~ PhD thesis entitled ~

STUDIES ON RESTRAINED STEEL BEAMS AND ITS MATERIAL CHARACTERIZATION UNDER HEATING AND COOLING FIRE

Submitted by

Suman Kumar Mushahary

Reg. No. 166104037

Supervised by

Prof Konjengbam Darunkumar Singh

Prof S Arul Jayachandran

Department of Civil Engineering
Indian Institute of Technology Guwahati
Guwahati – 781039, India

ABSTRACT

The present thesis is divided into three studies on the fire behavior of prismatic steel beams subjected to both heating and cooling. The first part is on (i) the material characteristics of mild steel E350 under heating and cooling. Then (ii) fire experimental investigations is carried out on the behavior 10.9 Grade bolts under both heating and cooling fire and (iii) the third part of the thesis is a numerical work on estimating the catenary forces that develop in restrained beams during heating and cooling. The thesis is presented in this order.

First, the mechanical properties, namely yield strength ($\sigma_{0.2,T}$), ultimate strength ($\sigma_{u,T}$) and elastic modulus (E_T) of mild steel E350 (equivalent to S355JR in EN 10025) are determined subjected to growth, cooling and post-fire phases in a non-standard fire condition. Based on the combined results from the present study and those from the literature, reduction factors for yield strength, ultimate strength and elastic modulus have been proposed, for growth, cooling and post-fire phases. In comparison to the growth phase, the rate of regain of the yield strength and elastic modulus are found to be relatively slower in the case of cooling phase. Additionally, in general, it has been seen that, the mechanical properties have been able to regain as they cool down after being heated to temperatures lesser than 600 ^{o}C Further, stress strain models corresponding to a) growth and cooling phases; and b) ambient temperature and post fire phase have been proposed.

Second, an experimental study is presented to evaluate the tensile and shear capacity of 10.9 Grade bolt in heating and cooling fire with an emphasis in the cooling phase properties. In total 44 specimens are tested and results are presented for the steady state tensile and shear tests conducted at room temperature, growth, cooling and postfire phases with peak temperature of heating from 600 - 800^{o}C. Based on the study, it has been seen that the growth phase data (as the temperature increases) follows an inverted S pattern while in cooling phase (as the

temperature decrease from peak temperature) the strength is regained linearly upto ~400^{o}C, without much strength enhancement as the specimens cools farther to the postfire phase. The strength drop in tensile tests is higher than the shear tests when the temperature increases from 500^{o}C to 600^{o}C in growth phase. Based on the present and previous experimental data, different reduction factors are proposed for tensile and shear behavior at growth phase on contrary to the single material proposed in EN1993-1-2. The strength regain in cooling phase is higher in shear tests than tensile tests. The tensile and shear strength reduces by ~46-67% and ~67-79% respectively (as compared to strength in room temperature) at postfire phase when the specimens are heated to 600-800^{o}C. Based on present experimental study, tensile and shear reduction factors are proposed in cooling phase.

Third, a numerical investigation is carried out assess the catenary forces in axially restrained beams in heating and cooling phase of fire. Catenary forces are developed in restrained steel beams that are subjected to elevated temperatures and then a subsequent cooling due to thermal expansion and material plastification. Catenary forces are higher in cooling phase fire than the forces at the end of heating/ growth phase fire. Hence a structural fire investigation must include the entire spectrum of the fire – start of the heating to end of cooling. Unlike the conventional (numerical) fire investigations, in the present work different materials properties are employed in growth and cooling phase. To enable the above, a new heating scheme is developed which can handle two different set of material properties in growth and cooling phases of fire. Parametric studies are carried out based on cross sectional slenderness, cross sectional shape, load ratio and extent of axial restraint. To augment the fire behaviour interpretation, moment capacity of the beams are estimated at elevated temperatures. The maximum temperature that may be sustained on the restrained beams are estimated for growth phase fire. The internal force at the end of cooling phase fire is evaluated, if the beam is heated up to the maximum temperature. Analytical models are developed based on force moment equilibrium relation for restrained beam in heating and cooling fire. Failure modes are discussed for typical beams with varying slenderness. An example has been worked out to show the implication of internal force on safety of restrained beam in heating and cooling fire.

In summary, the thesis contributes to the body of knowledge on heating and cooling in fire structural engineering.

STATEMENT OF ORIGINALITY

I do hereby declare that the matter embodied in this thesis is the result of investigations carried out by me in the Indian Institute of Technology Guwahati (IITG), Assam, India. In keeping with the general practice of reporting scientific observations, due acknowledgments have been made wherever the work described is based on the findings of other investigators.

IIT Guwahati

Date:

Suman Kumar Mushahary

CERTIFICATE

This is to certify that the thesis titled: "**Studies on restrained steel beams and its material characterization under heating and cooling fire**" being submitted by Mr Suman Kumar Mushahary to the Indian Institute of Technology Guwahati, India for the award of degree of Doctor of Philosophy is a record of genuine research work carried out by him under our supervision.

This thesis work, in my opinion is worthy of considering for the award of degree of Doctor of Philosophy in accordance with the regulation of the institute.

Date:

Dr. Konjengbam Darunkumar Singh

Professor
Department of Civil Engineering
Indian Institute of Technology Guwahati, India

Place:

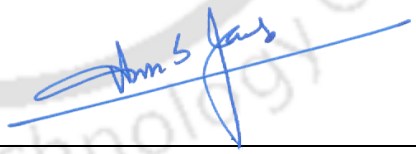

Date:14-07-2022

Dr. S Arul Jayachandran

Professor
Department of Civil Engineering
Indian Institute of Technology Madras, India

Place:IIT Madras, Chennai

ACKNOWLEDGEMENT

The whole journey into this PhD phase has been quite a long one. I quote these two sayings which has been instrumental in my upbringing.

'PhD is just a training for your future endeavor'- KD Singh

'Meeting deadline is important. You need not be perfect every time'- Arul SJ

It took me a while to inculcate these two major ideas. The first quote encouraged me to take up as many learning opportunities I could. This motivated me to learn - building human relationship, teaching and mentoring, explore unsolved scientific problems and most importantly improve myself personally on daily basis. The second one compelled me to finish the tasks that I take-up and fulfil my commitments where sometime perfection might cost considerable amount of time or you may just procrastinate. With this, I am blessed with endless support and motivation from my supervisors - Prof K Darunkumar Singh and Prof Arul S Jayachandran. Prof Arul has been always an elderly friend to me who played a major role in shaping my career as an engineer and researcher and has been inspiring me ever since my junior year at IIT Madras. While, Prof KD Singh facilitated me with all technical and material resources, insightful conversations, life skills and many more.

I thank my doctoral committee members - Prof AK Singh, Prof H Sharma and Prof S Bag for their valuable suggestions during annual seminars at IIT Guwahati. I thank the staff for the support provided at Central Workshop - Gwmchar Baro, Jiten Basumatary, Upen Gohain and at CIF - Dr. Ashim Malakar. I thank M/S Metalscope, Pondicherry who provided me with steel (E350) for mechanical testing.

The journey would never have been joyous if I had not met these amazing people who stood by me. I cherish the company of my friends and acknowledge their technical support - Dr.

Abhishek Saha (PhD IITG), Bidyut Bikash Borah (BTech IITM), Tapas Tripura (MTech IITG, now PhD IITD), Dr. Jashnav Pancheti (PhD QUT), Dr. Sevugan Rajkannu (PhD IITM), Dr. Akshay Mangal (PhD IITM), Soumi Rajbanshi (PhD IITG), Dr. Apurba Das (PhD IITG), Dr. Jyotirmoy Haloi (now NITS), Dr. Anjaly Pillai (PhD IITG) and Dr. Rahul Verma (PhD IITG). I thank my colleagues in my lab - Prasanta Kar (now CBRI Roorkee) and Dr T Ghisan Singh (now IITJ). Food and travel have been an important part in this journey. I thank - Manoj, Rupam, Gagan, Shukleswar Da and Baido, Dipak and Pranjeet for the immense love they showered with the food they prepared for me and my friends. I also thank for the support and encouragement that I received from my juniors at IITG - Hashmat Ahmed (MTech 2021), M Bharath (MTech 2021), Shravani Dhamane (MTech 2022), Navneet Diniya (MTech 2022), Shrikant Kanike (MTech 2021), Khogendrajit (BTech 2019), Thamsing Marem (BTech 2022), Harsh Jaiswal (MTech 2022), Luptesh Pradhan (MTech 2022), Himanshi Shrivastava (MTech 2022), Sanjoy Pal (MTech 2022), Abhay Rangoonwala (MTech 2022), Sanchit Saxena (currently PhD scholar), Vaibhav Patel (MTech 2022), Ayushi Athiya (MTech 2022), Faiz Akram (MTech 2022), Jayawant Ghadage (currently PhD scholar) and many more.

I am in debt, for their support and love, to my parents - Rahini Kumar Mushahary and Ilabati Mushahary and brother - Anup Kr Mushahary. And, last, but not the least, to the Almighty, who keeps giving me all the energy, health and humility to keep moving on and keep exploring

June 2022 Suman Kr Mushahary

IIT Guwahati (166104037)

Table of Contents

List of Figures

List of Tables

Notations

$\sigma_{0.2}$ or $\sigma_{0.2,20}$	0.2% proof stress at room temperature (~20^{o}C)
$\sigma_{0.2,T}$	0.2% proof stress at elevated temperature - T^{o}C
σ_y or $\sigma_{y,20}$ or f_y or $f_{y,20}$	Yield strength at room temperature (~20^{o}C)
σ_y or $\sigma_{y,T}$ or f_y or $f_{y,T}$	Yield strength at elevated temperature (~20^{o}C)
$\sigma_{t2.0,T}$	Stress at 2% of total strain
σ_u or $\sigma_{u,20}$ or f_u or $f_{u,20}$	Ultimate strength at room temperature (~20^{o}C)
$\sigma_{u,T}$ or $f_{u,T}$	Ultimate strength at elevated temperature - T^{o}C
E or E_{20}	Elastic modulus at room temperature (~20^{o}C)
E_T	Elastic modulus at elevated temperature - T^{o}C
$\varepsilon_{0.2}$ or $\varepsilon_{0.2,20}$	Strain corresponding to 0.2% proof stress at room temperature (~20^{o}C)
$\varepsilon_{0.2,T}$	Strain corresponding to 0.2% proof stress at elevated temperature - T^{o}C
ε_p or $\varepsilon_{p,20}$	Strain corresponding to initiation of strain hardening at room temperature (~20^{o}C)
ε_u or $\varepsilon_{u,20}$	Strain corresponding to ultimate strength at room temperature (~20^{o}C)
$\varepsilon_{u,T}$	Strain corresponding to ultimate strength at elevated temperature - T^{o}C
ε_r or $\varepsilon_{r,20}$	Strain corresponding to rapture at room temperature (~20^{o}C)
$\varepsilon_{r,T}$	Strain corresponding to rapture at elevated temperature - T^{o}C
n_T and m_T	Strain hardening coefficient
τ_v or $\tau_{v,20}$	Shear strength at room temperature (~20^{o}C)
k_{rT}	Reduction factor for tensile strength

k_{rS}	Reduction factor for shear strength
K_a	Axial stiffness
K_r	Rotational stiffness
A_g	Gross beam area
L_b	Length of beam
I	Moment of inertia in major axis
u_x, u_y or u_z	Translational degree of freedom in x, y or z direction
θ_x, θy or θz	Rotational degree of freedom in x, y or z direction
χ	Load ratio
β	% of axial restraint
$\lambda_{L,20}$	Cross sectional slenderness ratio at room temperature (~ 20^{o}C)

Abbreviations

CT	Cooling phase temperature
GT	Growth phase temperature
RT	Room temperature
PT	Post-fire temperature
N	Total number of specimens
GL	Gauge length (extensometer)
t	Thickness of plate
N_{Cmax}	Maximum internal compressive force
T_{Cmax}	Temperature during maximum internal compressive force
T_z	Temperature during the heating phase when the internal force is zero
N_{Tcr}	Internal force at critical temperature
T_{cr}	Maximum temperature the beam can sustain for given geometric (length, cross section), boundary and loading condition
N_{Fmax}	Maximum internal tensile force at the end of cooling phase.
OES	Optical emission spectroscopy
UTM	Universal testing machine
RP	Reference point

CHAPTER 1: INTRODUCTION

1.1 Fire hazard

Major fire incidents like the 1 and 2 World Trade Centre (WTC) in New York City (2001) (Usmani et al. 2003) (see Figure 1.1), Plasco Building in Tehran (2017) (Aghakouchak et al. 2021) (see Figure 1.2), Chennai Silk in Chennai (2017) are some of devastating fire accidents. In WTC 1 and 2 fire, the periphery columns and then the internal columns buckled due to reduction in buckling resistance as the temperature increased in the building. In Plasco Building (Aghakouchak et al. 2021), the external column buckled outward at the beam column junction due to thermal expansion of the beams. In the Plasco Building, the fire has initiated in the morning (~8AM, local time) and it collapsed in the noon (~ 12 PM, local time). The temperature within this building has been reducing at the time collapse. Similarly, the fire in Chennai Silk has doused after a long duration (initiated in morning) when suddenly the building collapse (in the evening). In all the above examples, these buildings underwent structural collapse after being exposed to elevated temperature for a long duration. When the building is exposed to long duration of fire (>2-3 hours), the load carrying capacity of structural members reduces drastically. Although some building collapsed during the heating phase, i.e., when temperature is increasing (eg., WTC 1 and 2) while others collapsed during the cooling phase, i.e., when temperature is decreasing (eg., Plasco Building and Chennai Silk). Sometimes, during the later stage of fire (when the temperature is decreasing), firefighters try to control the fire and get into the building. The lives of these firefighters are endangered, if the building collapse during that stage. So, it is important that buildings do not collapse at that time. Hence,

it is important to understand the structural response of the building during a realistic fire (natural fire).

1.2 Behavior of restrained beams in fire

Design of steel structures in fire (ANSI/AISC 360 2016; EN 1993-1-2 2005) is taken care by reducing the member capacity through certain reduction factors (with respect to temperature). Thermal expansion and material plasticity induce different types of internal forces (like axial compression and tension in beams, moments in columns etc.,) in building system due to increase in temperature. These internal forces, which otherwise, will not develop in a non-fire scenario, can be governing forces in building in fire that can trigger catastrophic failure in building. Hence, it is important to access these forces. These forces are assessed in literatures for heating fire (incremental fire type). However, the actual fire scenario in buildings has heating and cooling fire, where, the temperature increases in a compartment due to availability of fuel or ventilation (also called growth phase fire) and after certain period of time, when the fuel exhausts, the temperature starts to drop (also called cooling phase fire). It has been observed in some of the experiments that the internal forces in beams are much higher when the temperature drops than the scenario where the temperature is increasing. In literature, the internal force in growth phase fire has been well discussed, however there is very little understanding on the internal force during cooling phase fire.

1.3 Mechanical properties of steel at elevated temperature

Steel undergoes different degrees of strength deterioration at elevated temperature. The strength reduction is well discussed in literatures and codes. However, these reductions are based on heating fire (growth phase fire). It has been observed in literature, which are based on mechanical strength of steel in post fire, that the steel does not regain complete strength when the fire douses completely. Internal forces are transferred from beams to adjacent members through connections. Out of two types of connection in steel building (bolted and welded connection), bolted connections are more prominent in time constrained construction projects. Since, the resistance of bolts reduces at elevated temperature, the bolts are required to have adequate strength to resist the internal forces during fire. And there has been no or very limited

data on mechanical strength of steel plate and bolt in cooling phase Hence, it is important assess the mechanical strength of steel plate and bolts in cooling phase fire.

1.4 Motivation

Steel building system comprises of restrained beams as main structural element. In these beams, large internal forces are developed during fire. The beams are made of readily available hot rolled steel sections or built-up sections. And the restrain in the beam is gained through the presence of adjacent members, for which there should be proper stress follow through the connections. As mentioned above, it is important to understand the mechanical strength of steel material (plate) and bolt in heating and cooling fire. In order to understand the internal forces, we can measure them through experimental investigation or numerical studies. Experimental programs are costly exercise; hence, numerical studies are carried out. It is important to have exact material properties in the numerical model to assess the internal forces more accurately.

1.5 Objectives of the study

In this thesis, the behaviour of axially restrained beams is studied in heating and cooling fire, for which. numerical investigation is carried out. In order to exactly assess the internal forces, precise mechanical properties of a typical steel grade and bolt grade are experimentally evaluated in heating and cooling fire. The research objectives of this thesis are listed below:

1. Experimentally assess the mechanical properties of typical steel grade – E350 in heating and cooling fire.
2. Experimentally assess the tensile and shear strength of 10.9 Grade bolt in heating and cooling fire.
3. Numerically estimate the internal forces of axially restrained steel beam in heating cooling fire. The mechanical properties estimated in the first objective is incorporated in the numerical models.

1.6 Thesis outline

This thesis is structured with six chapters. These chapters are briefly discussed below:

Chapter 1 introduces the basic concepts of fire in building, member response during fire, material degradation due to increase in temperature.

Chapter 2 presents brief review of works on restrained beams in fire, strength degradation in mild steel and bolt.

Chapter 3 covers the study on mechanical properties of E350 steel in heating and cooling fire. Tensile coupon tests are tested in room and elevated temperature. 2 tests are carried out in room temperature, 8 tests in growth phase, 17 tests in cooling phase and 9 tests in post fire tests. Chemical analysis is carried out for room temperature and heat treated (heated upto 400^{o}C, 500^{o}C, 600^{o}C, 700^{o}C, 800^{o}C, 900^{o}C and 1000^{o}C) specimens. Microstructural studies are also carried out in the heated treated specimens. Mechanical properties, such as tensile strength, yield strength, elastic modulus, yield strain etc., are evaluated for each of the tested specimens. Material properties are compared with existing material model and other experiments for growth phase study. Based on least mean error (MAPE), reduction factors are proposed for growth phase and cooling phase properties. Stress strain relationship is proposed for all the tests based on experimental outcome.

Chapter 4 discuss the experimental investigation on the tensile and shear strength of 10.9 Grade HSS bolt in heating and cooling fire. Tensile and shear testing fixture is developed. M10 and M8 size bolt is chosen for tensile and shear test respectively. To evaluate the tensile strength of 10.9 Grade bolt, 3 tests in room temperature, 5 tests in growth phase, 9 tests in cooling phase and 3 tests in post-fire tests are carried out. While 5 tests in room temperature, 6 in growth phase, 9 in cooling phase and 4 in post fire are carried out to estimate shear strength. The results are compared with existing models and results from other experiments. Reduction factors are proposed for growth phase and cooling phase for tensile and shear strength. Load – displacement relationship and failure modes are discussed.

Chapter 5 explores the internal forces in restrained beam in heating and cooling fire. The numerical model is developed for a restrained beam at elevated temperature. The model is validated against two experimental work on restrained beam at elevated temperature and natural fire. Different material properties are applied during heating and cooling phases of fire. A new heating scheme is developed which can handle different material properties in heating and cooling phase. Parametric studies are carried out based on cross sectional slenderness and aspect ratio, amount of axial restraint and load ratio. The moment capacity of the beams is evaluated at elevated temperature. Maximum temperature (T_{cr}) that the beam can sustain for given load ratio and axial restrained is estimated. The maximum internal force is found at the end of cooling phase if the beam is heated upto T_{cr}. Failure modes are discussed for some of the typical beam cross sections. Based on force- moment equilibrium, analytical formulation is proposed.

Chapter 6 sums up the complete study carried out in the thesis work and provides suggestions for future research.

The numerical and analytical results for all the cross sections with different levels of axial restraint and load ratio considered in this study is presented in *Appendix – A*.

The numerical model for a typical simulation procedure in cooling phase is presented in annotated form in the *Appendix - B*. The annotated form shows the various intricated parts of the numerical model, like – nodes, elements, material properties, coupling, springs, boundary and loading condition etc., and their linkage within the Abaqus framework.

Figures

Figure 1-1 Fire in World Trade Centre (courtesy: www.britannica.com)

Figure 1-2 Plasco Building fire (courtesy: www.nbcnews.com)

CHAPTER 2: BACKGROUND

2.1 Layout of literature review

This chapter cover the following topics:

1. Mechanical properties of mild steel at elevated temperature
2. Strength of bolt at elevated temperature
3. Forces in restrained beams in fire

2.2 Mechanical properties of mild steel at elevated temperature

Fire is a major hazard that has devastating effects, especially on steel structures. In the literature, effects of fire on structural members or buildings, have been reported, primarily considering two fire scenarios in buildings: *viz.*, (i) standard fire (or ISO fire) (Flint et al. 2007) with incremental heating temperature and (ii) realistic fire (Bailey et al. 1996; El-Rimawi et al. 1996; Franssen 1990; Gernay and Franssen 2015) –like parametric fire (EN 1991-1-2 2002), localized fire (Ramesh et al. 2020), travelling fire (Rackauskaite et al. 2017) etc. with incremental heating and followed by decremental cooling temperature (see Figure 2.1). Based on the direction of change of temperature with time, realistic fire (see Figure 1) may be divided into three phases: (i) growth (heating) phase, (ii) cooling phase and (iii) post-fire phase. Various codes (e.g. (ANSI/AISC 360 2016; AS 4100 2016; EN 1993-1-2 2005)) on steel structural design at elevated temperature provide suitable reduction factors to enable the design of structural members in growth phase. In addition to that, there are several works to estimate the material properties of steel (e.g. (Aziz and Kodur 2016; Chen et al. 2006; Hu et al. 2009; Imran

et al. 2018; Kankanamge and Mahendran 2011; Kirby and Preston 1988; Li et al. 2003; McCann et al. 2015; Neuenschwander et al. 2017; Outinen and Makelainen 2004; Ranawaka and Mahendran 2009; Singh and Singh 2019a; Torić et al. 2017; Yuan et al. 2016)) at elevated temperature (see Figure 2.2, 2.3 and 2.4). The gas temperatures adopted while performing these experiments are only growth phase / standard fire conditions, and exclude the cooling phase fire situations. Further, there are number of published works where the post-fire properties of steel (e.g., (Aziz and Kodur 2016; Chen et al. 2019; Gunalan and Mahendran 2014; Kesawan and Mahendran 2018; Lu et al. 2016; Outinen and Makelainen 2004; Singh and Singh 2019b; Smith et al. 1981)) have been investigated. From these works on post-fire properties of steel, it has been observed that some permanent change/ reduction in mechanical properties of steel occur when heated to certain temperature above 550-650 ˚C, which may not recover once it cools down. From these observations, it is inferred that the material properties in the growth phase cannot be directly used to understand the mechanical response of structures in cooling phase. However, in the literature, many researchers have performed numerical investigations using fire condition which has growth phase and cooling phase (e.g., (Elhami Khorasani et al. 2019; Fischer et al. 2019; Gernay and Khorasani 2020; Jiang et al. 2015; Jiang and Li 2017; Lamont et al. 2004; Rackauskaite et al. 2017)) wherein material properties of growth phase have been used in the cooling phase, essentially due to the unavailability of cooling phase properties. Experiments on restrained beams (Li and Guo 2008; Ramesh et al. 2020) and slab (Guo 2012; Guo and Bailey 2011) under both growth and cooling phases, reveal that that large axial forces have been induced in members due to plastic deformations and thermal contraction (Guo and Bailey 2011) during the cooling phase, emphasizing the key importance of understanding the cooling phase material behavior and response. In some cases (Ramesh et al. 2020; Wang 2000), the connections have failed due to tensile yielding of bolts during cooling phase. Accurate and reliable estimation of cooling phase material properties will serve as key inputs in the evaluation of stress flow in the beams during the cooling phase. To the best of authors' knowledge, no studies are available in the published literature to understand the mechanical properties of steel in the cooling phase for any grade of carbon steel.

2.3 Strength of bolt at elevated temperature

Bolted connections are popular in steel buildings due to their ease of fabrication and installation. However, during a fire event, bolts undergo drastic reduction of strength and stiffness. In a general compartmental fire, these connections (Guo and Bailey 2011; Li and Guo 2008; Shaheen et al. 2020; Wang 2000) need to sustain different internal forces due to two stages (namely, heating and cooling) of compartment or natural fire(Li and Guo 2008). At the ambient temperature, the axially restrained beams transfer load to the adjacent members through shear and moment. In the event of fire, in addition to the forces due to gravity loads (Yin and Wang 2004), the connections (e.g. bolted connections) have to sustain additional forces during the cooling phase(Li and Guo 2008). These additional forces may arise due to plastic deformation (during growth phase) (Shaheen et al. 2020) and strain reversal (El-Rimawi et al. 1996; Franssen 1990) (or strength regain). These forces must be effectively transferred to the adjacent members during the cooling phase through the bolted connection. It has been observed from postfire experiments (e.g. (Lou et al. 2012)) that the bolts do not completely regain strength when the specimens are heated above ~400-500oC, indicating that the growth and cooling phase responds are different (i.e., the strength of the bolt with respect to temperature is not same in growth and cooling phase). Amongst a variety of high strength steel bolts used in construction industry (e.g. 8.8 Grade, 10.9 Grade etc.), 10.9 grade is very popular. However, while examining the strength regain in high strength steel (HSS) bolts (Ketabdari et al. 2019) and mild steel (Chen et al. 2019, 2020b; Singh and Singh 2019b; Zhang et al. 2021) at post fire stage, HSS bolts regain much lower strength than the mild steel. Hence, it is important to estimate the strength (tensile and shear) of bolts in various stages (heating and cooling) of fire. Tension and shear are the primary failure modes in bolts. And the tensile - shear relationship ($\tau_{y,T} = \sigma_{y,T}/\sqrt{3}$) may not hold good all the time (Li et al. 2020; Song et al. 2020). Hence, it is important to evaluate the tensile and shear strength of bolt in heating and cooling fire.

2.4 Restrained beams at elevated temperature

Steel beams are primarily designed to resists bending, shear or lateral torsional buckling in framed structure at elevated temperature. The beams are designed based on the simply

supported boundary condition. While, most of the beams are axially or rotationally restrained (see Figure 2.5). At elevated temperature, axial forces are induced in the beam due to thermal expansion and restrains at beam connection/support. These axially restrained beams can sustain higher temperature as compared to simply supported beams (Liu et al. 2002; Yin and Wang 2004) . Due to material degradation with increase in temperature, the beams undergo large deflection. Catenary forces are developed in these beams due to the occurrence of large deflection (see Figure 2.6). Catenary forces are axial in nature and hence are more capable to withstand higher temperature as compared to flexure (axial resistance is more preferred over flexural resistance due to availability of higher reserved strength). These forces have been earliest observed in the Cardington fire tests (Wang 2000). The earliest work on restrained beam at elevated temperature initiates with the full scale experimental investigation (Liu et al. 2002) on restrained beam in elevated temperature. Later, Numerical (Dwaikat and Kodur 2011; Kodur and Dwaikat 2009; Li et al. 2007; Pournaghshband et al. 2019; Tan and Huang 2005; Yin and Wang 2004) and analytical (Dwaikat and Kodur 2011; Sun and Burgess 2016; Yin and Wang 2005) studies are carried out to understand the effect of other parameters. However, the gas temperature considered in these studies (Dwaikat and Kodur 2011; Kodur and Dwaikat 2009; Li et al. 2007; Pournaghshband et al. 2019; Sun and Burgess 2016; Tan and Huang 2005; Yin and Wang 2004, 2005) are incremental in nature, i.e., growth phase fire (see Figure 2). But, in compartmental fire (such as the fire in a building), cooling phase fire succeeds the growth phase which is not considered in these assessments (Dwaikat and Kodur 2011; Kodur and Dwaikat 2009; Li et al. 2007; Pournaghshband et al. 2019; Sun and Burgess 2016; Tan and Huang 2005; Yin and Wang 2004, 2005). It is displayed in the limited experiments (2 tests) conducted on restrained beam in natural fire (Li and Guo 2008), that the axial forces in the beams are much higher (in the order of about 200%) in cooling phase than in growth phase. In the Cardington fire tests (Wang 2000), bearing failure of bolts has been observed when the beam is allowed to cool after a heating cycle. Since, connections at beam-column junction are designed to transfer loads through shear or bending. So, failure of bolts in bearing indicate that there is development of large tensile forces (in plane force) at the connection. Hence, it is important to estimate these forces during cooling phase.

2.5 Summary on literature review

Based on the present literature survey, following conclusions are drawn:

1. The mechanical properties of steel can vary in heating and cooling phase. There is no study on mechanical properties on mild steel in heating and cooling fire
2. It is important to assess the forces in connection during cooling phase. For the stability of the connections (bolted connections), it is important to evaluate the mechanical strength of bolts in heating and cooling fire. There is very limited study on HSS bolt in heating and cooling phase.
3. There is development of internal forces in beams during cooling phase. It is important to assess these forces. The present research has been limited to assessing these forces in growth phase fire only. There is a need to extend the present study to cooling phase fire as well.

Based on these gap areas, objectives listed in the previous chapter (see Section 1.4) are framed

Figures

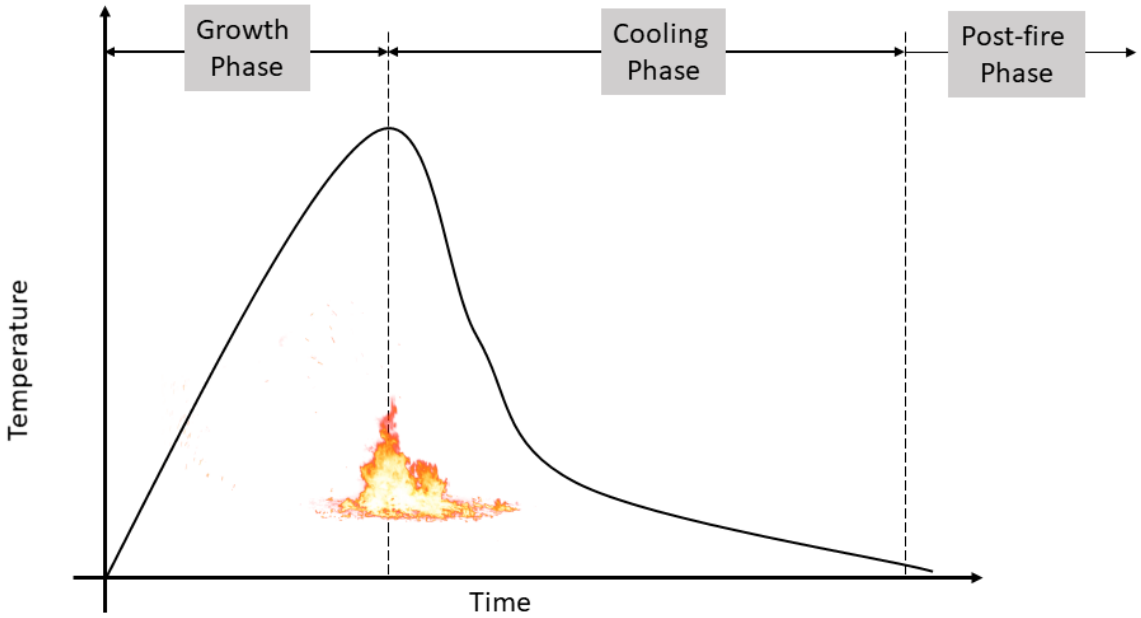

Figure 2-1 Typical realistic fire curve

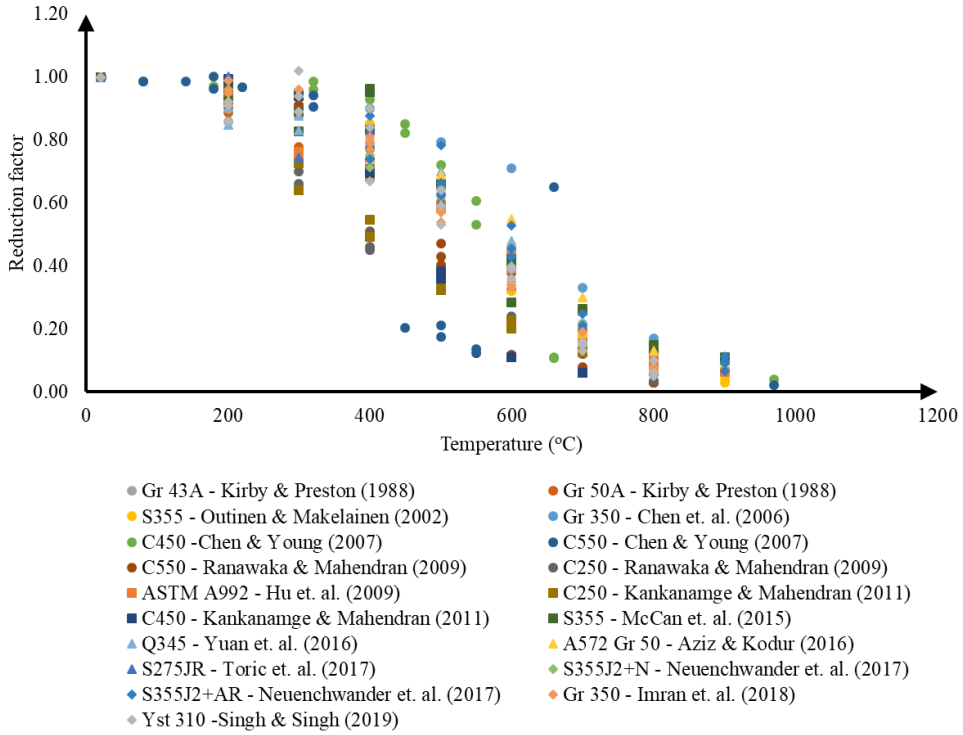

Figure 2-2 Yield strength reduction factor at elevated temperature

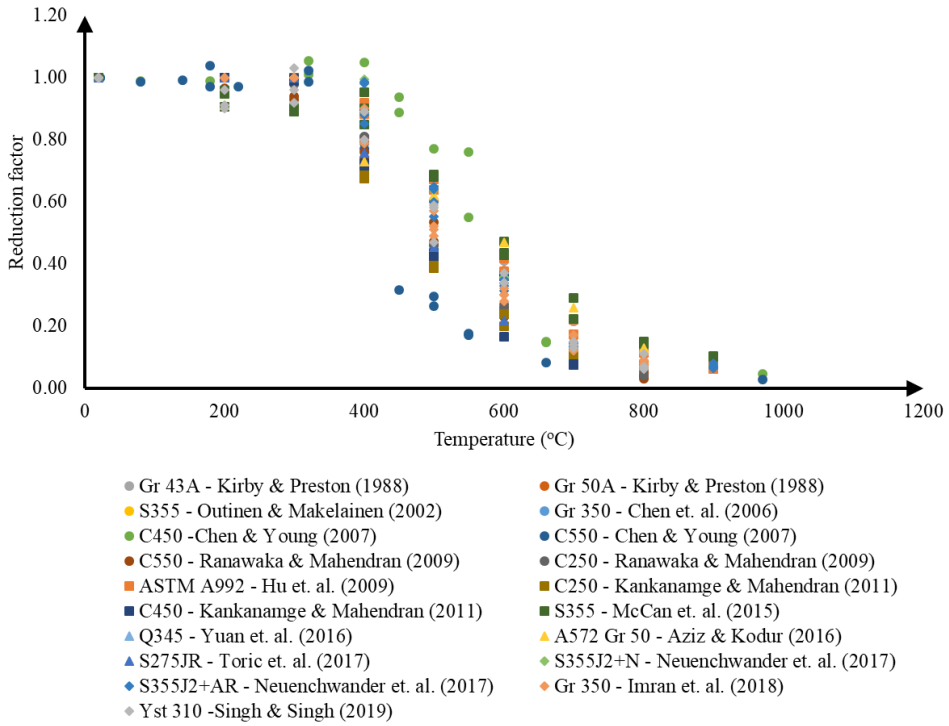

Figure 2-3Ultimate strength reduction factor at elevated temperature

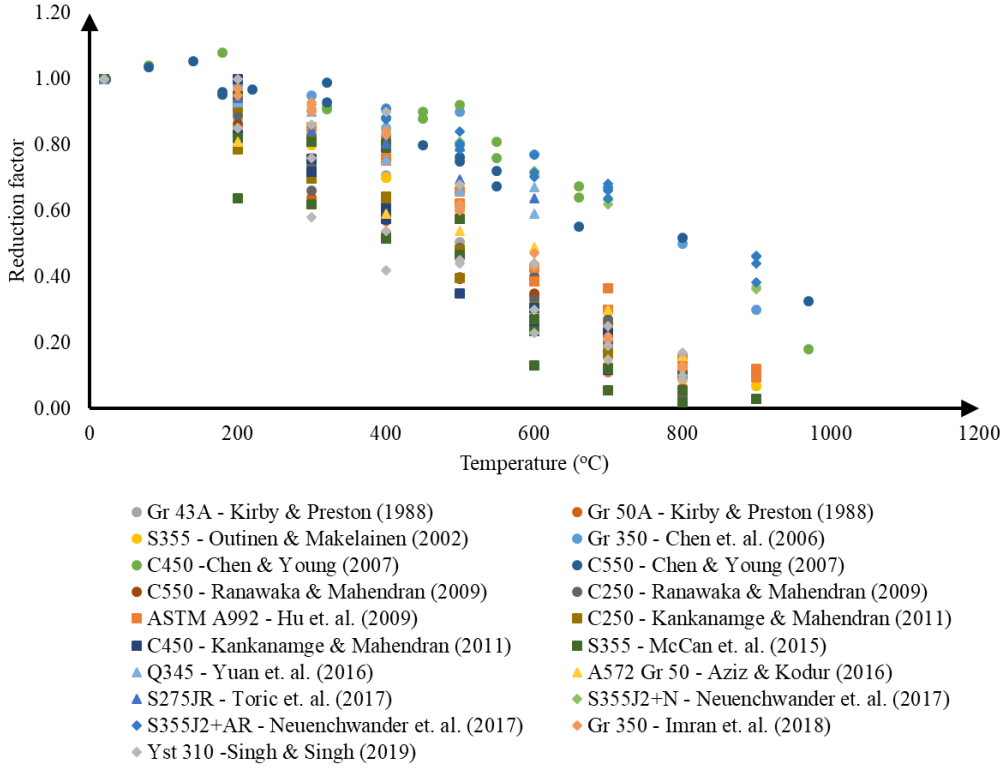

Figure 2-4Elastic modulus reduction factor at elevated temperature

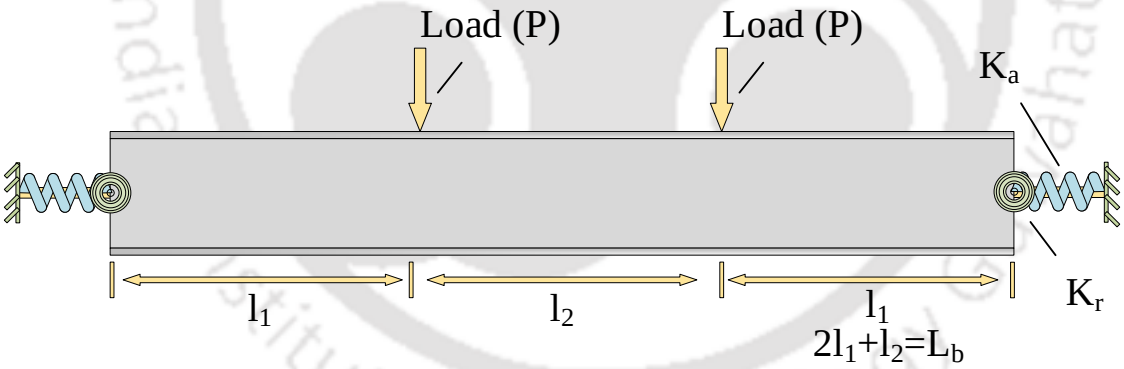

Figure 2-5 Schematic diagram for an axially and rotationally restrained beam under four-point bending load

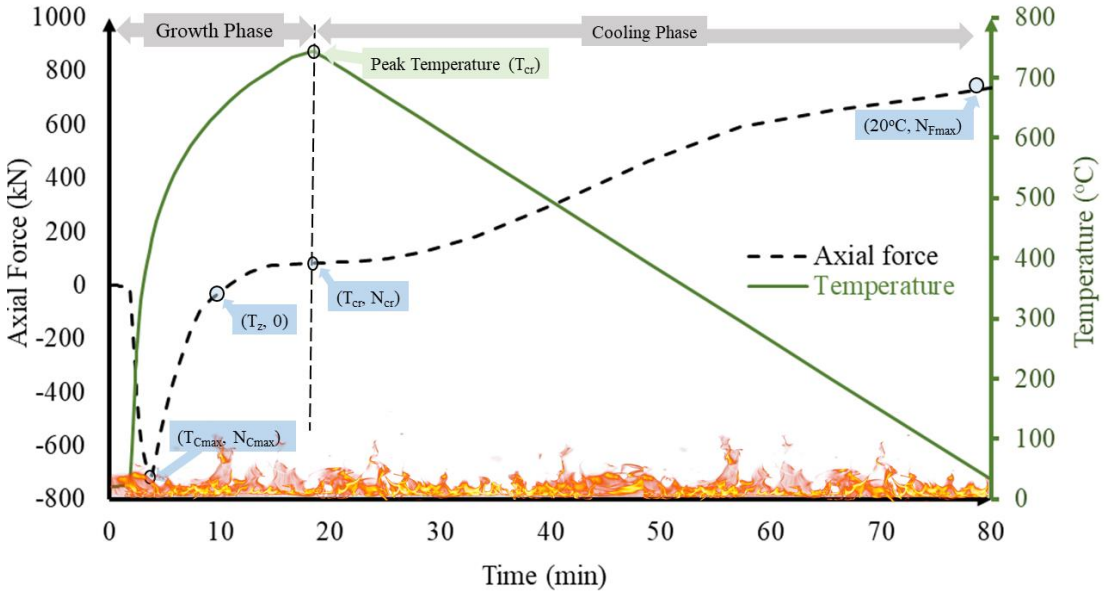

Figure 2-6 Typical representation of internal forces in a restrained beam in natural fire

CHAPTER 3: MECHANICAL PROPERTIES OF E350 STEEL IN HEATING AND COOLING FIRE

3.1 Background

In this chapter, an attempt has been made to investigate the mechanical properties of mild steel grade - E350 (IS 2062 : 2011) (IS 2062 2011) in the cooling phase, along with the properties in growth and post-fire phases. E350 grade mild steel with a nominal yield strength of 350 MPa, is a commonly used grade in the Indian construction industry; and also conforms to other international codes such as Grade 50 in ASTM A572/A572M (A572/A572M 2018), S355JR in BS 10025 (EN 10025-2 2019) etc. Hot-rolled E350 mild steel are popularly used in India, for making built-up sections for girders and piers. Results of post-fire optical emission spectroscopy (OES) and micro-structure studies are also presented. Further, some of the experimental results are compared with existing experimental data from the literature and design reduction factors are proposed. Finally, appropriate stress-strain models at elevated temperature are also provided which can be directly used for advanced numerical analysis

3.2 Experimental procedure

A controlled experimental programme has been carried out at the Central Instrument Facility of Indian Institute of Technology Guwahati. The experimental schemes are divided into three parts, *viz.*, (i) growth phase, (ii) cooling phase and (iii) post-fire phase (see Figure 2.1). Different procedures are adopted in each of these phases, which have been discussed in the subsequent sections.

A total of 36 tensile coupon tests have been carried out, out of which two are at room temperature, eight at growth phase, seventeen at cooling phase and nine at post-fire phase. The initial temperature at the inception of fire is the room temperature (RT) which is maintained at 20^{o}C. In order to identify the specimens with different temperature and temperature path, sample identifier (Sample ID) has been employed. Sample ID is denoted by RT-20-20 where the first number 20 represents the intermediate / initial temperature (20˚C), which is separated by a hyphen and the second number - 20 is the temperature (20˚C) at which the experiment is carried out. If more than a single trial is conducted, then numbers will be denoted within parenthesis. Likewise, similar representations are made for growth phase (e.g. GT-20-600), cooling phase (e.g. CT-600-300) and post-fire phase (e.g. PT-600-20). Here, GT-20-600 means the sample is tested at 600˚C in growth phase after being heated from room temperature (20˚C) with GT denoting growth phase; CT-600-300 denotes sample is tested at 300˚C in cooling phase after being heated to a maximum temperature (600˚C) with CT means cooling phase temperature and PT-600-20 implies sample is tested at room temperature (20˚C) in post-fire case (PT denoting post-fire temperature) after being heated to maximum temperature of 600˚C.

3.2.1 Test method

In the literature, generally, two procedures have been adopted to evaluate mechanical properties at elevated temperature *viz.*, (i) steady state testing and (ii) transient state testing. In steady state testing, (Imran et al. 2018; Li and Young 2017; McCann et al. 2015; Neuenschwander et al. 2017; Singh and Singh 2019a; Torić et al. 2017; Yuan et al. 2016), the specimen is heated up to a target temperature (or peak temperature) and then it is held steady at that temperature and the load is applied until failure of the specimen. While in the transient state testing (Kirby and Preston 1988; Outinen and Makelainen 2004; Ye and Chen 2012; Yuan et al. 2016), specimen is loaded up to a certain stress level and then incremental temperature is added. Stress - strain and temperature – strain relationships are obtained from steady state and transient state testing methods (Ye and Chen 2012) respectively. Hence, in order to readily obtain stress strain relationship (Imran et al. 2018) and reduction factors, steady state tensile testing method has been adopted in this study. .

3.2.2 Test specimen and the set-up

The samples for testing have been extracted as rectangular strips of dimension 400 mm x 30 mm from larger sheet of E350 of nominal thickness of 5 mm. Only one thickness (i.e. t = 5 mm) has been taken up for this study. EC 3 (EN 1993-1 2005), BS 5950-1 (BS 5950-1 2000), AS4100 (AS 4100 2016) and IS 800 (IS 800 2007) suggest uniform nominal strength upto 40mm, 16 mm, 12 mm and 20 mm respectively. Hence, the strength obtained from the present single thickness (i.e., t = 5mm < 20mm) will be indicative of the nominal strength for E350. The mid-span of the rectangular strips has been cut using wire cut EDM (electric discharge machining) to form flat dog bone tensile coupon. Flat sub sized coupon of dimensions 6 mm wide and 25 mm gauge length have been prepared in accordance to the ASTM E8 (ASTM E8/E8M 2016) (see Figure 2-a). The dimensions are measured using a digital Vernier calliper, which is capable to measure up-to second decimal of a millimeter. A longer grip of about 150 mm in length on top and bottom (i.e. at the ends) has been provided to insert the specimen into the muffle furnace; also, for the safety of the actuator and cross-head grips during the experiment.

The experiment has been conducted in a 250 kN servo hydraulic universal testing machine (see Figure 3). A ceramic rod-type 25 mm gauge length high temperature extensometer is used to measure the strain in the specimen. The loading is carried out through displacement control mode. Elastic modulus and yield strength are estimated based on the initial portion of the stress-strain graph. Usually, slower displacement rate is provided during the initial loading in order to avoid over-shoot of the stress value. Over shoot of stress value (yield strength) occurs during a higher displacement rate due to dynamic strain effect. Once, the yielding has taken place the displacement rate is increased for the rest of the test till rupture. Hence, two loading rates are employed in this test. Initial loading rate in growth or cooling phase is 0.1 mm/min up to 0.2% strain and then 0.5mm/min (Huang and Young 2014) for the remaining of the test. The loading rate is within the specification suggested in ASTM E8(ASTM E8/E8M 2016) which allows the strain rate in between 0.05 and 0.5 mm/mm/min.

The chemical composition by weight has been evaluated using optical emission spectroscopy (OES) and the average value has been reported in Table 3.1. In order to evaluate the mechanical

properties, namely yield strength ($\sigma_{0.2}$), ultimate strength (σ_u), elastic modulus (E), strain percentage at yielding ($\varepsilon_{0.2}$) and strain percentage at rupture (ε_u), sub-sized coupon according to ASTM E8 (ASTM E8/E8M 2016), has been prepared. The mechanical properties of the base material – E350, at room temperature, are presented in Table 3.2.

3.2.3 Heating protocol for growth phase

The specification from ASTM E21 (ASTM E21 2017) has been followed to conduct the experiments (see Figure 3.1) in the growth phase. The tensile coupons have been exposed to desired elevated temperatures using electric furnace that is capable to heat up to 1400^{o}C. There are two internal thermocouples in the furnace embedded in the refractory material lining to display the gas temperature inside the chamber. Additionally, three external K-type thermocouples (see Figure 3.2) capable of measuring in the range 0^{o}C– 1024^{o}C have been kept in touch to the specimen within the gauge length in three sides with the fourth side having the high temperature extensometer. The thermocouple, having a sensor module MAX 6675, is connected to a micro-controller (ESP 8266) for processing of the outputs from thermocouple which is connected to a laptop computer via an USB data cable. The specimen is heated at the rate of 10^{o}C/min until the peak temperature is attained. This heating rate is similar to the rate of temperature increase in protected steelwork (Li and Young 2017; McCann et al. 2015). The specimen is then allowed to heat for 20 minutes at a constant temperature once the pre-determined temperature is attained (Singh and Singh 2019a) such that the temperature gradient within the chamber is minimised. The temperature from the thermocouple has been taken as the specimen temperature, which is found to be very close to the temperature provided by the internal thermocouple of the chamber. During heating, the heating chamber is sealed using glass wool in order to avoid thermal leakage.

3.2.4 Test method for Cooling Phase

Cooling phase properties are very important parameters to assess the stability of the structures while the gas temperature is reducing. In the present case, the cooling-phase experiments have been carried out after coupons have been heated to a maximum temperature of 800^{o}C. It has been observed that the reduction in mechanical properties for change of temperature from 800^{o}C (GT-20-800) to 900^{o}C (GT-20-900) is relatively low (~2-4%), so, the experiments for

cooling phase temperature corresponding to a peak temperature of 900°C has not been conducted. The coupons used in this section are of similar dimension as used in the growth phase (see Section 2.3). Although, cooling rates play a significant role in micro-structural phase transformation, however, in the scope of this study, it has been limited to only one cooling rate (i.e., cooling in furnace/ chamber). In the heating protocol, after the specimen temperature reaches the peak intermediate temperature the specimen is retained for 20 mins and then allowed to cool in the chamber upto the target temperature. Once, the target temperature is achieved, the specimen is allowed to soak heat for another 20 minutes before testing. The loading procedure in these experiments is similar to the one employed for the growth phase, as mentioned in Section 2.2.

3.2.5 Test method for Post-fire Phase

Post-fire material properties are very important since such properties are required to re-assess the strength after an event of fire, in order to, efficiently rehabilitate a fire-damaged building. In this study, the post-fire experiment has been carried out after sub-sized specimens have been heated at temperatures ranging from 200°C to 1000°C at an interval of 100°C. Initially, the sub-sized tensile coupon (see Figure 3.1 b) is prepared in accordance with ASTM E8 (ASTM E8/E8M 2016) with a total specimen length of 100 mm. In order to assess the post-fire material properties, the specimen is heated in an external furnace till a certain peak temperature and then allowed to cool in the furnace. Then, the specimen is tested at ambient temperature. The heating of the specimen is carried out in a muffle furnace, which is capable to reach upto 1400°C. The specimen is heated at a rate of 10°C/ min. Once the target temperature is achieved, the specimen is allowed to stay in that temperature for 30 minutes. Then the specimen is allowed to cool in the furnace/chamber. Dimensions are measured after the specimen surface has been rubbed with emery paper to remove burned out surface material. Testing (Huang and Young 2014; Singh and Singh 2019b) is then carried out with an initial loading rate at 0.05mm/min upto 0.2% strain and then 0.5mm/min for the remaining of the test.

3.2.6 Chemical analysis and microstructure study of post-fire specimens

The chemical composition of the post-fire specimens is evaluated using OES (see Table 3.3). In carbon steel, proportions of carbon, silicon and manganese play an important role in deciding

the strength and ductility of the material. The post-fire specimens for chemical analysis and microstructure study, has been prepared by allowing the specimen cool in the chamber along with post-fire coupons. Micrographs of the unstressed post-fire samples are obtained to understand the microstructure of the heat - treated materials. The post-fire samples are extracted using EDM. They are then placed in epoxy resin moulds for ease of handling. The samples are then grounded on emery paper and velvet cloth with polishing-colloidal solution. The micrographs are obtained for samples extracted from the unstressed post fire specimen. Nital (96% methanol + 4% nitric acid) is used to etch the surface for 5 seconds before observing the sample in the optical microscope.

3.3 Results and discussions

Results of the tensile tests conducted in this study are presented (see Figure 3.3) for a typical test at room temperature, growth phase, cooling phase and post-fire phase. The reduction of the mechanical properties *viz.*, yield strength, ultimate strength and elastic modulus of E350 mild steel in elevated temperature are then discussed. The elastic modulus is evaluated as the ratio of difference of stress and strain values at 10% and 50% of $\sigma_{0.2}$ as specified in ISO 6892 (ISO 6892-1 2016). The stress strain responses generated at the elevated temperature do not have a distinct yield plateau. Hence, the yield strength is determined using 0.2% proof stress method. The mechanical properties are presented in Tables 3.4, 3.8 and 3.10, for growth phase, cooling phase and post-fire phase respectively. The reduction factor ($\sigma_{0.2,T}/\sigma_{0.2,20}$, $\sigma_{u,T}/\sigma_{u,20}$ or E_T/E_{20}) is the ratio of properties at temperature T^oC, say yield strength ($\sigma_{0.2,T}$), ultimate strength ($\sigma_{u,T}$) or elastic modulus (E_T) to the properties in standard room temperature (20^oC) such as yield strength ($\sigma_{0.2,20}$), ultimate strength ($\sigma_{u,20}$) or elastic modulus (E_{20}). Yield strength, ultimate strength and elastic modulus at different phases have been discussed in the following section. Observations from chemical analysis and microstructure study have also been discussed below.

MAPE technique[56] has been adopted in this work to obtain appropriate reduction factor by minimising the mean error of the predicted value against the experimental data. Khorasani et al. (Khorasani et al. 2015) successfully adopted the MAPE technique to show the goodness of the various material models (ANSI/AISC 360 2016; EN 1993-1-2 2005; Luecke et al. 2013) at elevated temperature. MAPE is given as

$$MAPE = \frac{1}{N}\sum_{i=1}^{N}\left|\frac{A_i - a_i}{A_i}\right| \quad (3.1)$$

where A_i = experimental data point; a_i = proposed/predicted (using one of the models) data point; and N = number of data points.

The experimental data points are considered only at discrete temperature of 20, 200, 300, 400, 500, 600, 700, 800 and 900 ^oC for growth phase and additional 100^oC and 1000^oC for post-fire phase. Some of the experimental data are linearly interpolated to the nearest discrete temperature if the experimental data point does not exist at that discrete temperature. For example, in Neuenschwander *et al.*, (Neuenschwander et al. 2017), $\sigma_{0.2,T}/\sigma_{0.2,20}$ at 400^oC and 550^oC for 60mm (S355J2+N) are presented as 0.75 and 0.58 respectively. hence the $\sigma_{0.2,T}/\sigma_{0.2,20}$ at discrete temperature (T = 500^oC) is linearly interpolated as 0.64. Since, design values cannot be taken higher than the nominal values. In case of few of the data points, where the reduction factor is more than unity (in post-fire results) has been rounded to unity.

3.3.1 Growth phase

Eight temperatures are chosen in this study, namely, 200^{o}C to 900^{o}C with an interval of 100^{o}C. Yield strength ($\sigma_{0.2,T}$), stress at 2% total strain ($\sigma_{t2.0,T}$), ultimate strength ($\sigma_{u,T}$), yield strain ($\varepsilon_{0.2,T}$), maximum strain at ultimate load ($\varepsilon_{0.2,T}$), strain at rupture (ε_r) Elastic modulus (E_T) and reduction factors–for the growth phase are provided in Table 3.6. The reduction factors at growth phase are compared with the EC 3(EN 1993-1-2 2005), AISC 360(ANSI/AISC 360 2016) and AS 4100(Standards Australia 1998) and other 38 sets of experimental result (Aziz and Kodur 2016; Chen et al. 2006; Hu et al. 2009; Imran et al. 2018; Kankanamge and Mahendran 2011; Kirby and Preston 1988; Li et al. 2003; McCann et al. 2015; Neuenschwander et al. 2017; Ranawaka and Mahendran 2009; Singh and Singh 2019a; Torić et al. 2017; Yuan et al. 2016) on mild steel ($\sigma_{0.2,20}$ = 250-410 MPa) at elevated temperature (see Table 3.5). Unlike previous studies(Luecke et al. 2013), which have been focused only on hot rolled steel, the present database has different types of carbon steel, namely, hot rolled plates (HR) (Aziz and Kodur 2016; Chen et al. 2006; Hu et al. 2009; Kirby and Preston 1988; Li et

al. 2003; Neuenschwander et al. 2017; Torić et al. 2017) and coupons extracted from cold formed tubular members (CF-T) (Imran et al. 2018; McCann et al. 2015; Singh and Singh 2019a; Yuan et al. 2016) from very recent experimental studies. The comparison studies have not included the experimental results from cold formed sheets (Kankanamge and Mahendran 2011; Ranawaka and Mahendran 2009), since $\sigma_{0.2,T}/\sigma_{0.2,20}$ reduces drastically once it exceeds 200^{o}C.

It can be seen (see Figure 3.4). that there is about 20% increase in the yield strength when the temperature reaches 300^{o}C, but it quickly decreases as temperature rises. The ultimate strength (see Figure 3.5) follows a similar trend as that of the yield strength. Higher reduction in the elastic modulus (see Figure 3.6) can be observed when the temperature rises to 500^{o}C. The elastic modulus shows higher value when compared to in EC 3(EN 1993-1-2 2005) which also has been reported by several authors (Imran et al. 2018; McCann et al. 2015; Yuan et al. 2016) and has been found to be in good agreement. A sharp fall in the strength and the elastic modulus when the temperature proceeds from 500^{o}C to 600^{o}C, can be seen. This may be related to due to the phase transformation occurring from face-centred cubic lattice to body-centred cubic lattice. There is just 10% fall in strength and modulus before 500^{o}C, while it falls down by 80% and 70% in strength and elastic modulus when it reaches 600^{o}C.

The reduction factors for growth phase (see Table 3.6), that have been proposed using MAPE technique, have been compared with EC 3 (EN 1993-1-2 2005), AS 4100 (AS 4100 2016), AISC 360 (ANSI/AISC 360 2016), NIST (Luecke et al. 2013), Imran *et al.* (Imran et al. 2018) and Singh and Singh (Singh and Singh 2019a). The proposed $\sigma_{0.2,T}/\sigma_{0.2,20}$ (MAPE = 13.8%) have a lower value than EC 3 (MAPE = 24.7%) and AISC 360 (MAPE =27.7%) upto 500^{o}C, while it follows a similar trend as AS 4100 (MAPE = 28.7%) and NIST (MAPE =22.0%). From 500^{o}C to 700^{o}C, all the prediction (ANSI/AISC 360 2016; AS 4100 2016; EN 1993-1-2 2005; Luecke et al. 2013) give slightly higher $\sigma_{0.2,T}/\sigma_{0.2,20}$ than the proposed $\sigma_{0.2,T}/\sigma_{0.2,20}$. The proposed $\sigma_{u,T}/\sigma_{u,20}$ (MAPE = 12.2%) remains higher than the AISC 360(ANSI/AISC 360 2016) (MAPE = 28.9%) model. The proposed E_T/E_{20} (MAPE = 28.3%) closely matches with prediction provided by EC 3 (MAPE= 28.7%) and AISC 360 (MAPE = 29.7%). The prediction for E_T/E_{20} suggested by NIST (MAPE =138%) is highly unsafe, since the NIST prediction passes through the upper bound data points. The proposed reduction factors have the lowest %

error among other predictions (ANSI/AISC 360 2016; AS 4100 2016; EN 1993-1-2 2005; Imran et al. 2018; Luecke et al. 2013; Singh and Singh 2019a) (see Table no. 3.7). Hence, the proposed reduction factors at growth phase can be used by designers for mild steel at elevated temperature.

3.3.2 Cooling phase

As mentioned earlier, cooling phase mechanical properties are important parameters which allows assessment of the strength of the building which may not have already collapsed when it has reached the peak temperature. However, at some point when the building is cooling down there might be excessive plastic deformations, which induce additional stress in the members. In order to estimate the stress flow in the building during the cooling phase, the mechanical properties (see Table 3.8) have been evaluated.

In Figures 3.7 to 3.11, the reduction factors for specimens in certain desired temperature in the growth phase and those cooled down to upto that target temperature. There has been no experimental data available in the previous literature to estimate the mechanical properties in cooling phase. Hence, few of the tests are repeated to check the validity of the present test - two temperature paths namely 600-300 and 800-500 are repeated. While comparing the results for the ultimate tensile strength and elastic modulus, it has been observed that the standard deviation is less than 1%. The specimen is cooled to either of lower temperature - 200^{o}C, 300^{o}C, 400^{o}C, 500^{o}C or 600^{o}C. (see Figures 3.7 to3.112) after being heated up to a maximum temperature of 800^{o}C.

In Figure 3.12 to 3.15, the reduction factors are presented as a function of temperature for heating and cooling fire. For example, in Figure 3.12 the temperature path denotes the temperatures of growth phase which starts at 0^{o}C, traverses upto 500^{o}C and the cooling down to lower temperatures. In the growth phase, as the temperature increases from 500^{o}C (GT-20-500) to 600^{o}C (GT-20-600), there is a steep fall of yield strength (61%) and elastic modulus (63%). However, a relatively lower regain (36% for yield strength and 2% for elastic modulus) of the mechanical properties, has been observed in the during the cooling phase (from CT-800-600 to CT-800-500). It may be noteworthy to mention that the observed difference in the rate

of reduction and regain corresponding to growth and cooling phases are in contrast to the assumption of equal reduction and regain rates reported in literature (e.g., (Fischer et al. 2019; Jiang et al. 2015; Jiang and Li 2017; Lamont et al. 2004; Rackauskaite et al. 2017)).

The reduction factor for cooling phase has been proposed in Table 3.9. It may be noteworthy to mention that such cooling phase data presented in this paper, have not been made available in the public domain, to the best of the author's knowledge.

3.3.3 Post-fire phase

Yield strength ($\sigma_{0.2,T}$), ultimate strength ($\sigma_{u,T}$), yield strain ($\varepsilon_{0.2,T}$), strain at onset of hardening ($\varepsilon_{p,T}$) strain at rupture ($\varepsilon_{r,T}$) Elastic modulus (E_T) and reduction factors ($\sigma_{0.2,T}/\sigma_{0.2,20}$, $\sigma_{u,T}/\sigma_{u,20}$ or E_T/E_{20}) for the post-fire phase are provided in Table 3.10 & 3.11. These values are compared with the experimental results (see Figures 3.16 to 3.18) (Aziz and Kodur 2016; Gunalan and Mahendran 2014; Kesawan and Mahendran 2018; Lu et al. 2016; Smith et al. 1981) where post-fire material properties have been evaluated. The experimental dataset comprises of studies on HR (Aziz and Kodur 2016; Lu et al. 2016; Smith et al. 1981) and CF-T (Kesawan and Mahendran 2018; Lu et al. 2016; Singh and Singh 2019b). Some studies (Aziz and Kodur 2016; Lu et al. 2016) have adopted have two distinct cooling processes, namely air-cooling (indicated as AC) and water cooling (indicated as WC) while other studies (eg., (Gunalan and Mahendran 2014; Singh and Singh 2019b; Smith et al. 1981)) adopted only air cooling process.

In the present study, the reduction factor shows that yield strength (see Figure 3.16) and ultimate strength (see Figure 3.17) is steadily maintained as the temperature increases to 600^{o}C, while there is steady decrease in yield strength and ultimate strength when the temperature crosses 600^{o}C. Similar observations are found in literature (e.g. (Aziz and Kodur 2016; Kesawan and Mahendran 2018; Lu et al. 2016)). It has been observed that there is not much reduction in the elastic modulus (see Figure 3.18) which is comparable to other literature (e.g.(Aziz and Kodur 2016; Chen et al. 2019; Kesawan and Mahendran 2018; Lu et al. 2016)).

The reduction factors for post-fire phase have been proposed (see Table 3.11). Its goodness against various experimental studies has (Aziz and Kodur 2016; Kesawan and Mahendran

2018; Lu et al. 2016; Singh and Singh 2019b) been assessed using MAPE technique. The proposed $\sigma_{0.2,T}/\sigma_{0.2,20}$ (MAPE = 8.3%) and $\sigma_{u,T}/\sigma_{u,20}$ (MAPE = 5.0%) remain close to unity till 600°C and then drop by 29% and 12% respectively as the temperature reaches 1000°C. The proposed E_T/E_{20} (MAPE = 2.9%) remains close to unity for all the ranges of temperature, indicating that the elastic modulus is less affected due to heating and cooling cycle. The proposed design reduction factors provide the least MAPE compared to other reduction factors that are proposed by other authors (Aziz and Kodur 2016; Gunalan and Mahendran 2014; Kesawan and Mahendran 2018; Lu et al. 2016; Singh and Singh 2019b).

3.3.4 Chemical and microstructure analysis

The results of the microscopy are presented (see Figure 3.19) for various temperatures (20°C, 400°C, 600°C, 700°C, 800°C and 900°C). The chemical analysis shows that there is negligible difference in the chemical composition of the heat-treated samples. Similar observations are reported in previous literature (Huang and Young 2017),

At 20°C, it can be seen (see Figure 3.19) that E350 steel microstructure displays ferrite (α-iron) and pearlite microstructure represented by black (pearlite) and white (ferrite) patches (Callister and Rethwisch 2014). Upon heating, the grain size tends to increase at 400°C and then it decreases again at 600°C. A relative increase in grain size attributes to decrease in strength. Beyond 600-675°C, the ferrite – pearlite microstructure transforms to austenite (*γ-iron*) microstructure. Upon allowing it to be cooled very slowly, the austenite microstructure transforms to α-ferrite and iron carbide phase. It can be seen that for 700°C to 900°C, the grain boundary appeared to be coarser as the temperature increased. However, when the steel is not allowed to cool at a very slow rate once the phase transition is attained, γ-iron tends to transform into martensite. Martensite phase is attributed to a higher strength (Huang and Young 2017) than that of unheated ferrite-pearlite phase. It can be seen in the samples for 700°C to 900°C, that the martensitic phase represented by the dark patches dominates as the temperature increases. Hence, although there may be decrease in strength due to increased grain size, however, the strength reduction is nullified by formation of martensitic phase, which may add strength to the specimen.

3.4 Stress - strain relationship

In order to carry out advanced numerical investigation, appropriate material models have to be adopted. The complete domain of stress strain curves for mild steel at room temperature and elevated temperature have been represented using two material models. The stress strain curve at room temperature consists of a distinct yielding zone as seen for any typical hot rolled mild steel, while, the curve at elevated temperature comprises of a rounded curve at yielding without any distinct yielding plateau as it directly goes into strain hardening zone post yielding.

3.4.1 Stress strain model for room temperature and post-fire phase

The materials that are tested at room temperature and post heat treatment has distinct yield plateau. Mander model (Mander 1983) is widely used to model structural steel at room temperature that provided distinct yield plateau. Tao et. al. (Tao et al. 2012) modified this model to accurately fit the experimental data. In the present work, Tao et. al. model (Tao et al. 2012) has been adopted to fit into the experimental data, which has been presented (see Equation 3.2) below.

$$\varepsilon = \begin{cases} \dfrac{\sigma}{E_T} & 0 < \sigma \le \sigma_{0.2,T} \\ \varepsilon_{u,T} - \left(\dfrac{\sigma - \sigma_{u,T}}{\sigma_{u,T} - \sigma_{0.2,T}} \right)^r \left(\varepsilon_{u,T} - \varepsilon_{p,T} \right) & \sigma_{0.2,T} < \sigma \le \sigma_{u,T} \end{cases} \tag{3.2}$$

where E_T, $\sigma_{0.2,T}$ and $\sigma_{u,T}$ is the elastic modulus, 0.2% proof stress and ultimate stress respectively; $\varepsilon_{p,T}$ and $\varepsilon_{u,T}$ is the maximum yielding strain and ultimate strain respectively; $r = (\varepsilon_u - \varepsilon_p)/(q_T \times 0.2E_T(\sigma_{u,T} - \sigma_{0.2,T}))$ is the inverse of strain hardening parameter. q_T has been inserted in the strain hardening parameter for better fit of the values.

3.4.2 Stress strain model for growth and cooling phase

The Ramberg - Osgood model (Hill 1944; Ramberg and Osgood 1943) is widely used material model to define metal plasticity with rounded stress-strain curve. This model is extended by Mirambell and Real (Mirambell and Real 2000) who proposed modified Ramberg – Osgood

model – a two stage model to incorporate the behaviour at post yielding. Rasmussen (Rasmussen 2003) further simplified the two stage model and proposed strain-hardening parameter which ensures that the curve is extended upto the ultimate stress. Gardner and Nethercot (Gardner and Nethercot 2004) extended the Mirambell and Real model, using 1% proof stress value instead of ultimate stress. This is done due to two reasons: firstly, in ductile materials, the amount of change of strain value in the strain-hardening region is very slow as it approaches the ultimate stress and secondly, to able to incorporate the same model for compression in addition to tension, where necking phenomena is not observed. Gardner et. al. (Gardner et al. 2010) modified their previous work and proposed material model at elevated temperature which required minimum parameters from the experiments. In the present work, the material model (see Equation 3.3) at elevated temperature by Gardner et. al. (Gardner et al. 2010) has been adopted to fit the experimental curve.

$$\varepsilon = \begin{cases} \dfrac{\sigma}{E_T} + 0.002\left(\dfrac{\sigma}{\sigma_{0.2}}\right)^{n_T} & \text{for } \sigma \le \sigma_{0.2,T} \\ \dfrac{\sigma-\sigma_{0.2,T}}{E_{0.2,T}} + \left(0.02 - \varepsilon_{t0.2,T} - \dfrac{\sigma_{t2.0,T}-\sigma_{0.2,T}}{E_{0.2,T}}\right)\left(\dfrac{\sigma-\sigma_{0.2,T}}{\sigma_{t2.0,T}-\sigma_{0.2,T}}\right)^{m_T} & \text{for } \sigma_{0.2,T} \le \sigma < \sigma_u \end{cases} \tag{3.3}$$

where E_T, $\sigma_{0.2,T}$ and $\sigma_{t2.0,T}$ are properties measured at elevated temperature for elastic modulus, 0.2% proof stress and stress at 2% total strain respectively. $E_{0.2,T}$ is given by $E_{0.2,T} = E_T/(1+0.002nE_T/\sigma_{0.2,T})$. The co-efficients n_T and m_T are exponential values. The coefficients n_T and m_T are evaluated through an iterative process, such that the difference in area within the experimental curve and the predicted curve is minimum; also the difference between the ultimate strain for the experimental and predicted curves is minimum. Comparison for the above models against the experimental stress strain curve have been presented (see Figure 3.20). It can be observed, that there is good agreement between the fit and the experimental data.

3.5 Summary and conclusion

In this chapter investigation is carried out to estimate the mechanical properties, namely yield strength, ultimate strength and elastic modulus of mild steel E350 subjected to growth, cooling

and post-fire phases of heating and cooling fire with maximum temperature of 800^{o}C with special emphasis on the mechanical properties in cooling phase. Chemical analysis and microstructure study have also been conducted on unstressed post fire specimens. Based on the results, key conclusions are presented below;

1) Reduction factors ($\sigma_{0.2,T}/\sigma_{0.2,20}$, $\sigma_{u,T}/\sigma_{u,20}$ or E_T/E_{20}) have been proposed for growth, cooling and post-fire phases based on present study and previously reported experimental studies.
2) In comparison to the growth phase, the rate of regain of the yield strength and elastic modulus are found to be slower in the case of cooling phase. Additionally, in general, it has been seen that, the mechanical properties have been able to regain, for elevated temperatures not exceeding 600°C.
3) The microstructure study of the unstressed post-fire specimens shows large grain size when heated beyond 600^{o}C leading to fall of strength, however, there is less significant strength reduction owing to bainite formation.
4) Further, stress strain models corresponding to a) growth and cooling phases; and b) ambient temperature and post fire phase have been proposed.

The experimental investigation exhibits that the mechanical properties in cooling phase are found to be usually lower than that in the growth phase. Hence, appropriate mechanical properties for growth and cooling phases need to be incorporated for accurate and reliable response under real fire scenarios.

Tables

Table 3.1 Chemical Composition of E350

Sample ID	C	Si	Mn	P	S
RT-20-20	0.146	0.326	1.753	0.0043	0.001
IS 2062:2011	0.200	0.450	1.550	0.045	0.040

Table 3.2 Mechanical properties of E350

Sample ID	σ_y (MPa)	σ_u (MPa)	E_{20} (GPa)	$\varepsilon_{0.2}$ (%)	ε_p (%)	ε_u (%)	ε_r (%)
RT-20-20 (1)	429	544	211	0.43	1.9	9.6	19.2
RT-20-20 (2)	427	542	208	0.43	1.7	8.4	16.5
Average	428	543	210	0.43	1.8	9.0	17.8

Table 3.3 Chemical composition of E350 post-fire specimens

Sample ID	C	Si	Mn	P	S
PT-20-20	0.1685	0.0137	1.286	0.0045	0.0055
PT-400-20	0.1188	0.0143	0.786	0.005	0.0074
PT-500-20	0.1486	0.0195	1.294	0.0046	0.0066
PT-600-20	0.1513	0.0176	1.301	0.0046	0.0068
PT-700-20	0.0819	0.0166	0.787	0.0051	0.0075
PT-800-20	0.005	0.0143	0.788	0.005	0.0071
PT-900-20	0.1674	0.0163	1.251	0.0047	0.0083
PT-1000-20	0.1115	0.0109	0.778	0.0049	0.0054

Table 3.4 Mechanical Properties for E350 at growth phase

Sample ID	$\sigma_{0.2,T}$ (MPa)	$\sigma_{t2.0,T}$ (MPa)	$\sigma_{u,T}$ (MPa)	$\varepsilon_{0.2,T}$ %	$\varepsilon_{u,T}$ %	$\varepsilon_{r,T}$ %	E_T (GPa)	n_T	m_T	$\sigma_{0.2,T}/\sigma_{0.2,20}$	$\sigma_{u,T}/\sigma_{u,20}$	E_T/E_{20}
GT-20-200	392	425	488	0.39	13	23.0	201	8.0	2.0	0.91	0.90	0.96
GT-20-300	497	550	603	0.44	10.3	20.2	208	8.0	2.8	1.16	1.11	0.98
GT-20-400	426	461	500	0.41	13	25.4	205	9.9	2.3	0.99	0.92	0.97
GT-20-500	361	409	431	0.38	7.9	22.4	197	7.0	4.5	0.84	0.79	0.94
GT-20-600	99	115	118	0.29	2.5	35.8	77	9.5	2.9	0.23	0.22	0.37
GT-20-700	90	98	101	0.34	4.9	38.6	70	8.5	3.8	0.21	0.19	0.33
GT-20-800	51	53	55	0.41	3.3	56.5	24	9.0	1.8	0.12	0.10	0.12
GT-20-900	36	41	45	0.40	6.74	28.3	18	3.5	2.5	0.08	0.08	0.08

Table 3.5 List of experimental studies on mechanical properties of mild steel at elevated temperature

Source	Grade	Nominal σ0.2,20 (MPa)	Maximum temperature (oC)	No. of specimens *	Remark
(Kirby and Preston 1988)	Grade 43A, 50B	275, 345	900	18	HR
(Li et al. 2003)	16Mn	345	700	7	HR
(Neuenschwander et al. 2017)	S355	355	1000	20	CF-T
(Chen et al. 2006)	XLERPLATE 350	350	900	9	HR
(Hu et al. 2009)	ASTM A992	345	900	18	HR
(McCann et al. 2015)	S355	355	800	24	CF-T
(Yuan et al. 2016)	Q345	345	600	12	CF-T
(Aziz and Kodur 2016)	ASTM A572 Grade 50	345	800	8	HR
(Outinen et al. 2001)	S355J2+N, S355J2+AR	355	900	34	HR
(Torić et al. 2017)	S275JR	275	600	6	HR
(Imran et al. 2018)	Grade 350	350	800	32	CF-T
(Singh and Singh 2019a)	YSt-310	310	800	24	CF-T

* The number of specimens indicates to the number of test data taken from the experiment for comparison in the present work.

Table 3.6 Proposed reduction factors at growth phase

Sample ID	$\sigma_{0.2,T}/\sigma_{0.2,20}$	$\sigma_{u,T}/\sigma_{u,20}$	E_T/E_{20}
GT-20-20	1.00	1.00	1.00
GT-20-200	0.92	0.99	0.93
GT-20-300	0.89	0.98	0.84
GT-20-400	0.79	0.88	0.79
GT-20-500	0.62	0.60	0.61
GT-20-600	0.39	0.34	0.31
GT-20-700	0.18	0.15	0.13
GT-20-800	0.08	0.08	0.09
GT-20-900	0.07	0.07	0.06

Table 3.7 Comparison of various prediction with existing experimental data for growth phase

	$\sigma_{0.2,T}/\sigma_{0.2,20}$	$\sigma_{u,T}/\sigma_{u,20}$	E_T/E_{20}
Present study	13.8	12.2	28.3
EC3	24.7	--	28.7
AS4100	28.7	--	43.8
AISC360	27.7	28.9	29.7
NIST	22.0	--	138.0
Imran et al.	16.7	19.3	30.7
Singh & Singh	19.4	16.5	--
N	183	149	183

Table 3.8 Mechanical Properties for E350 at cooling phase

Sample ID	$\sigma_{0.2,T}$ (MPa)	$\sigma_{t2.0,T}$ (MPa)	$\sigma_{u,T}$ (MPa)	$\varepsilon_{0.2,T}$ %	$\varepsilon_{u,T}$ %	$\varepsilon_{r,T}$ %	E_T (GPa)	n_T	m_T	$\sigma_{0.2,T}/\sigma_{0.2,20}$	$\sigma_{u,T}/\sigma_{u,20}$	E_T/E_{20}
CT-400-200	465	510	548	0.42	6.7	15.1	212	8.0	2.3	1.08	1.01	1.01
CT-500-200	399	422	492	0.42	14.7	27.6	178	8.0	1.6	0.93	0.91	0.84
CT-600-200	433	499	560	0.49	14.7	16.7	148	6.5	2.5	1.01	1.03	0.70
CT-700-200	350	425	488	0.45	9.5	17.6	141	6.0	3.2	0.81	0.90	0.67
CT-800-200	351	390	446	0.35	9.6	17.7	229	5.0	2.0	0.82	0.82	1.09
CT-500-300	409	447	503	0.46	9.29	17.5	191	6.0	2.0	0.95	0.93	0.91
CT-600-300 (1)	397	423	502	0.50	11.4	20.2	157	9.9	1.5	0.93	0.92	0.74
CT-600-300 (2)	402	425	505	0.49	13.1	22.8	161	9.9	1.5	0.94	0.93	0.76
CT-700-300	409	433	489	0.47	15.3	22.5	177	9.9	2.0	0.95	0.90	0.84
CT-800-300	320	387	467	0.41	12.9	23.1	153	8.0	2.9	0.75	0.86	0.73
CT-600-400	380	415	465	0.45	9.9	23.0	155	3.5	2.1	0.89	0.85	0.73
CT-700-400	372	386	484	0.47	14.6	21.9	136	9.9	1.1	0.87	0.89	0.65
CT-800-400	343	437	532	0.42	12.7	24.6	153	4.5	3.2	0.80	0.98	0.73
CT-700-500	269	341	360	0.36	5.7	20.0	164	3.5	5.5	0.63	0.66	0.78
CT-800-500 (1)	230	316	358	0.38	9.0	27.5	131	1.5	4.5	0.54	0.66	0.62
CT-800-500 (2)	274	319	363	0.43	9.3	28.4	121	5.0	2.7	0.64	0.67	0.57
CT-800-600	122	148	153	0.30	5.3	31.4	117	9.9	8.0	0.28	0.28	0.55

Table 3.9 Proposed reduction factor for cooling phase

Sample ID	$\sigma_{0.2,T}/\sigma_{0.2,20}$	$\sigma_{u,T}/\sigma_{u,20}$	E_T/E_{20}
CT-500-300	0.92	0.90	0.84
CT-500-200	0.93	0.90	0.84
CT-600-400	0.89	0.85	0.70
CT-600-300	0.93	0.93	0.70
CT-600-200	0.97	0.98	0.70
CT-700-500	0.63	0.66	0.65
CT-700-400	0.80	0.86	0.65
CT-700-300	0.80	0.87	0.88
CT-700-200	0.81	0.89	0.89
CT-800-600	0.28	0.28	0.55
CT-800-500	0.54	0.66	0.62
CT-800-400	0.71	0.82	0.73
CT-800-300	0.72	0.82	0.73
CT-800-200	0.73	0.82	1.00

Table 3.10 Mechanical Properties for E350 at post-fire phase

Sample ID	$\sigma_{0.2,T}$ (MPa)	$\sigma_{u,T}$ (MPa)	E_T (GPa)	$\varepsilon_{0.2,T}$ (%)	$\varepsilon_{p,T}$ (%)	$\varepsilon_{u,T}$ (%)	$\varepsilon_{r,T}$ (%)	q_T	$\sigma_{0.2,T}/\sigma_{0.2,20}$	$\sigma_{u,T}/\sigma_{u,20}$	E_T/E_{20}
PT-200-20	414	532	196	0.32	2.02	12.54	21.86	1	0.96	0.98	0.93
PT-300-20	428	537	196	0.32	2.02	11.46	21.65	1	1.00	0.99	0.93
PT-400-20	454	568	234	0.39	1.38	7.17	14.22	1	1.06	1.04	1.11
PT-500-20	435	531	191	0.46	2.76	10.23	19.65	1	1.01	0.98	0.91
PT-600-20	444	537	189	0.46	3.18	10.66	18.29	1	1.03	0.99	0.90
PT-700-20	400	489	188	0.44	2.94	10.91	20.86	1	0.93	0.90	0.89
PT-800-20	341	450	212	0.39	3.26	14.89	28.83	0.7	0.79	0.83	1.00
PT-900-20	263	397	216	0.35	2.30	12.46	22.02	0.7	0.61	0.73	1.02
PT-1000-20	253	421	169	0.40	1.84	12.07	21.21	0.7	0.59	0.77	0.80

Table 3.11 Proposed reduction factor for post-fire

Sample ID	$\sigma_{0.2,T}/\sigma_{0.2,20}$	$\sigma_{u,T}/\sigma_{u,20}$	E_T/E_{20}
PT-200-20	1.00	1.00	1.00
PT-300-20	1.00	1.00	0.97
PT-400-20	1.00	1.00	1.00
PT-500-20	0.96	0.98	0.99
PT-600-20	0.97	0.98	0.99
PT-700-20	0.84	0.90	0.99
PT-800-20	0.74	0.90	1.00
PT-900-20	0.83	0.92	0.96
PT-1000-20	0.71	0.88	0.93

Table 3.12 Comparison of various prediction with existing experimental data for post fire phase

	$\sigma_{0.2,T}/\sigma_{0.2,20}$	$\sigma_{u,T}/\sigma_{u,20}$	E_T/E_{20}
Proposed model	8.3	5.0	2.9
Lu model (AC)	11.0	5.9	3.0
Lu model (WC)	11.9	7.3	3.5
Aziz model (AC)	14.3	10.7	--
Aziz model (WC)	9.9	6.1	--
Kesawan model	26.4	23.3	17.4
Singh Model	26.7	20.8	21.8
N	151	151	102

Figures

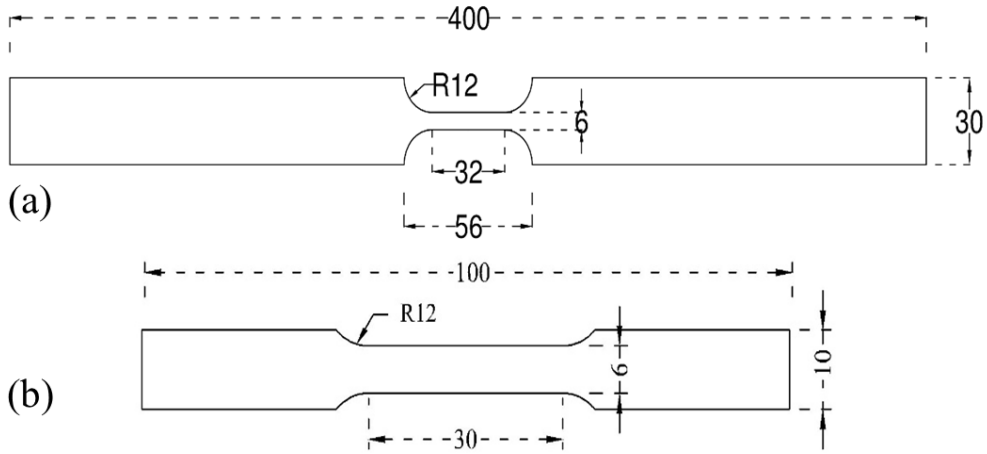

Figure 3-1 Tensile Coupon for (a) growth phase, cooling phase and (b) room temperature and post-fire phase (dimension in millimetres)

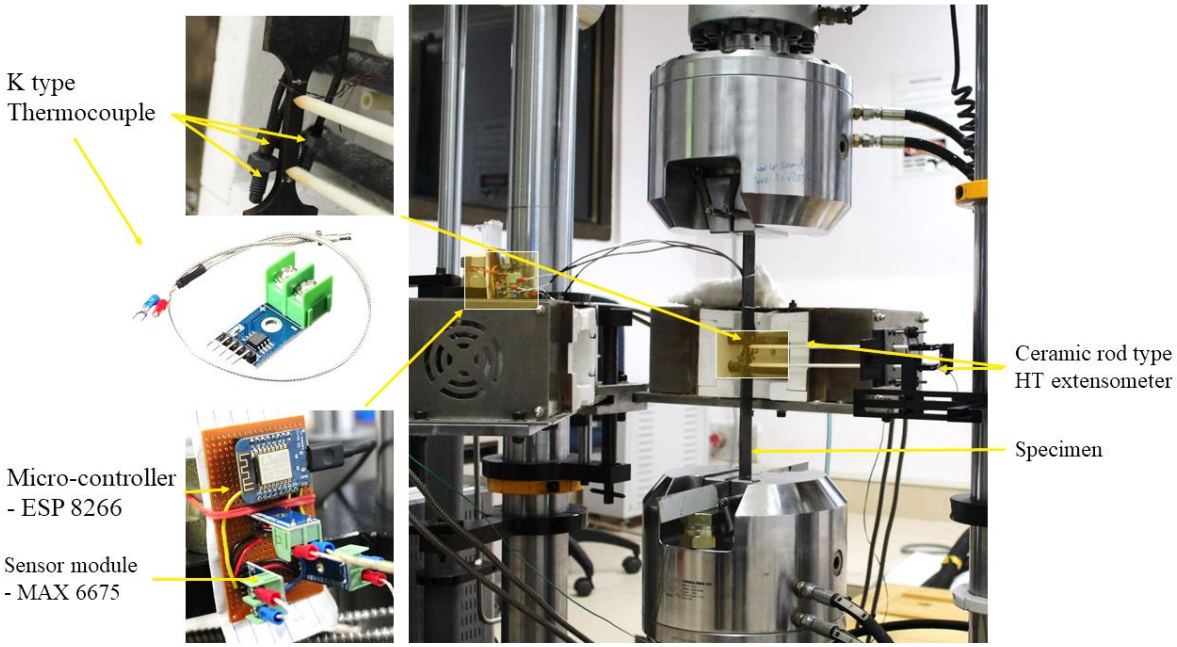

Figure 3-2 Testing Setup. 250kN UTM

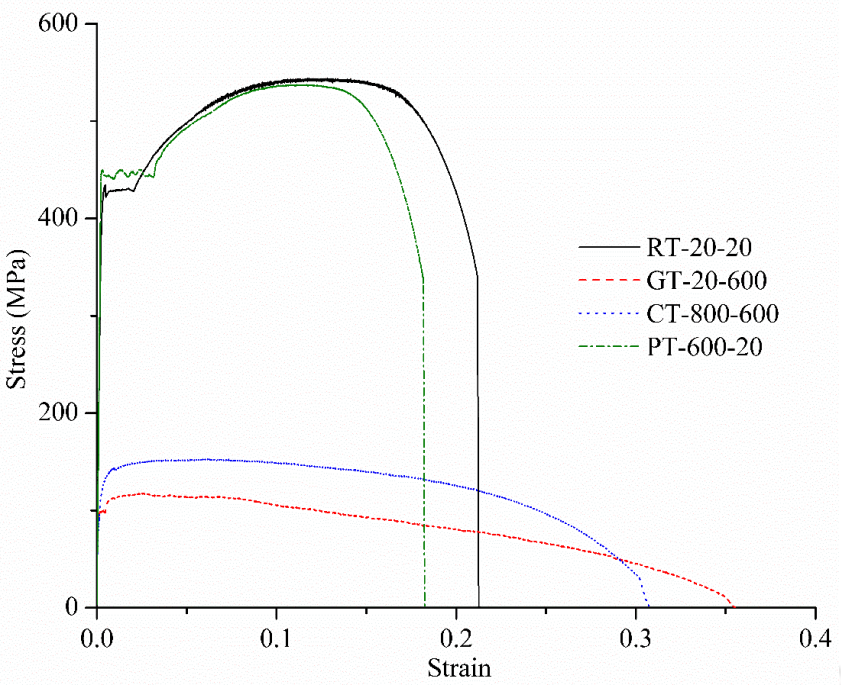

Figure 3-3 Typical Stress strain relationship from the experiment

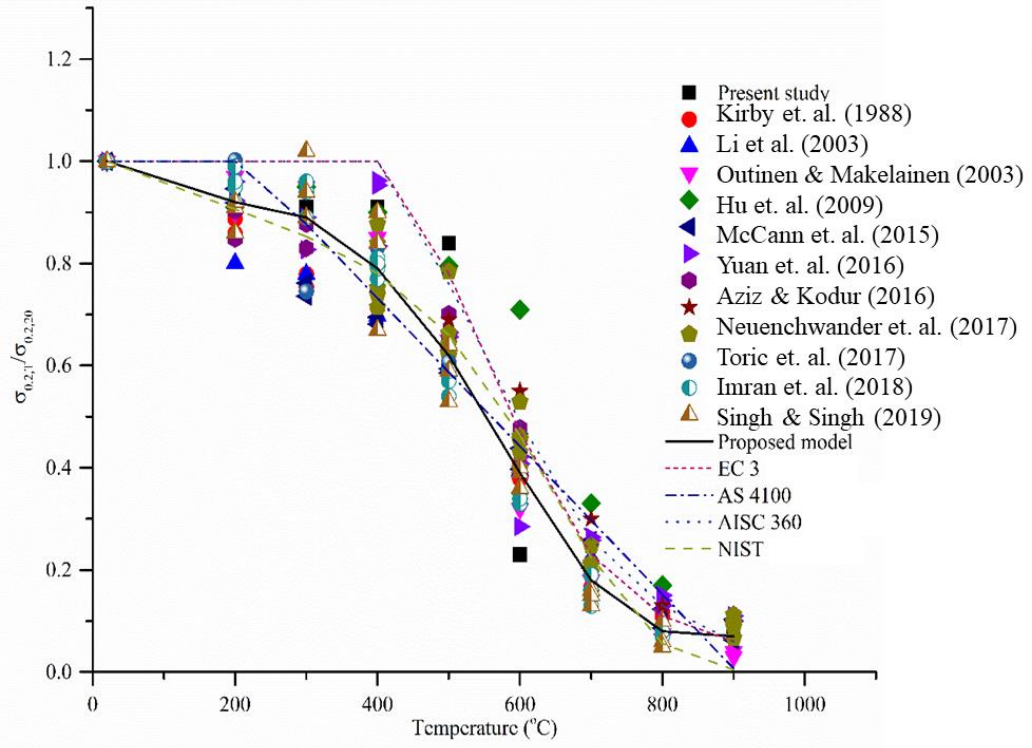

Figure 3-4 Yield strength reduction factor for present study and proposed curve

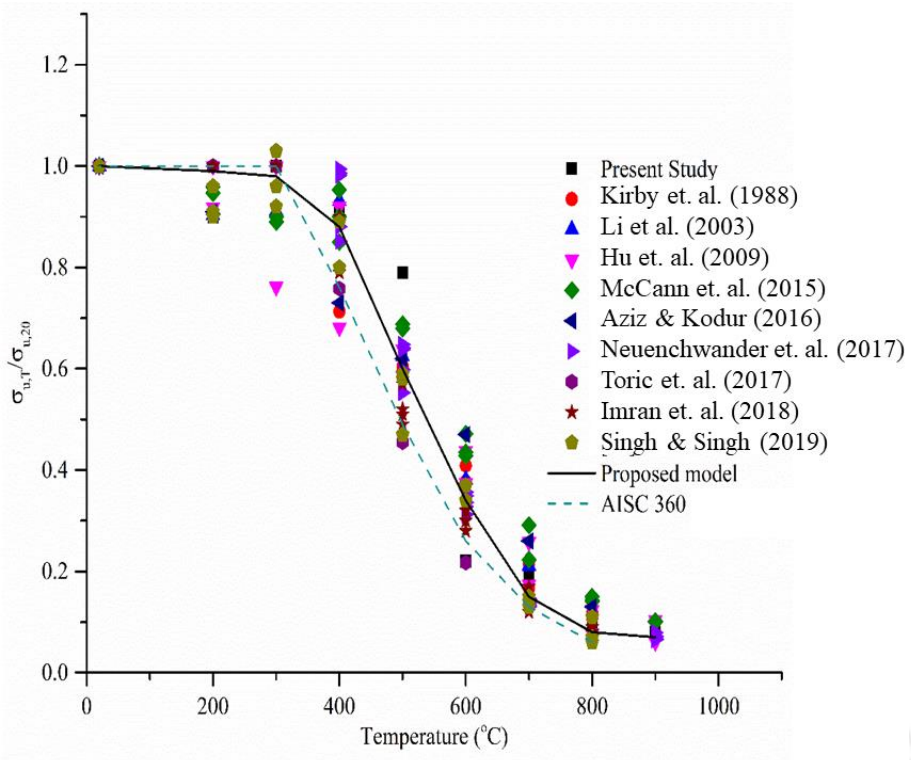

Figure 3-5 Ultimate strength reduction factor for present study and proposed curve

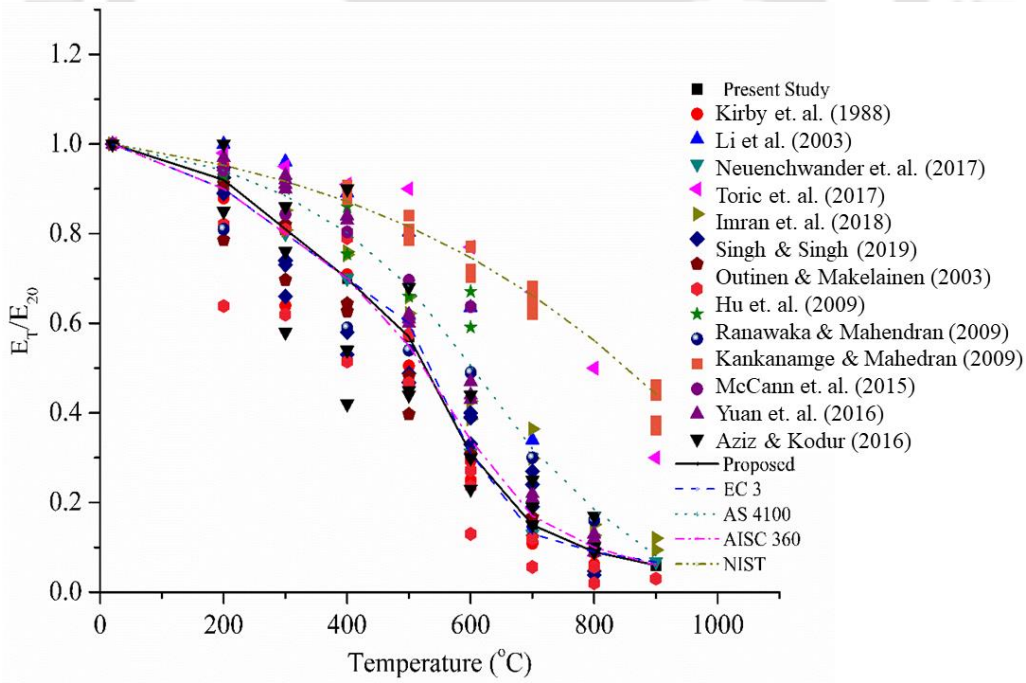

Figure 3-6 Elastic modulus reduction factor for present study and proposed curve

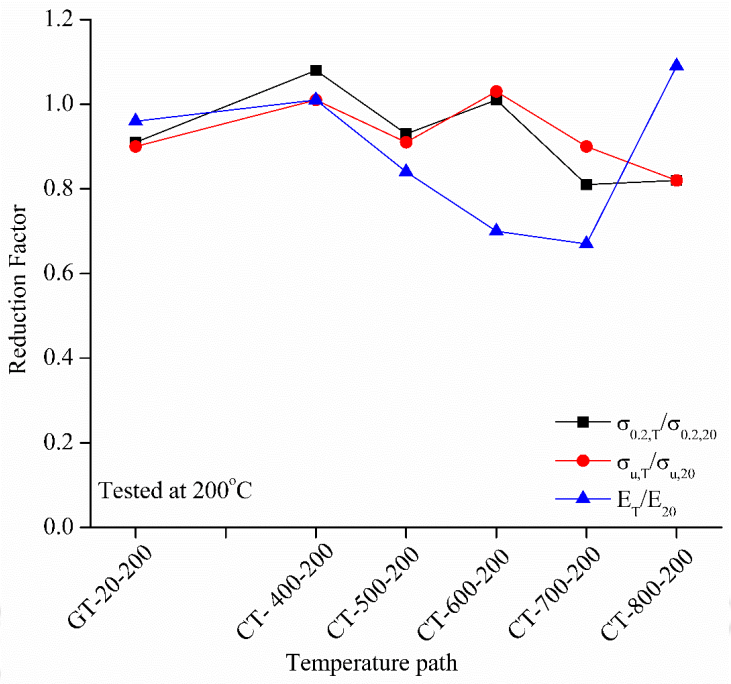

Figure 3-7 Comparison of reduction factor at growth phase and cooling phase where the specimen is tested at 200°C

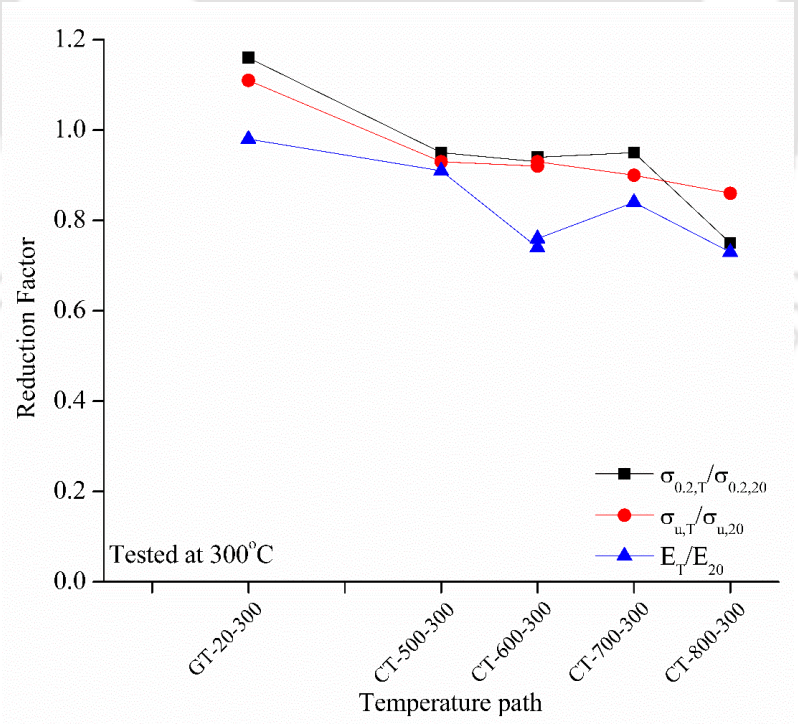

Figure 3-8 Comparison of reduction factor at growth phase and cooling phase where the specimen is tested at 300°C

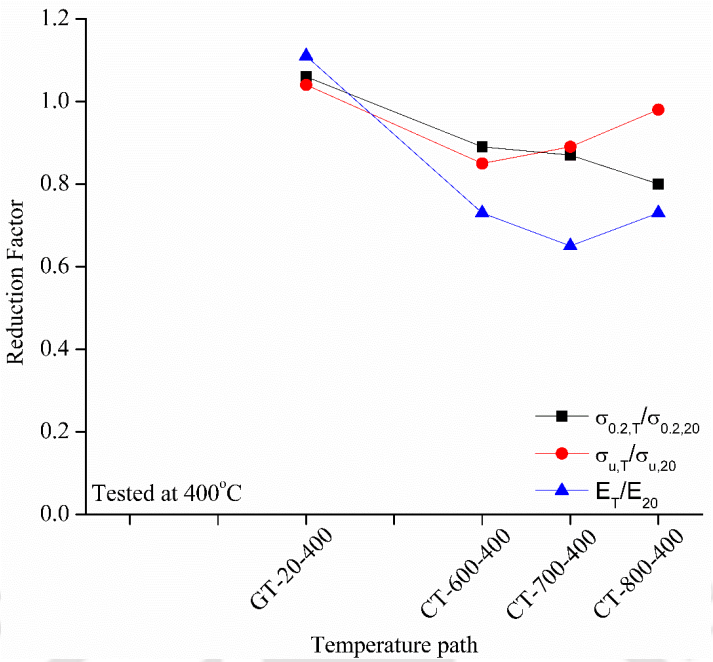

Figure 3-9 Comparison of reduction factor at growth phase and cooling phase where the specimen is tested at 400°C

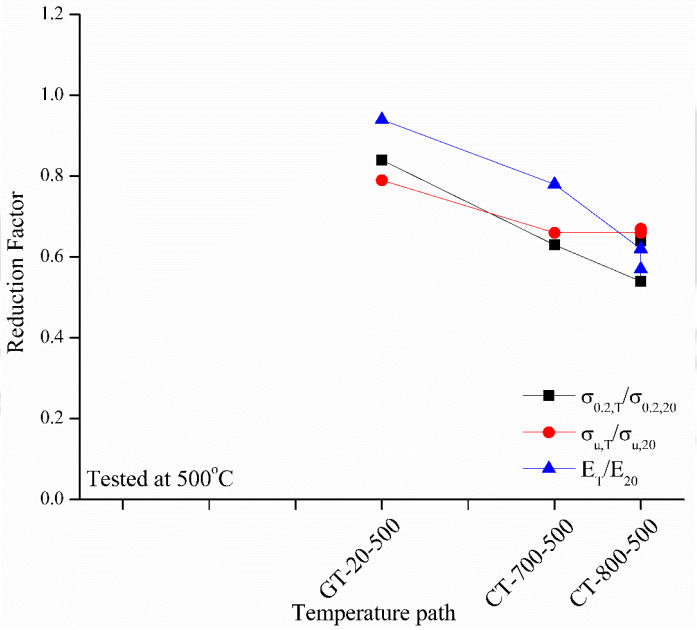

Figure 3-10 Comparison of reduction factor at growth phase and cooling phase where the specimen is tested at 500°C

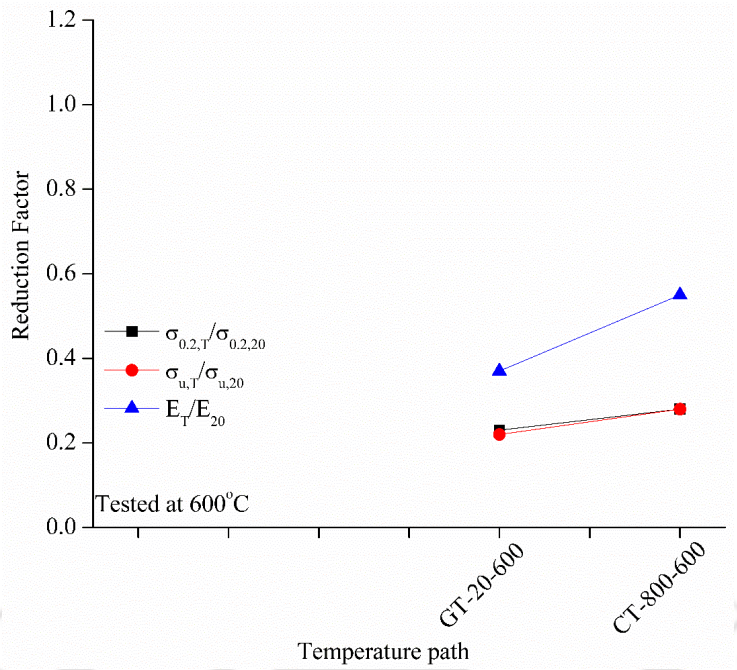

Figure 3-11 Comparison of reduction factor at growth phase and cooling phase where the specimen is tested at 600ºC

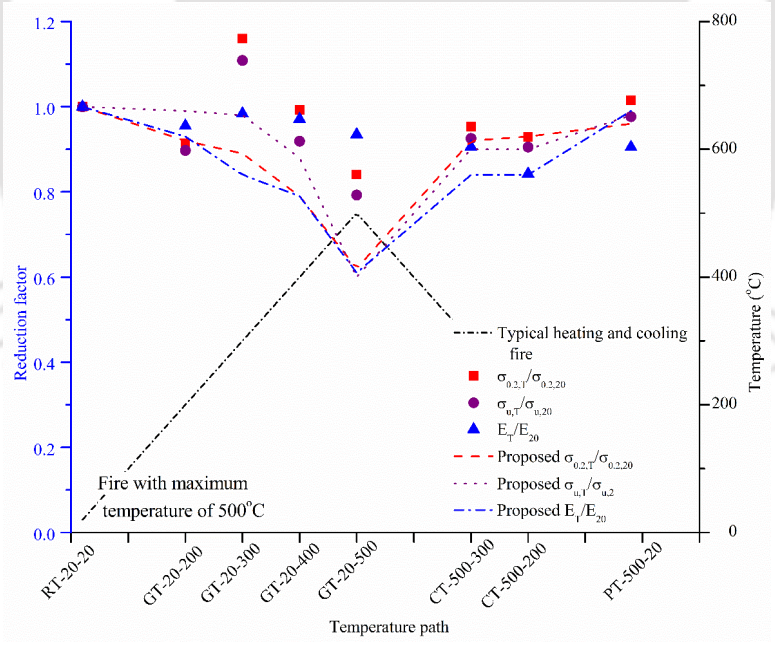

Figure 3-12 Comparison of reduction factor for a typical heating and cooling fire with maximum temperature of 500ºC

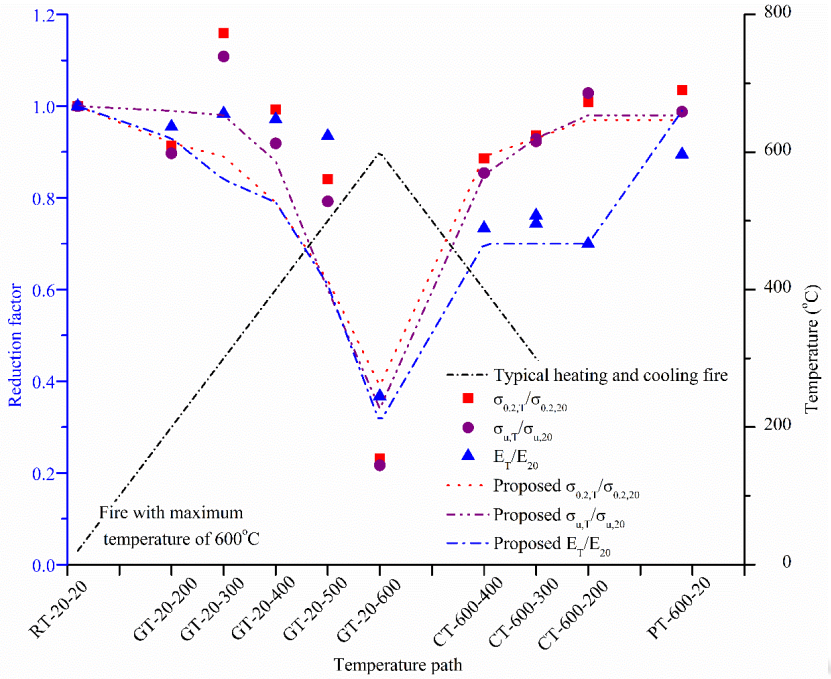

Figure 3-13 Comparison of reduction factor for a typical heating and cooling fire with maximum temperature of 600°C

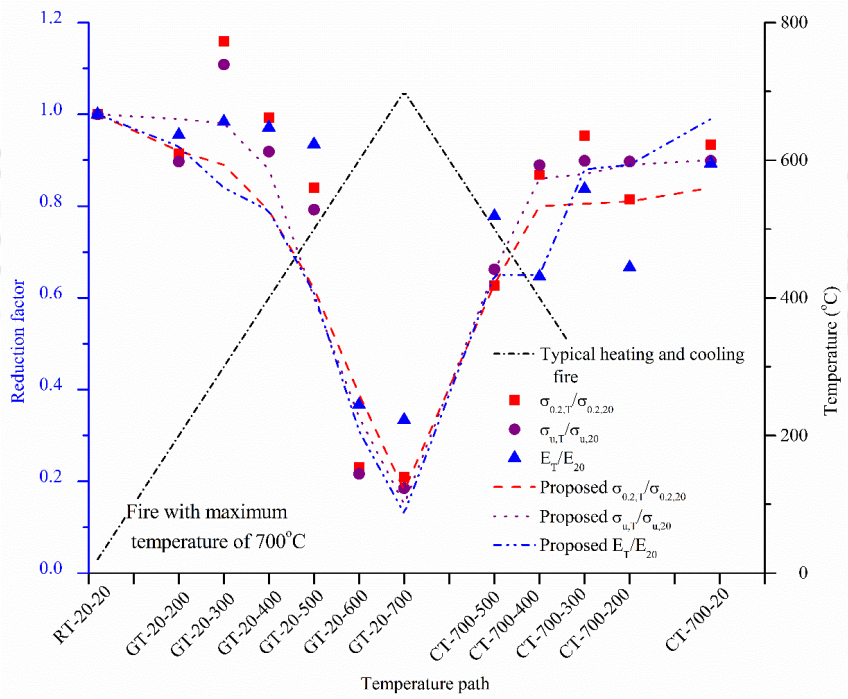

Figure 3-14 Comparison of reduction factor for a typical heating and cooling fire with maximum temperature of 700°C

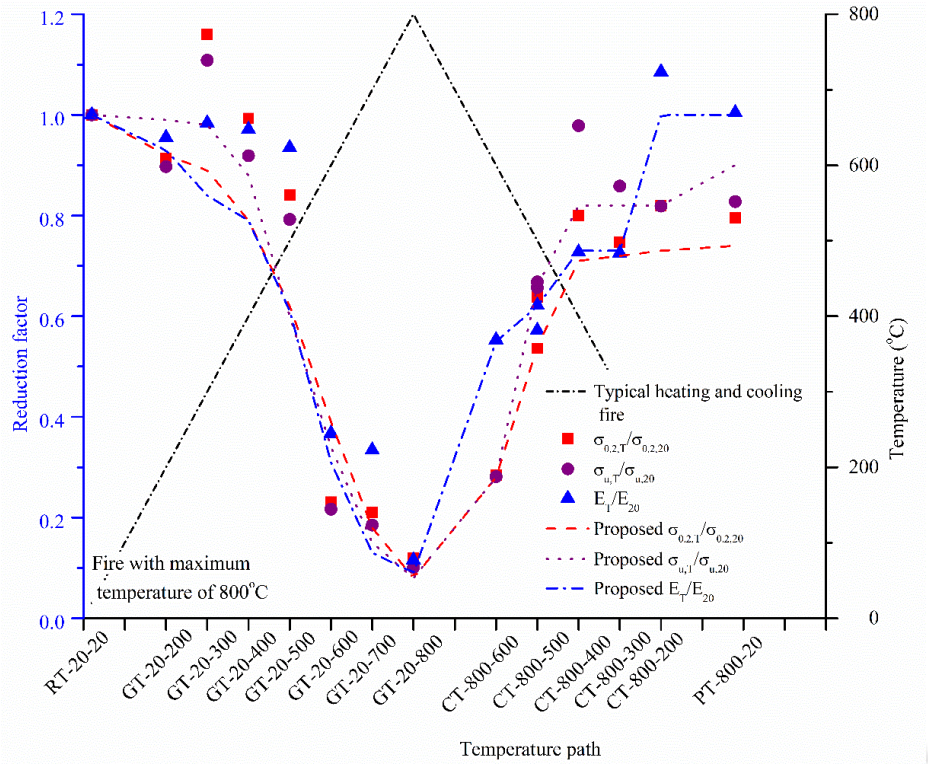

Figure 3-15 Comparison of reduction factor for a typical heating and cooling fire with maximum temperature of 800ºC

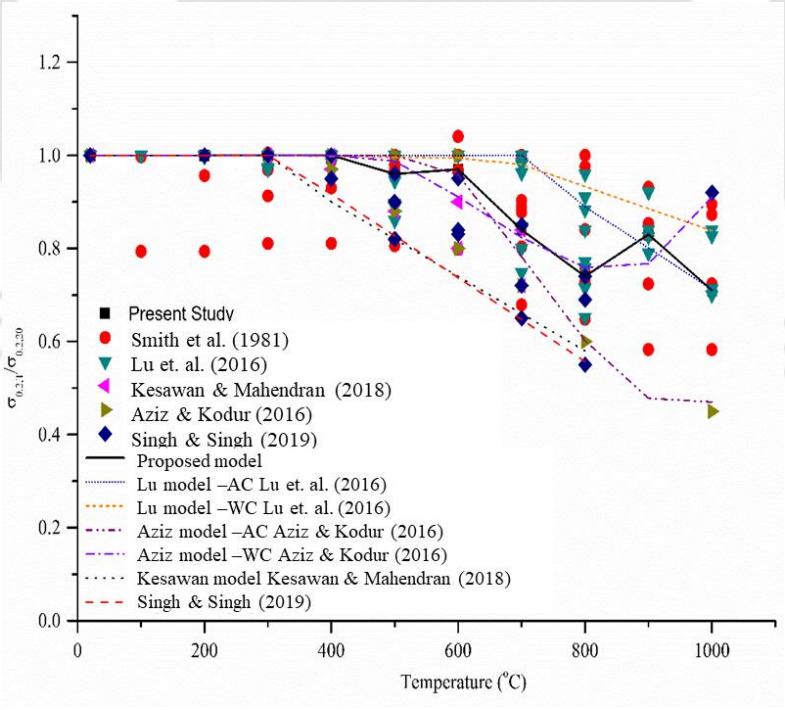

Figure 3-16 Yield strength reduction factor for post-fire specimen

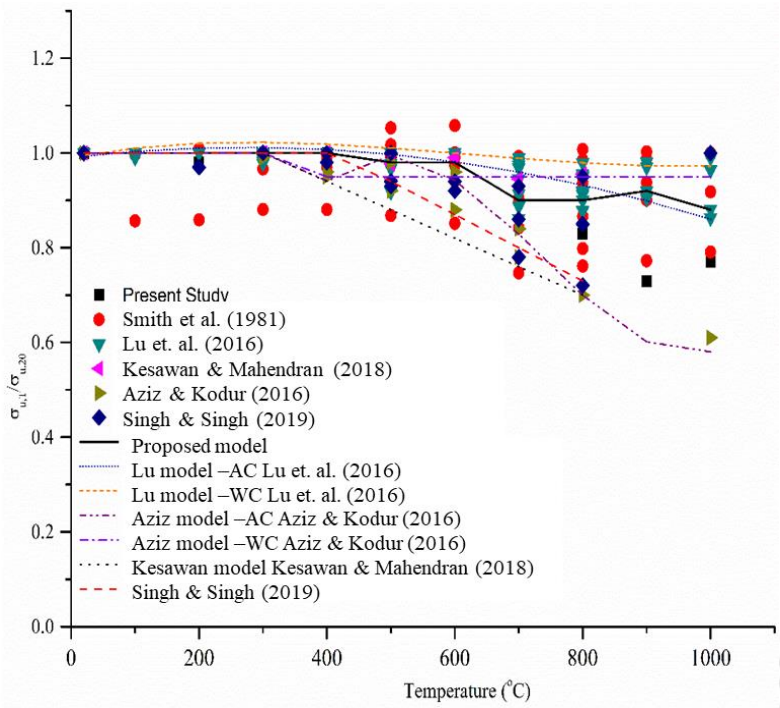

Figure 3-17 Ultimate strength reduction factor for post-fire specimen

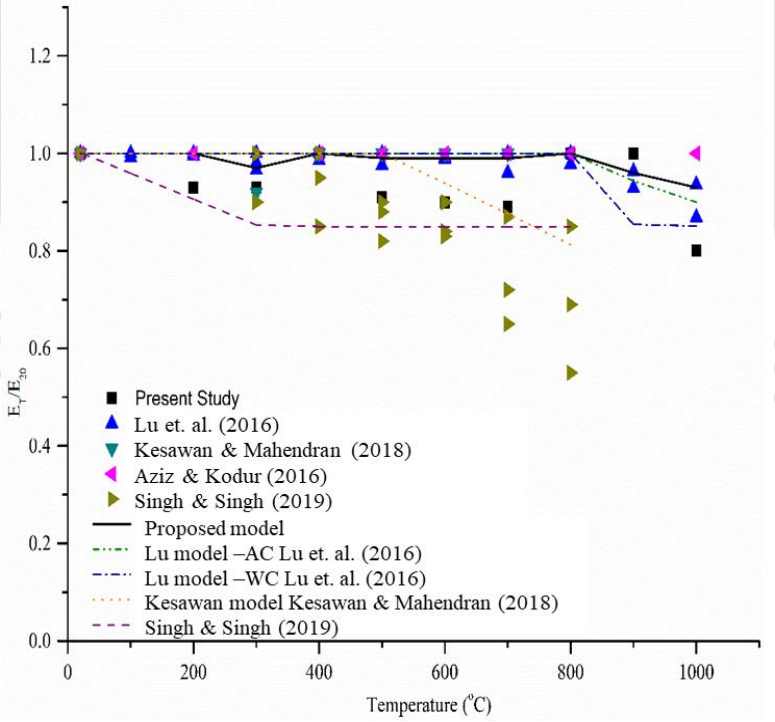

Figure 3-18 Elastic modulus reduction factor for post-fire specimen

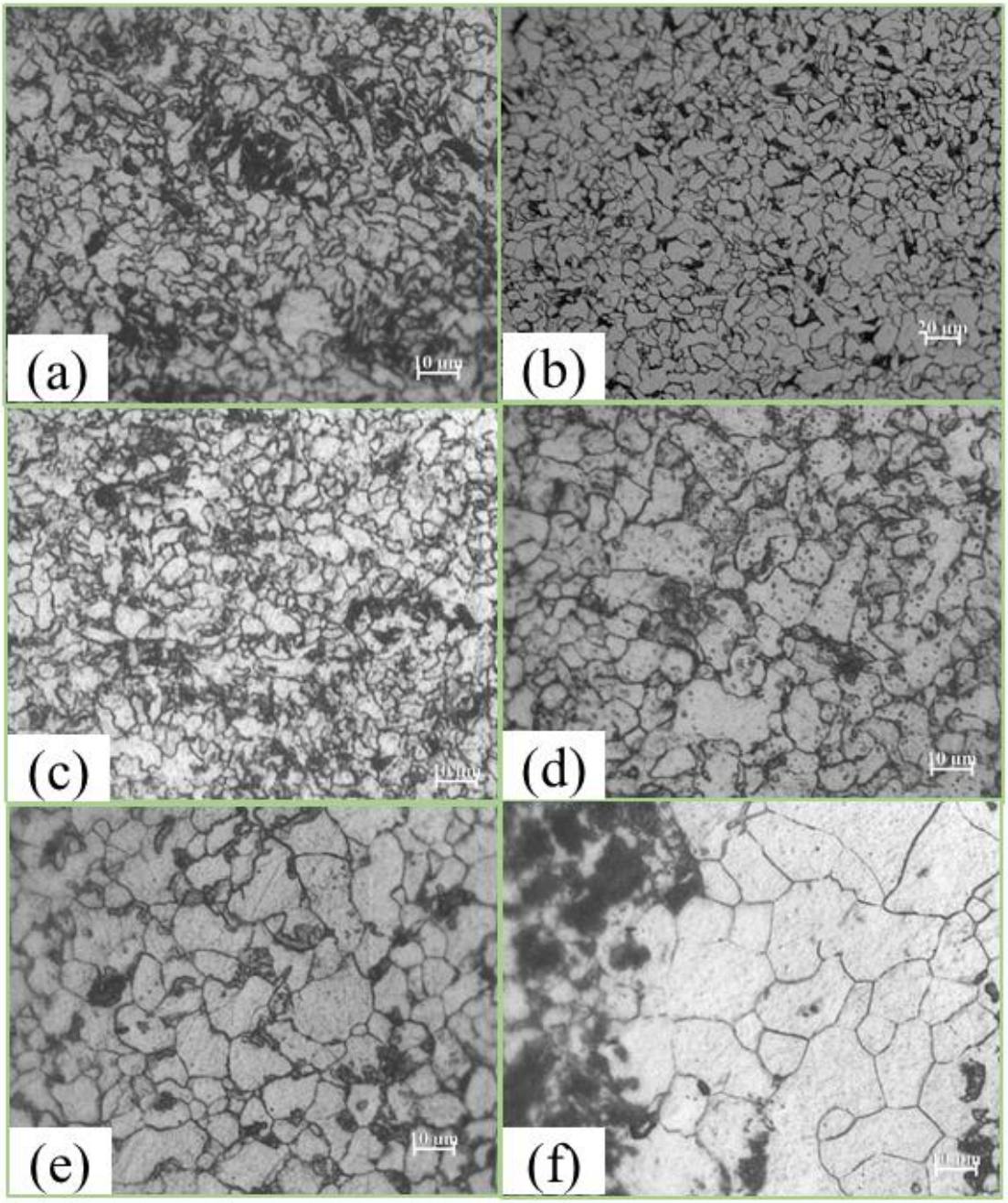

Figure 3-19 Micrographs of (a) unheated specimens and post-fire specimens heated upto (b) 400°C, (c) 600°C, (d) 700°C, (e) 800°C, (f) 900°C

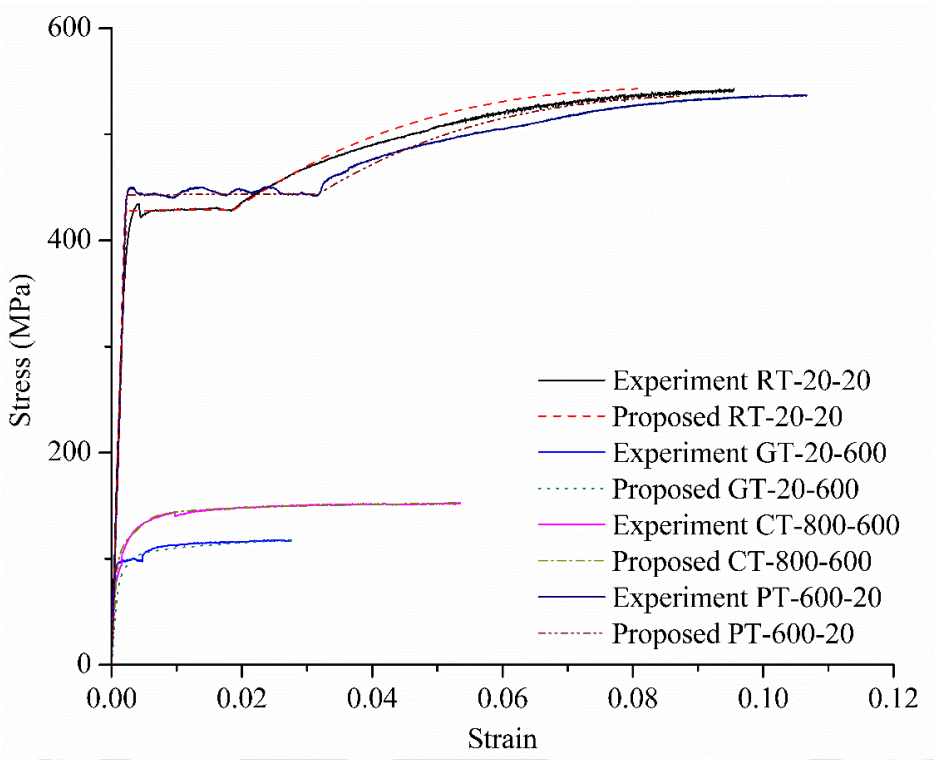

Figure 3-20 Comparison of experimental and proposed stress strain curves

CHAPTER 4: TENSILE AND SHEAR STRENGTH OF 10.9 GRADE BOLT IN HEATING AND COOLING FIRE

4.1 Background

In literature, growth phase studies have been reported for 8.8 (Hanus et al. 2011; Kirby 1995; Kodur et al. 2012) and 10.9 (Fan et al. 2013; Kodur et al. 2012; Lange and González 2012) Grade bolts. To the best of authors' knowledge, only Hanus et. al. (Hanus et al. 2011) has reported an experimental study on the tensile and shear strength of HSS bolt (8.8 Grade) in cooling phase. Further, it may be noted that experimental studies on 10.9 Grade bolt during cooling phase has not been reported in the literature. Hence, an attempt has been made in this chapter to experimentally assess both the tensile and shear strength of 10.9 Grade bolt in heating and cooling phases. The results of the tests are presented in the form of reduction factor in growth and cooling phases. Further, comparisons are also made against previous literature (Fan et al. 2013; Kodur et al. 2012; Lange and González 2012; Peixoto et al. 2017; Wang et al. 2005; Yang et al. 2011) and codal provisions (e.g. -(ANSI/AISC 360 2016; BSI 1990; EN 1993-1-2 2005)). Based on experimental data from the literature and current study, new reduction factors are proposed.

4.2 Experimental procedure

4.2.1 Test procedure

Special loading set-ups are designed and fabricated at IIT Guwahati to estimate the tensile and shear strength of the 10.9 grade bolt at elevated temperature (see Figure 4.1). These fixtures are attached to the well calibrated 250 kN displacement controlled universal testing machine (UTM)/loading frame (see Figure 4.1) available at Central Institute Facility (CIF, IITG). Heat is applied to specimen through an electric furnace attached to the UTM that is capable to heat upto 1400^{o}C with a heating rate of 10^{o}C/min.

4.2.2 Test fixture

The tensile and shear testing set-up is made from an ultra-high strength EN24 steel. The tolerance and dimensions for the tensile testing set-up satisfies the guidelines provided in ISO 898-1 (ISO 898-1 2009). Each of the tensile and shear testing set-up is composed of two fixtures made out from circular shaft. On one end, it has threaded hole for connecting it to the loading frame/ UTM. At the other end of the tensile fixture, slots are provided such that the bolt head and the nut which is fixed into the bolt can be slided inside these slots. As the initial preload is applied, the fixtures move away from each other, thereby, the bolt head and nut can no longer slide outward due to tension. Single shear test is carried out in the shear set-up. The circular shaft is longitudinally cut into half at other end for the shear-fixture. Bolt hole is drilled into that flat half. After the shear-fixture is fixed into the loading frame, bolt hole is aligned and the bolt is inserted and the nut is screwed and tightened.

4.2.3 Specimens

10.9 grade high strength steel bolts (make: TVS India; complying to DIN 931 standard) are sourced from local market. M10 partially threaded (nominal diameter = 10mm) and M8 full - threaded specimens (nominal diameter = 8mm) are considered for tensile and shear tests respectively (see Figure 1). Usually, the minimum diameter of bolt used in construction industry is higher than M10 bolt (minimum M12 in India(IS 800 2007), ½ inch in US(ANSI/AISC 360 2016)). However, M10 and M8 bolts are considered in this study for

tensile and shear tests respectively due to the limitation of current experimental set-up and it is expected that the general behavior will be similar for even higher diameter bolt since similar manufacturing procedure is applied (except for the expected increase in load capacities for higher bolt). It may be noted that the very limited data is available in the literature for diameter ≤ M12 and the present experimental results are likely to contribute to dataset of smaller diameter bolts.

The specimens are identified using sample identifier (Sample-ID). Sample ID for a tensile tests (T) for a specimen at 800^{o}C in growth phase (GT) is represented as T-GT-20-800. Here, the first letter T denotes tensile state of loading, the next two letters - GT denote growth phase temperature, the next number -20 denotes initial temperature and the last number denotes the temperature (target temperature) when the specimen is loaded and tested till failure. Similarly, other sample IDs are provided for tensile (eg. room temperature: T-RT-20-20; cooling phase: T-CT-800-400, in here 800 is the peak temperature - 800^{o}C upto which the specimen is heated and tested at 400^{o}C at cooling phase; post fire phase: T-PT-700-20) and shear (eg. room temperature: S-RT-20-20; growth phase: S-GT-20-700; cooling phase: S-CT-600-300; post-fire phase: S-PT-600-20) tests.

A total of 44 specimens are tested. For tensile tests, 3, 5 (temperature: 400^{o}C, 500^{o}C, 600^{o}C, 700^{o}C and 800^{o}C), 9 and 3 specimens are tested for RT, GT, CT and PT respectively. While for the shear tests 23 specimens are tested (RT: 5 specimens, GT: 5 samples, CT: 9 specimens and PT: 4 specimens). From the previous studies (like in (Kodur et al. 2012)), it has been seen that only 20-30% drop in strength is observed below 400^{o}C (Kodur et al. 2017), hence no test is carried out for temperature lower than 400^{o}C in growth phase. Above 800^{o}C, steel loses around 92-94% of its strength (e.g. (Singh and Singh 2019a)), hence tests are not carried out for temperature above 800^{o}C. Since, steel loses 50% of its strength beyond 550^{o}C, hence the strength related to peak temperature – 800^{o}C, 700^{o}C and 600^{o}C becomes more critical. Hence, CT and PT tests are executed for peak temperature – 800^{o}C, 700^{o}C and 600^{o}C.

The diameters of the shaft and the threaded region for all the M10 bolts are measured using digital Vernier caliper and found to be ~9.81mm and ~8.71 mm respectively. The length of the bolt is measured as 140mm for tensile test. While for the shear tests, the shaft and threaded

portion diameters for all the M8 bolt are ~7.79 mm and ~6.82 mm respectively. The length of the M8 bolt is measured as 60mm.

4.2.4 Heating Method

In steady state testing method, the specimen is first heated to the target temperature and then mechanically loaded at that temperature till the specimen fails. Since, it desirable to obtain peak strength at any temperature, hence, steady state testing over transient state testing method has been adopted in this study for the heating and loading procedure.

For all the tests, after the specimen is placed in testing set-up, a small preload of 1kN is applied to the specimen, before initiating the actual loading procedure in order to nullify the initial noise in the data which can arise due to slippage within the testing fixture. The temperature in the electric furnace can be changed through a temperature controller module. This module displays the temperature inside the furnace through in-built thermocouples which are placed behind the tungsten heating rods. In GT and CT tests, load controlled mode is adopted during heating of the specimen. By enabling the load-controlled mode, the specimen is allowed to expand during heating without any additional stress. The specimen is heated at 10^{o}C/ min following the works of Gardner (McCann et al. 2015) and Ben (Li and Young 2017). Once, the target temperature is reached, the specimen is soaked in that temperature for 30 minutes (ASTM E21 2017) so that the thermal gradient within the specimen is minimized, then the loading protocol is changed to displacement-controlled mode (as no more thermal expansion is expected). For the cooling phase, after the specimen is heated at 10^{o}C/min, till the peak temperature, the specimen is soaked for 30 mins and then allowed to cool naturally inside the furnace till the target temperature is reached. The specimen is then soaked for another 30 mins before loading. In order to save time, the post fire specimens are heated in a separate muffle furnace which can accommodate more than one specimen at a time. The post fire specimens are heated at 10^{o}C/min which is then allowed to soak for 30 mins before letting it to cool naturally in the furnace. The post fire specimens are taken out of the muffle furnace and loaded in the UTM. No additional thermocouple is placed inside the furnace, since, it is found in the authors' previous work (refer to Chapter 3) that the additional 3 K-type thermocouples and the in-built thermocouple did not show significant variation. This also indicates that 30 minutes of

soak time is adequate to minimize the thermal variation within the furnace and the built-in thermocouples show representative temperature.

4.2.5 Loading method

All the specimens are loaded through displacement control mode. The displacement is applied at the rate of 0.5mm/min (ASTM E8/E8M 2016). Once, the peak load is achieved, after a significant drop in the load displacement curve, the experiment is stopped. Since, rupture of the bolt may damage the furnace.

4.2.6 Chemical composition

The chemical composition of the specimens at RT is carried out using optical emission spectroscopy (OES) in accordance to ASTM E 415. The chemical composition for M10 and M8 specimens is provided in Table 4.1. It can be seen that the present steel grade for the bolt material conforms to IS 1367 (Part 3): 2002 (IS 1367-3 2002)/ ISO 898-1:1999 (ISO 898-1 2009).

4.3 Results and discussion

Experimental results for tensile and shear tests are presented in Tables 4.2 and 4.3. In this present study, due to the difficulty in extracting the exact elongation for the bolt in the experimental set-up (inadequate space for HT extensometer placement) for the tensile test study, the displacement is monitored from the actuator movement. Typical actuator displacement - load relations are presented in Figures 4.2 and 4.3 for tension and shear behavior respectively. The tensile and shear strength are estimated from the peak load and measured (actual) area for each bolt. Reduction factor for tensile strength (k_{rT}) and shear strength (k_{rS}) are obtained as the ratio of ultimate strength ($\sigma_{u,T}$) at the target temperature to the average strength ($\sigma_{u,20}$) of the specimens tested at room temperature for tensile and shear tests respectively. The reduction factors for tensile and shear strength of 10.9 bolts are discussed for growth, cooling and post fire phase in Table 4.2 and 4.3. As, the scope of the present study is to estimate the peak load, the possible differences that may arise while estimating the displacement from actuator and in actual bolt elongation in not likely to have any influence.

Typical modes of failure in tension and shear are presented in Figures 4.4 and 4.5 respectively. Testing of specimens at elevated temperature is a time-consuming exercise, hence a single experiment is conducted for each parameter. Couple of experiments (like T-RT-20-20, S-RT-20-20 and S-GT-20-800; see Table 4.2 and 4.3) are repeated and the results show very less variability (< 2%) which indicate good repeatability of the experimental outcomes.

4.3.1 Tests at Room Temperature (RT)

All the specimens for the tensile test study are half threaded bolt, except 1 full threaded bolt is tested at RT (room temperature). While in shear tests, 2 half threaded bolts are tested at RT, while the remaining are full threaded bolts. The elastic modulus and 0.2% proof stress values are extracted from the full threaded specimen using a 25mm gauge length RT extensometer. The elastic modulus and 0.2% proof stress for the full threaded bolt (T-RT-20-20(3)) is 190GPa and 1006MPa respectively; while, the strain at the peak load is 1.38%. The average ultimate tensile load and peak stress of the specimen at RT are 63.1kN and 1061MPa respectively. Based on the test results, the mechanical properties of all the 3 specimens tested at RT confirms to that of 10.9 Grade as per ISO (ISO 898-1 2009). From the shear tests, the shear failure plane is found to lie at the threaded portion of the bolt. The full threaded M8 bolts are considered for the study at elevated temperature. The average ultimate shear stress capacity at RT is 710 MPa.

4.3.2 Tests at Growth Phase (GT) Temperature

Results for tensile (Fan et al. 2013; Kodur et al. 2012; Lange and González 2012; Wang et al. 2005) and shear (Fan et al. 2013; Kodur et al. 2012; Peixoto et al. 2017; Yang et al. 2011) tests by other authors are plotted along with the reduction factors from the present study in Figures 4.6 and 4.7 for growth phase. EN1993-1-2 (EN 1993-1-2 2005)/AISC 360:16 (ANSI/AISC 360 2016) and BS 5950-8 (BSI 1990) provide separate reduction factors for bolt material and carbon steel, while AS 4100 (AS 4100 2016) is silent about the same which are also presented in Figures 4.6 and 4.7.

k_{rT} (reduction factor in tension) for the present study reduces by 33% when the temperature reaches 500^{o}C and falls drastically by 67% at 600^{o}C. For the shear strength in growth phase, k_{rS} (reduction factor in shear) increases 11% above unity when the bolt is heated to 400^{o}C,

which dropped by 27% and 57% at 500°C and 600°C respectively. This indicates that the fall in shear strength is not as significant as that of tensile strength as the temperature increases from 500°C to 600°C. Usually, at around 550°C, the densely packed face-centered cubic atomic structure is transitioned to loosely packed body centered cubic packing(Callister and Rethwisch 2014). Because, of this reason, a sharp fall in tensile and shear strength may have been observed whenever the bolt is heated beyond 550°C. The increment in shear strength when the specimen is heated from 20°C at 400°C, may be attributed to Portevin-LeChatelier effect (Manach et al. 2014; Yilmaz 2011; Zuev et al. 2017), where the ultimate strength is improve due to solute diffusion and dislocation of defects. This effect occurs due to certain loading rate and temperature. Similar observations are also reported in previous studies (Imran et al. 2018; Rokilan and Mahendran 2020; Wang and Chen 2021). In the Figures 4.6 and 4.7, the data-points at 300°C are cluttered around unit reduction factor (k_{rT} or k_{rS} = 1.00) after a dip (k_{rT} or k_{rS} < 1.00) as the temperature increases from 20°C to 300°C for the study conducted by Kirby(Kirby 1995), showing the prominence of Portevin-LeChatelier effect. The slight difference in reduction factor at elevated temperature among other authors (Fan et al. 2013; Hanus et al. 2011; Kirby 1995; Kodur et al. 2012; Lange and González 2012; Peixoto et al. 2017; Wang et al. 2005; Yang et al. 2011) and present study may be attributed to different manufacturing process (like forging process, alloying chemicals composition, rate of cooling and tempering temperature) employed in various countries. As the temperature increases beyond 500°C, the drop in tensile strength is higher than the shear strength.

For comparison/prediction of the results in growth phase, mean absolute percentage error (MAPE) technique is applied in this study. This technique checks the efficacy of various material models at elevated temperature (see e.g. (Khorasani et al. 2015)). In this technique, new/existing reduction factor is evaluated/compared by reducing the mean error of the predicted/existing data point against the experimental data point. MAPE is given as

$$MAPE = \frac{1}{N}\sum_{i=1}^{N}\left|\frac{A_i - a_i}{A_i}\right| \tag{4.1}$$

where N = number of experimental data points; A_i= experimental data-point; a_i =proposed/existing (from one of the models in consideration) data-point. Linear interpolation is adopted whenever the experimental data points lies in between intermediate discrete data-points (of existing models). Sometimes, due to heating, the reductions factors lie above unity, indicating the strength of the material at that temperature to be higher than the nominal room temperature strength; however, it is difficult to consider such features in design. Hence, whenever the reduction factor is greater than unity, it is taken as unity in the present comparison. If the MAPE for any individual experimental data points exceeds unity, then such datapoints are considered as outlier and hence skipped. Lower MAPE indicates that the proposed/existing model is closer to the experimental results.

MAPE is calculated based on the present experiments and other tests (on tensile (Fan et al. 2013; Kodur et al. 2012; Lange and González 2012; Wang et al. 2005) and shear (Fan et al. 2013; Kodur et al. 2012; Peixoto et al. 2017; Yang et al. 2011) behavior) on 10.9 grade bolt (or strength equivalent to 10.9 Grade bolt like A490(Kodur et al. 2012; Peixoto et al. 2017), F10T(Yang et al. 2011)). The MAPE (see Table 4) for k_{rT} in the present study (MAPE = 19%) shows that it is more accurate (more accuracy is indicated by relatively lesser MAPE value) than the prediction provided by AS 4100 (AS 4100 2016) (MAPE= 20%) and BS 5950-8 (BSI 1990) (MAPE =22%). However, the EN1993-2 models (MAPE = 11%) (EN 1993-1-2 2005) more accurately predicts the behavior of the bolt at elevated temperature. AISC 360-16(ANSI/AISC 360 2016) concurs with the EN1993-1-2 model (EN 1993-1-2 2005) at elevated temperature and hence, no extra comparison study has been carried out here. The shear strength (k_{rS}) obtained from the present study (MAPE = 19.3%) is comparable to the existing models of EN1993-1-2 (EN 1993-1-2 2005) (MAPE = 19.7%). However, the shear test results devites away from other models of AS 4100 (AS 4100 2016) (MAPE = 25%) and BS 5950 - 8 (BSI 1990) (MAPE = 22%). The reduction factor follows a linear relationship with temperature after 215^{o}C in case of AS 4100(AS 4100 2016), which is not seen in the among the experimental results. Rather, an inverted S type pattern for the reduction factor (k_{rT} and k_{rS}) is seen with the increase of temperature. This type of pattern can been seen in the model provided by EN1993-2 (EN 1993-1-2 2005). Based on the experimental data (present study and other experiments) on tensile (Fan et al. 2013; Kodur et al. 2012; Lange and González 2012; Wang

et al. 2005) and shear tests (Fan et al. 2013; Kodur et al. 2012; Peixoto et al. 2017; Yang et al. 2011), a new model is suggested for k_{rT} and k_{rS} (see in Table 4.5) by minimization of error (between predicted and the experimental data). Beyond 500^{o}C, it is observed (see Figure 4.7) that the experimental data for shear tests are on the higher side (more strength) in comparison to those of EN1993-1-2 (EN 1993-1-2 2005) model (like the experimental shear strength is ~10-15% higher than EN1993 model at 600^{o}C - 800^{o}C). Hence, two separate reduction factors are proposed for tensile and shear strength. It may be noted that the present proposal is in contrast to the EN1993-1-2 model, wherein single reduction factor is proposed for both tensile and shear strength. The proposed model shows better prediction as indicated by the least value of MAPE (see Table 4; k_{rT} = 11%; k_{rS} = 7%).

4.3.3 Tests at cooling (CT) and post-fire (PT) phase

The results of the tests in cooling and post fire phase are presented in Tables 4.2 and 4.3. The results for the cooling and post fire phase study with other authors (8.8 grade bolt (Hanus et al. 2011), E350 grade plate (refer to Chapter 3), Q345 grade plate(Chen et al. 2020b)) is shown in Figures 4.8 and 4.9. The comparison is carried out with non-bolt material (i.e., E350 grade hot rolled plate (refer to Chapter 3) and Q345 cold formed plate (Chen et al. 2020b)) to signify the subtle differences in the bolt and normal steel materials response during the cooling phase. To the best of author's knowledge, these are the only two studies (Chen et al. 2020b) (refer to Chapter 3) available in the open literature that discuss the behavior of plate materials in cooling phase, hence comparison is made with only these works (Chen et al. 2020b) (refer to Chapter 3). In the present study, when the specimen is heated to 800^{o}C, 700^{o}C and 600^{o}C there is 46%, 52% and 67% regain of tensile strength (k_{rT}) respectively. And, around 70-80% regain the shear strength (k_{rS}) when the specimen is heated in between 700^{o}C - 800^{o}C and around 93% when heated upto 600^{o}C. The regain of tensile strength can be seen only upto 400^{o}C in cooling phase for tensile and shear tests, after which there is no longer strength enhancement.

The regain in strength is slower at CT than the drop in strength at GT (see in Figures 4.8 and 4.9). Such similar observation is also seen in previous study. In contrast to the general notion that the tensile and shear strength in GT and CT will be similar for a temperature with any heating and cooling cycle, they vary based on the temperature they are heated (see in Figure

4.10 and 4.11). Here, as the specimens are heated to higher temperature (peak temperature) and then tested at lower temperature in CT, the strength reduces for the same temperature (target temperature).

In comparison to the behavior at GT, where the strength reduces in an inverted S shaped manner as the temperature increase, the strength regain in CT is linear as the cooling temperature decreases from peak temperature to 400^{o}C. After 400^{o}C, the k_{rT} and k_{rS} regain is not significant when the specimen is heated upto 700^{o}C - 800^{o}C. When the specimen is heated upto 600^{o}C, the k_{rT} regains more than the k_{rS}. In contrasts to that of plate steel material (Chen et al. 2020b) (refer to Chapter 3) which regains around 90% of its strength at PT after being heated to 600-800^{o}C, the regains in strength for bolt material is lower (~50%-70%). The regain in strength in CT is higher in shear tests than in tensile tests.

Based on the present experimental studies, k_{rT} and k_{rS} are proposed for cooling phase (see Table 4.5).

4.3.4 Load - displacement relationships and failure modes

The load displacement relation for the tensile tests show that strain hardening is very limited in GT and CT. However, it is seen that in PT specimens (like T-PT-800-20 in Figure 2), distinctive yield plateau is visible. This is a behavior seen only in mild steel (Wang et al. 2021) without any cold-forming process. This indicated that the heating process may have removed that the effect of heat treatment and cold forging. The yield plateau decreases when the specimen is heated to lower temperature -700^{o}C (in T-PT-700-20) and disappears at 600^{o}C (in T-PT-600-20).

Mainly, two possible failure modes may occur in the pure tensile loading (Bull et al. 2015; Kirby 1995), namely: (i) necking of the bolt, where the bolt undergoes strain hardening or (ii) thread stripping, where the threads of the nut and bolt in contact with each other undergo large localised plastic deformation. In the present study, two nuts are kept for each bolt assembly, such that the thread stripping mode of failure is avoided which may lead premature failure (before reaching the peak capacity) of the bolt(Kirby 1995). Typical failure mode is presented

in Figure 4.4 for tensile tests. It has been observed that all the bolts have failed by necking at the threaded portion in the tensile testing (see RT 20(1), RT 20(3), PT 800 in Figure 4.4) with a visible cup cone pattern. For some specimens, which are stopped right after the peak load is achieved, localized strain hardening can be observed at the threaded portion as the cross section reduces locally (see RT-20(2) in Figure 4.4). A smooth shear plane is observed for specimens that failed in shear (like in RT-20-20 in Figure 4.5), with a slight undulation at one edge at RT. For other specimens at GT, CT and PT, the bolts undergo slight plastic deformation and with rough shear surface (like in PT-700-20 and CT-800-500) or smooth shear plane (like in CT-700-400).

4.4 Summary and conclusion

Experimental investigation has been carried to assess the tensile and shear capacity of high strength steel 10.9 grade bolt in heating and cooling fire with emphasis on the mechanical respond of the bolts in cooling phase. 44 specimens are tested and the results for tensile and shear tests are presented for room temperature (RT), growth phase (GT), cooling phase (CT) and postfire phase (PT). Based on the experimental study the following conclusions are made:

1) The growth phase reduction factor data is compared with other experimental results and existing material models and an appropriate reduction factors have been proposed. It has been seen that the growth phase data follows an inverted S pattern as seen in previous literature. The strength reduction in tensile tests is higher than the shear tests when the temperature increases from 500^{o}C to 600^{o}C in GT. Reduction factors are proposed separately for tensile (k_{rT}) and shear (k_{rS}) strength in GT for 10.9 Grade bolt.
2) For the peak temperatures: 600-800^{o}C at cooling phase considered in this study, a near linear strength regain can be seen upto 400^{o}C, after which there is no much significant regain in strength. The reduction factors regain upto ~46-67% and ~67-79% in tensile and shear capacities respectively at PT when the specimens are heated to 600-800^{o}C, which is lower than the strength regain found in mild steel. In comparison to the 8.8 grade bolt results in cooling phase, the strength regain is higher in 10.9 grade bolt upto ~400^{o}C. However, if the specimen is heated to 600^{o}C, the 10.9 grade regains lower

strength than the 8.8 grade bolt in post fire phase. Based on the present experimental study, reduction factors – k_{rT} and k_{rS} are proposed in cooling phase.

3) The load displacement curve shows that when the specimens are heated upto 700-800^{o}C distinctive yield plateau is observed for specimens tested at PT phase.

Tables

Table 4.1 Chemical composition of 10.9 grade bolts in w/w (%)

	C	Si	Mn	P	S	Cr	Mo	Ni	Al	Nb
M8	0.148	0.169	0.631	0.010	0.006	0.274	0.027	<0.005	0.029	0.006
M10	0.248	0.124	0.672	0.001	0.008	0.243	0.044	<0.005	0.034	0.006
	Co	Cu	Sn	Ti	V	W	Pb	B	Ceq	
M8	0.017	0.010	0.036	<0.001	0.004	<0.010	0.0025	0.0004	0.315	
M10	0.020	0.014	<0.001	0.043	0.004	<0.010	0.0049	0.0005	0.420	

	C*		P	S	B	$^{o}C^{\varphi}$
	min	max	max	max	max	Min
IS 1367 (Part3): 2002/ ISO 898-1:1999	0.15	0.35	0.035	0.035	0.003	340

* Carbon content is presented for carbon steel with additives (e.g. B, Mn or Cr) quenched and tempered

$^{\varphi}$Tempering temperature

Table 4.2 Tensile test results for M10 10.9 bolts

Sample ID	Peak Load (kN)	Peak Stress (MPa)	k_{rT}
T-RT-20-20 (1)	63.9	1074	
T-RT-20-20 (2)	63.1	1061	1.00
T-RT-20-20 (3)[#]	62.4	1049	
T-GT-20-400	52.6	884	0.83
T-GT-20-500	42.2	710	0.67
T-GT-20-600	20.9	351	0.33
T-GT-20-700	9.1	153	0.14
T-GT-20-800	4.6	77	0.07
T-CT-800-700	5.9	99	0.09
T-CT-800-600	14.0	235	0.22
T-CT-800-500	23.4	393	0.37
T-CT-800-400	31.7	533	0.50
T-CT-700-600	18.7	314	0.30
T-CT-700-500	25.6	430	0.41
T-CT-700-400	40.0	672	0.63
T-CT-600-500	40.4	679	0.64
T-CT-600-400	40.5	681	0.64
T-PT-800-20	28.8	484	0.46
T-PT-700-20	33.1	556	0.52
T-PT-600-20	42.1	708	0.67

[#]Full threaded M10 specimen tested at room temperature

Table 4.3 Shear test results for M8 10.9 bolts

Sample ID	Peak Load (kN)	Peak Stress (MPa)	k_{rS}
S-RT-20-20(1)[φ]	33	693	
S-RT-20-20(2)[φ]	34	714	
S-RT-20-20(3)	25.6	701	1.00
S-RT-20-20(4)	26.9	737	
S-RT-20-20(5)	25.8	707	
S-GT-20-400	28.9	792	1.11
S-GT-20-500	18.8	515	0.73
S-GT-20-600	11.1	304	0.43
S-GT-20-700	4.9	134	0.19
S-GT-20-800(1)	2.3	63	0.09
S-GT-20-800(2)	2.4	66	0.09
S-CT-800-700	3.8	104	0.15
S-CT-800-600	8.2	225	0.32
S-CT-800-500	13.4	367	0.52
S-CT-800-400	17.2	471	0.66
S-CT-700-600	9.3	255	0.36
S-CT-700-500	13.8	378	0.53
S-CT-700-400	18.8	515	0.73
S-CT-600-500	19.3	529	0.74
S-CT-600-400	24	657	0.93
S-PT-800-20	17.5	479	0.67
S-PT-700-20	17.6	482	0.68
S-PT-600-20	20.6	564	0.79
S-PT-500-20	21.5	589	0.83

[φ]Half - threaded M8 specimen tested at room temperature

Table 4.4 Comparisons of MAPE (%) for existing/proposed models with experimental data for growth phase

	k_{rT}	k_{rS}
Present study	*19.2*	*19.3*
EC 3 (bolt)	*11.4*	*19.7*
BS 5950-8 (bolt)	*22.7*	*22.5*
AS 4100 (plate)	*20.0*	*25.8*
Proposed	*11.2*	*7.3*
N	37	40

Table 4.5 Proposed reduction factor (k_{rT} and k_{rS}) for 10.9 grade bolt at growth phase in tension and shear

	k_{rT}	k_{rS}
RT-20-20	1	1
GT-20-100	0.95	0.95
GT-20-200	0.94	0.94
GT-20-300	0.93	0.93
GT-20-400	0.83	0.81
GT-20-500	0.56	0.60
GT-20-600	0.25	0.38
GT-20-700	0.11	0.18
GT-20-800	0.07	0.10
GT-20-900	0.05	0.02

Table 4.6 Proposed reduction factor (k_{rT} and k_{rS}) for 10.9 grade bolt at cooling and post-fire phase in tension and shear

	k_{rT}	k_{rS}
CT-800-700	0.09	0.15
CT-800-600	0.22	0.32
CT-800-500	0.37	0.52
CT-800-400	0.46	0.66
PT-800-20	0.46	0.67
CT-700-600	0.30	0.36
CT-700-500	0.41	0.53
CT-700-400	0.52	0.68
PT-700-20	0.52	0.68
CT-600-500	0.64	0.74
CT-600-400	0.64	0.79
PT-600-20	0.67	0.79

Figures

Figure 4-1 (a) Tensile testing set-up with RT extensometer; (b) Shear testing set-up; (c) Electric furnace around the tensile testing set-up

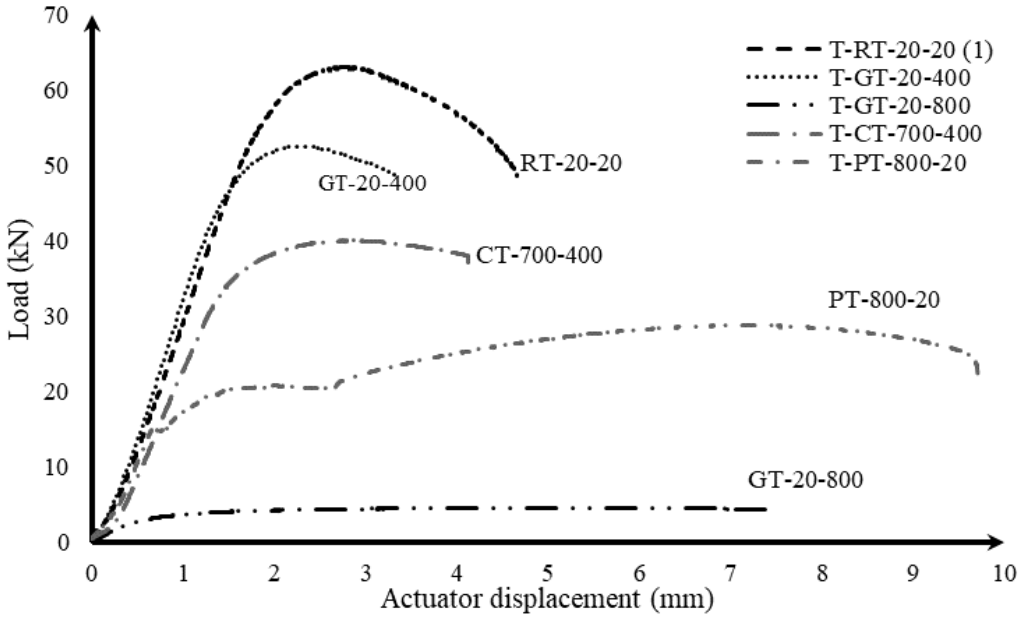

Figure 4-2 Typical load - displacement relation for the tensile test

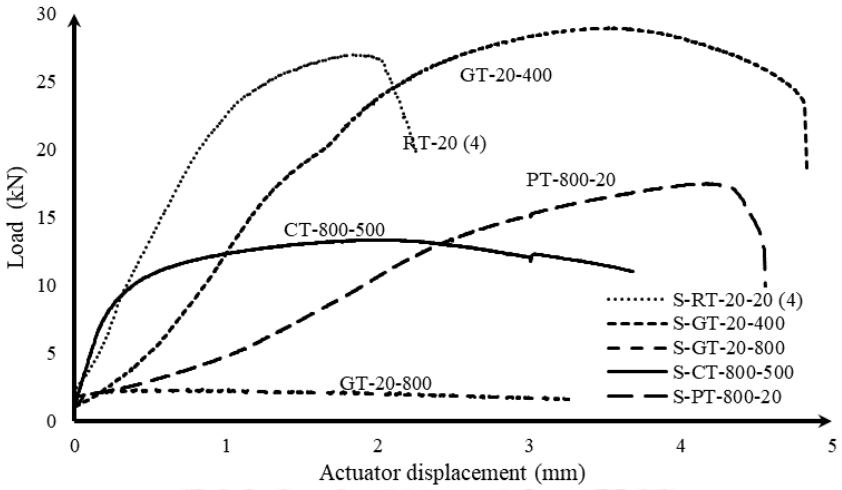

Figure 4-3 Typical load - displacement relation for the shear test

Figure 4-4 Typical tested specimens in tensile test

Figure 4-5 Typical tested specimens in shear tests

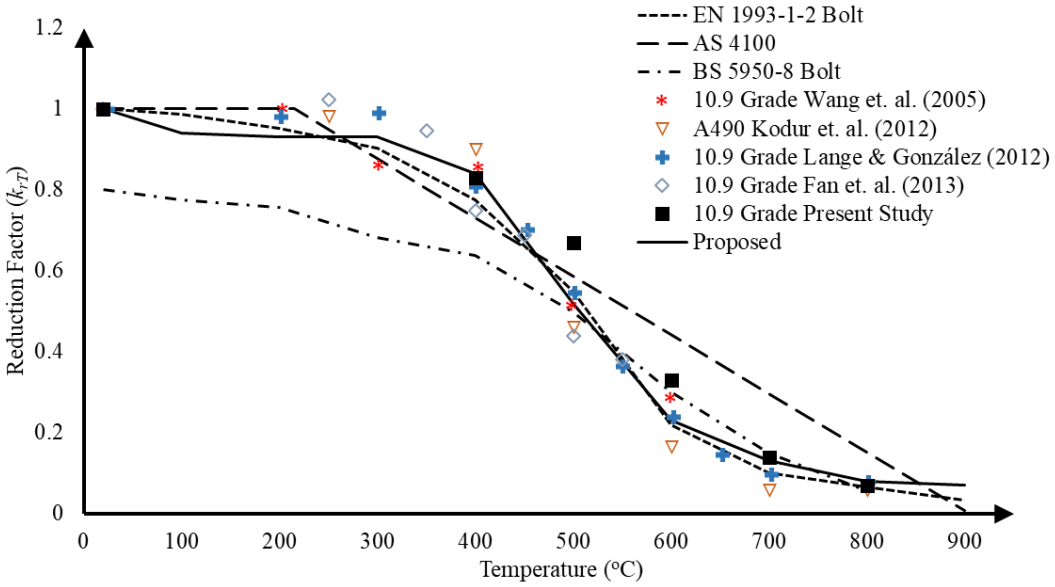

Figure 4-6 Tensile reduction factor (k_{rT}) for present study and other authors in growth phase

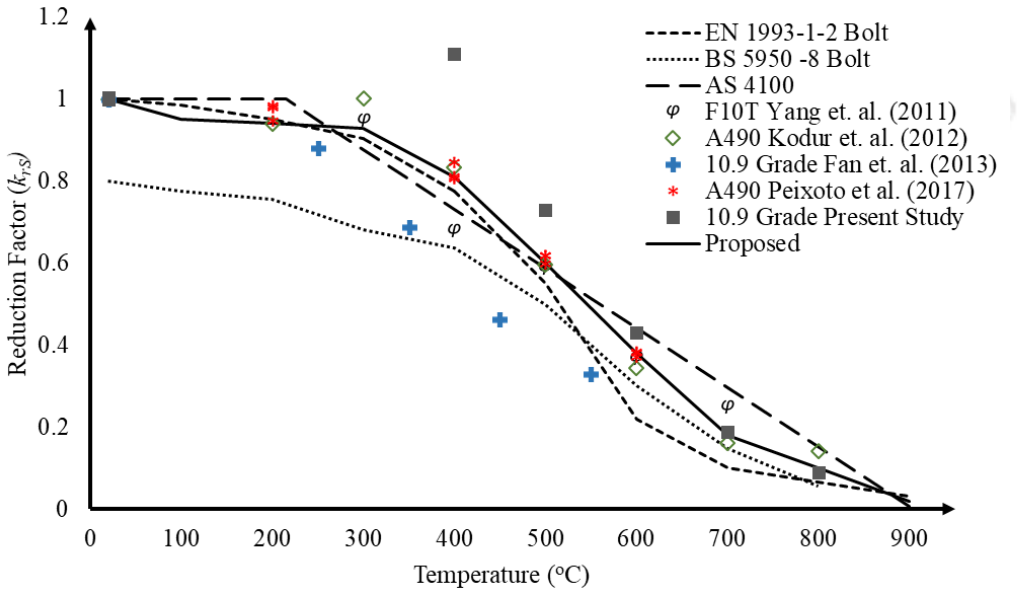

Figure 4-7 Shear reduction factor (k_{rS}) for present study and other authors in growth phase

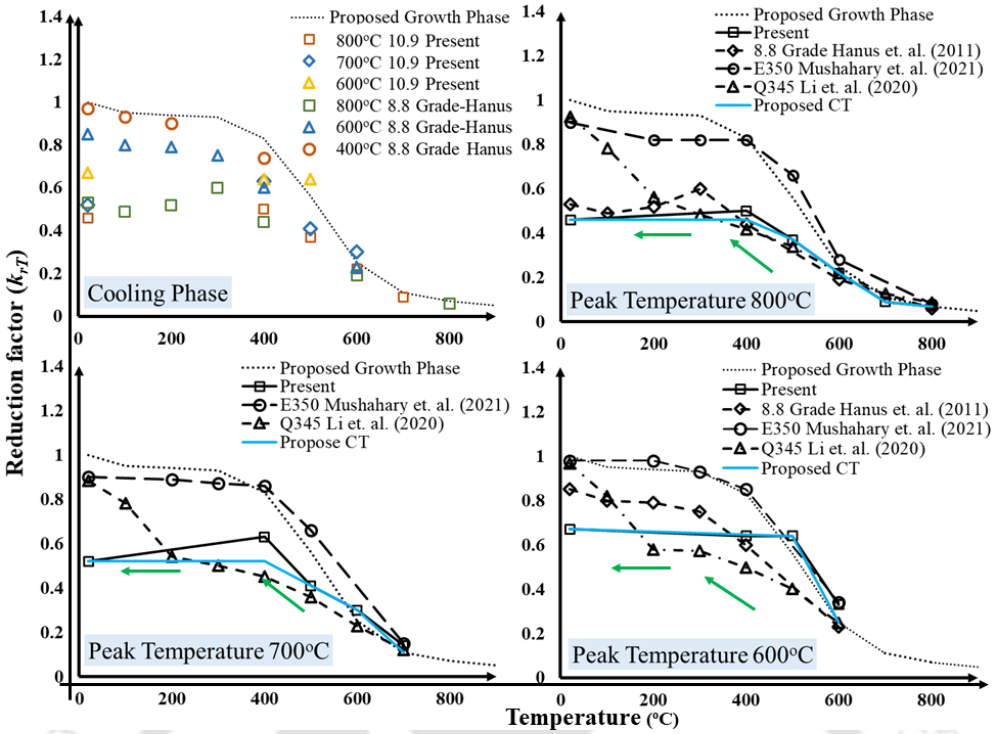

Figure 4-8 Tensile reduction factor (k_{rT}) for present study and other authors in cooling and post-fire phase

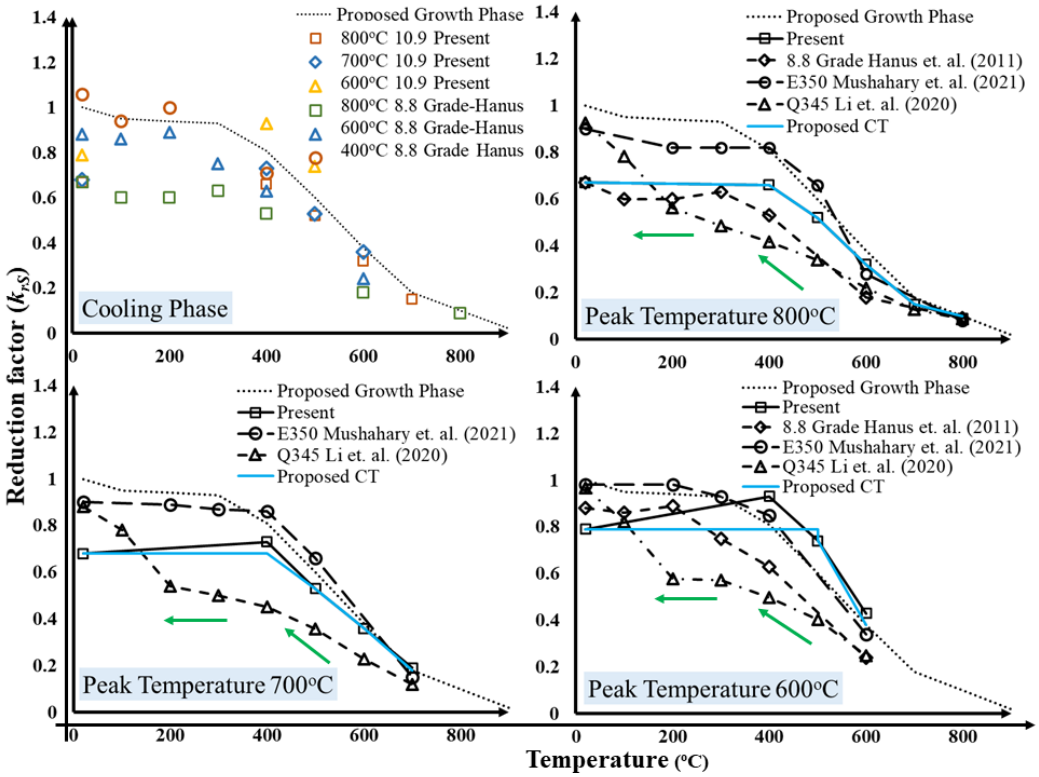

Figure 4-9 Shear reduction factor (k_{rS}) for present study and other authors in cooling and post-fire phase

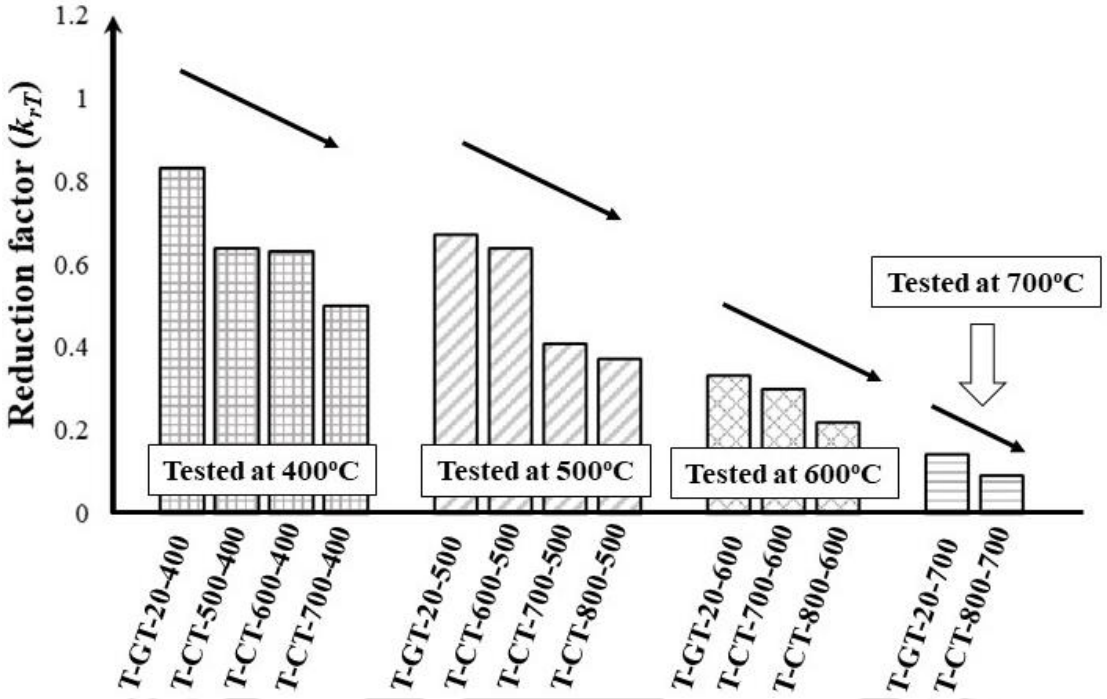

Figure 4-10 k_{rT} for the present study when the specimens are tested at 400°C, 500°C, 600°C and 700°C

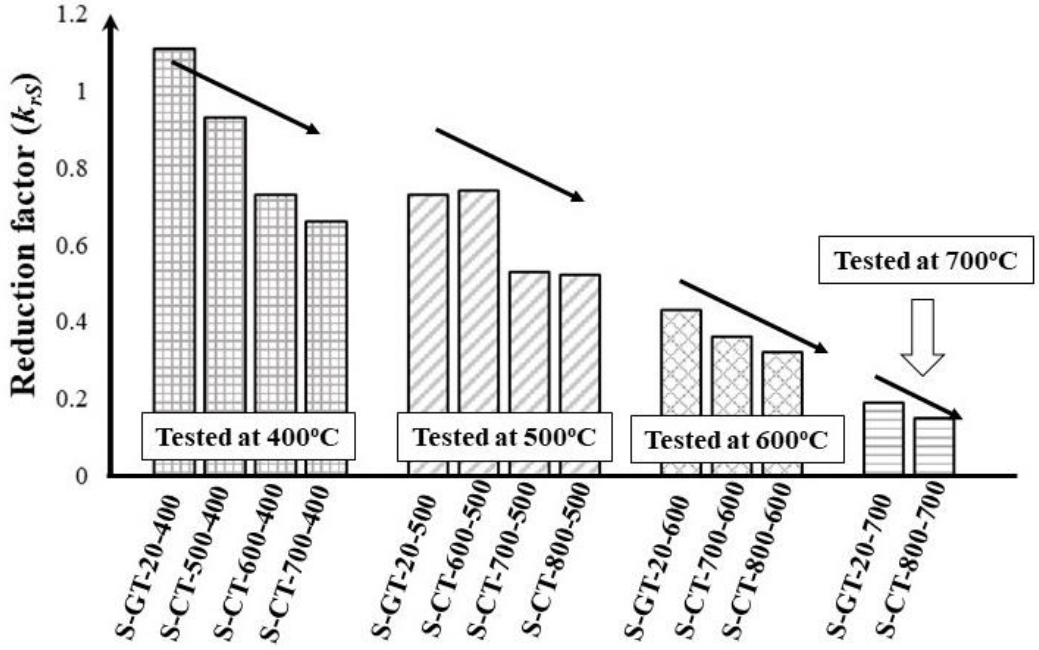

Figure 4-11 k_{rS} for the present study when the specimens are tested at 400°C, 500°C, 600°C and 700°C

CHAPTER 5: BEHAVIOUR OF AXIALLY RESTRAINED BEAMS DURING HEATING AND COOLING FIRE

5.1 Background

In the limited tests mentioned above, the effect of various parameters (such as the amount of axial restrain, amount of loading, cross sectional slenderness) is not discussed. The tests carried out in these studies (Li and Guo 2008; Liu et al. 2002) are compact sections. In order to gain better understanding on restrained beam in natural fire (heating and cooling fire), numerical investigation is carried in this chapter. In the present study, an attempt has been made to assess the influence of various parameters like beam cross sectional slenderness, axial restraint and amount of loading on beams. Usually, the dominant forces in steel building are due to gravity load. Reaction at the supports are transferred to adjacent member through shear connection. Shear connections are capable in providing axial restrain to the beam by resisting axial movement. Hence, only axially restrained beams are studied in this work. It has been found in the previous work (Chen et al. 2020b) (refer to Chapter 3) that material properties do not remain same in growth and cooling phases. In order to evaluate accurate response in cooling phase, different material properties are considered during cooling phase (as compared to the material properties in growth phase). Later, analytical model is proposed based on the results of the present numerical studies and moment - force equilibrium equation.

5.2 Model for numerical verification

The numerical models have been created using the commercial software - Abaqus 6.19(Abaqus 6.19 [computer Software] 2019) to estimate the responses of restrained beams at elevated temperature. Sequentially coupled thermo-mechanical analysis procedure has been adopted in this work. Here, the stress/ deformation field in the beam is dependent on the temperature field (e.g., internal forces developed in the beam due to thermal expansion, where thermal expansion is a resultant of change in temperature field), hence sequential coupled thermo – mechanical analysis is adopted.

5.2.1 Element type and meshing

Four-noded thermally coupled shell element with reduced integration (S4RT)(Rokilan and Mahendran 2022; Yin and Wang 2004) is adopted in this study. After various trials for mesh sensitivity, optimum mesh size is chosen (no. of elements in flange = 12; no. of elements in web = 20) such that computational effort is reduced and accurate results are obtained. In order to maintain stability of the analysis when the catenary action initiates, a pseudo-dynamic procedure (Yin and Wang 2004) has been adopted with a dissipated energy fraction of 2×10^{-4} and adaptive stabilization with maximum ratio of stabilization to strain energy as 0.05.

5.2.2 Boundary condition

In order to replicate the experimental conditions, various boundary conditions are applied to beam at supports and top flange (see Figure 5.3). Axial and rotations springs are added seperately at each member end to enact the axial and rotational restraints respectively. Spring2 element type is used in this study. Spring2 element simulates the presence of axial or torsional spring between two points/ nodes in a certain fixed direction. The different level of axial restrain (β) and rotational restrain (γ) are added as a fraction of axial stiffness ($K_a = E_{20}A_g/L_b$; E_{20}= elastic modulus of steel at room temperature; A_g= gross area of the beam; L_b = length of the beam) and rotational stiffness ($K_r = E_{20}I/L_b$; I = moment of inertia of the beam) respectively of the beam. For the four point bending scenario, two concentrated loads are applied on the beam at equal distance apart from the support (see Figure 5.1). Load is applied to the beam as

a fraction (i.e., load ratio - χ) of the maximum load corresponding to bending capacity of the beam (Dwaikat and Kodur 2011; Li and Guo 2008; Liu et al. 2002).

Kinematic coupling (see Figure 5.3) is used to condense the degrees of freedom of the beam-end cross section to a reference point. This reference point (RP-2 or RP-3) is connected to another reference point (RP-1 or RP-4) through two springs (axial and rotational spring). All the degrees of freedom at the end of the spring (RP-1 or RP-4) are arrested. The reference point (RP-2 or RP-3) at the beam end acts as the master node for the kinematic coupling. The axial (u_x) and rotational (θ_z) degree of freedom are relieved at the master node. For all the experiments, at RP-1 and RP-4, the beam is rotational restrained ($\theta_z \neq 0$). In order to provide lateral restraint to the beam at the top flange (as it is restrained with the presence of slab in real situation), the lateral displacement (u_z) is arrested at the top flange (see Figure 5.3). As, the beam is laterally restrained, it will not undergo laterally torsional buckling.

5.2.3 Heating procedure and parameters

Usually, a beam can be exposed to 3 sided fire or 4-sided fire based on exposed surface. 3 sided fire indicates to fire exposure where the top flange do not get directly exposed to fire as the deck slab sits on the top flange. 4 sided fire indicates the condition where the beam is exposed to fire on all the sides. 4 sided fire are more conservative fire scenario. However, in this study, the models are validated against 3 sided fire experiments (Li and Guo 2008; Liu et al. 2002) since, to the best of authors' knowledge, there is no experiment on restrained steel beam with 4 sided fire. There are three modes of heat transfer - conduction, convection and radiation. In real scenario, as the fire ignites at the source, the specimen gets heated up due to convection and radiation. So, the bottom flange and the web is heated through convection and radition mode of heating. The top flange in the experiments (Li and Guo 2008; Liu et al. 2002) is insulated using ceramic material. Hence, the heat transfers in the form of conduction The parameters for thermal input is provided as interaction: *Sfilm (convection) with convective heat transfer coefficient as 25 W/m^{2}K (EN 1993-1-2 2005) and *Sradiate (radiation) with coefficient of emissivity as 0.7 (EN 1993-1-2 2005). The thermal heat input applied in the validation study for comparision with the experimental results of Liu et. al (2002) and Li &

Guo (2008) (which are based on standard fire (ISO 834) and natural fire respectively) are taken from their respective work.

5.2.4 Material properties for validation

The stress-strain model is adopted from Eurocode (EN 1993-1-2 2005). Other thermal properties like specific heat, conductivity and thermal expansion are adopted from Eurocode (EN 1993-1-2 2005) for carbon steel. A modified heating scheme (see Section 5 – Modified heating scheme) is adopted in the FE model for the experiment on natural fire(Li and Guo 2008). The reduction factor incorporated in the modified heating scheme is presented in Figure 5.

5.2.5 Validation

The validation study is carried out based on the experimental investigation (Li and Guo 2008; Liu et al. 2002) on restrained steel beams at elevated temperature. Liu et al. (Liu et al. 2002) performed 15 fire tests on restrained steel beam (UB 172 x 102 x 19) with varying degree of load ratio (χ=20%, 30%, 50% or 70%), axial (β = 2%, 9% or 16%) and flexural restrain. Out of which, tests: FUR 13 (k_A= 8kN/mm; χ = *50%*), FUR 25 (k_A= 35kN/mm; χ = *50%*) and FUR 31(k_A= 62kN/mm; χ = *50%*) are presented for validation (see Figure 4) in this study. Out of the two tests conducted by Li & Guo (Li and Guo 2008) on 4.5m long restrained beams (H 250 x 250 x 8 x 12) of grade Q235B and Q345, the former beam (Grade: Q235B) is validated here (see Figure 5.5).

The validation studies are in good agreement with the experimental results (Li and Guo 2008; Liu et al. 2002) and other numerical simulation (Dwaikat and Kodur 2011; Liu and Davies 2001; Pournaghshband et al. 2019; Zhang et al. 2013). The unavoidable discrepancies that existed between the test and FE results are due to the variation in the actual and simulated temperature and the generalized elevated temperature stress-strain relationship assumed. The failure modes like formation of plastic hinge at the loading points and local buckling near the end supports as observed in the experiments (see Figure 5.4) have been captured well in the numerical study. Modified heating scheme (explanation provided in Section 5) is employed to

validate the test performed by Li & Guo (Li and Guo 2008). The different material reduction factor in growth and cooling phases are applied in the scheme (see Figure 5.5).

Having successfully validated these two works (Li and Guo 2008; Liu et al. 2002) on experimental investigation of restrained steel beam at elevated temperature, parametric studies have been carried out in the following section.

5.3 Parametric study

Numerical parametric studies are carried out considering various cross sectional slenderness, cross sectional aspect ratio, load ratio and boundary condition to investigate the resistance of restrained steel beams in natural fire. Beams with 9 different cross sections and each with length 3m are considered in this study (see Table 5.1). Three types of analysis are carried out in this study. Firstly, the moment capacity ($M_{FEA,T}$) of the beams is estimated for a beam at elevated temperature for a simply supported boundary condition. After having estimated the moment capacity, the maximum load that the beam can sustain is calculated. Secondly, the critical temperature (T_{cr}) is evaluated for the beam for varying load ratio (χ = 20%, 40% and 60%), axial restraint (β= 1%, 5%, 20%, 50% and 80%). As mentioned earlier, only axially restraint beams have been considered in this study. Thirdly, the beam is heated with natural fire with the peak temperature as the critical temperature (T_{cr}) that has been evaluated from the second analysis.

5.3.1 Material model in current study

As discussed in the earlier section, different material properties are incorporated in growth and cooling phases. To the best of author's knowledge, there are very few work which discuss material properties for mild steel in cooling phase: E350 (refer to Chapter 3), G345(Chen et al. 2020b), G550(Chen et al. 2020a). Out of these (Chen et al. 2020b) (refer to Chapter 3), only the work on E350 (refer to Chapter 3) discusses upon hot rolled steel in heating and cooling fire. Hence, the material properties for E350 (nominal $\sigma_{y,20}$ = 350MPa) such as reduction factor (see Figure 5.6) and stress strain models from recent study (refer to Chapter 3). have been considered in the present study.

5.3.2 Imperfection and residual stress

Initial imperfection leads to reduced capacity of the members. Eigenvalue buckling analysis is carried out to obtain the local and global buckling modes and the deformed geometry is assigned as the initial geometry (see Figure 5.7) for the thermo-mechanical analysis. The global imperfection amplitude is assumed as $L_b/1000$ (Pournaghshband et al. 2019).

Localised residual stresses are developed in the built-up section due to non-uniform cooling in the welding of flange-web junction. Linear stress profile (see Figure 5.8 a) has been adopted in this study for simplification, with a very close resemblance to ECCS model (see Figure 5.8 b). The residual stress is applied to the FE model using the predefined field option in Abaqus 6.19(Abaqus 6.19 [computer Software] 2019). The maximum compressive stress at flange and web is taken as $0.3\sigma_{y,20}$ and $0.1\sigma_{y,20}$ respectively and the maximum tensile stress is assumed as $0.3\sigma_y$ and $0.9\sigma_y$ at the flange and web respectively (see Figure 5.9).

5.3.3 Heating procedure in current FE study

In the parametric study, heat is applied on all the four sides of the beam (4-sided heating). Conduction mode of heat transfer is considered here. Heat is applied to the beam using thermal boundary condition.

5.4 Modified heating scheme (MHS)

In order to assess the maximum temperature (T_{cr}) that the member can sustain, standard fire curve (ISO 834 fire curve) is used as thermal input for growth phase (see Figure 5.10). The time temperature relation of standard fire has been provided in EN 1991-1-2; ($T = 20 + 345 \log(8t+1)$) here T is the temperature in ^oC and t is time in seconds). Once the peak temperature is reached, the beam is soaked for another 3 mins at that temperature. This is usually done during material testing experiments, in order to reduce thermal gradient within the furnace. However, since the heat is applied through conduction, there is least chance of thermal gradient being occurring in the numerical study, hence, a very small duration (of 3 mins) is kept for soaking. Then the beam is cooled at ~10^o/min.

In section 4.1, it has been discussed about using material properties in cooling phase that is different from material properties in growth phase. Say, the material has yield strength of $\sigma_{y,600}$ = 250MPa in growth phase at 600^{o}C and the material is cooled after it has reached the peak temperature of 750^{o}C has yield strength $\sigma_{y,600}$ = 200MPa in cooling phase at 600^{o}C. The FE for conventional heating scheme (CHS) does not allow keeping two different properties at the same temperature (temperature in growth phase and cooling phase). Hence, for the very first time, a modified heating scheme (MHS) has been developed which can consider different material properties for a natural fire simulation (growth and cooling phases).

In MHS (see Figure 5.10), fictitious heating cycle replaces the actual cooling cycle after the peak growth phase temperature (T_{cr}) is reached. In cooling phase, the fictitious temperature is the continuation of the heating (i.e., incremental temperature). Hence, the fictitious growth temperature is added after T_{cr} is reached in lieu of cooling phase temperature. The other parameters like specific heat, conductivity and thermal expansion are corrected according to the fictitious temperature. In this study, it is assumed as 100^{o}C of real temperature in cooling phase is equivalent to fictitious 50^{o}C (in growth phase). The validity of the modified heating scheme - MHS (see the dashed line in Figure 5.10) is checked with the conventional heating scheme -CHS (see the dotted line in Figure 5.10) keeping same material properties in growth and cooling phase. The MHS have shown exact match with the CHS. In the next simulation, the material properties are changed with different material properties in cooling phase (see the solid line in Figure 5.10). Since, the yield strength and elastic modulus are slightly lower than the growth phase, the MHS with different material properties (see the solid line in Figure 5.10) shows lower axial force (at the end of the simulation) than the MHS with same material properties (see the dotted line in Figure 5.10). Since, there is no other experimental data to verify this scheme (MHS), hence, from the above illustration, it is concluded that MHS is capable to handle different material properties in growth and cooling phase. Also, MHS scheme has been applied in the validation study above , which shows a very good agreement with the experimental results(Li and Guo 2008).

5.5 Result and discussion

As mentioned in earlier section, three types of analysis are conducted in this study to evaluate – $M_{FEA,T}$, T_{cr} and N_{Fmax}. In Section 5.1, the moment capacities of the beam at ambient and elevated temperature are presented. In Section 5.2, the parameters (load ratio -χ, axial restrain – β and cross sectional slenderness - $\lambda_{L,20}$) affecting the growth phase response of the beams are discussed. The maximum temperature in growth phase (T_{cr}) is evaluated from the second type of analysis. After having found the peak temperature – T_{cr}, a heating and cooling fire input is applied to the beam with peak temperature as T_{cr}. At the end of the third analysis, N_{Fmax} is estimated.

5.5.1 Moment capacity ($M_{FEA,T}$)

Numerical investigation to estimated moment capacity with various cross section is presented in Table 5.1. The cross sections are chosen with varying cross sectional slenderness ($\lambda_{L,20}$ = 0.165 to 0.996), cross sectional aspect ratio (B/D = 0.4 to 0.75), elemental slenderness (web – D/t_w = 30ε to 81.4ε; flange - $B/2t_f$ = 4.1ε to 20.3ε; where ε= $\sqrt{235/\sigma_{y,20}}$.=0.82; in accordance with local bucking classification mentioned in Eurocode (EN 1993-1 2005)). The beam dimensions are chosen such that the failure modes correspond to bending dominated situation (identified by mainly cross sectional yielding in the mid span). $M_{FEA,T}$ is evaluated for 20°C, 300°C, 400°C, 500°C, 600°C, 700°C and 800°C.

5.5.2 Effect of parameters in growth and cooling phase

The effect of axial restraint (β= 1%, 5%, 20%, 50% and 80%). with same load ratio (β =20% or 60%) for 2 beam cross sections (200×80×8×12 and 200×150×4.4×6) are presented in Figure 5.11. The axial force in compression (see for N_{Cmax} in Figure 11) increases as the axial restraint increase. 200×80×8×12 and 200×150×4.4×6 are a stocky ($\lambda_{L,20}$ = 0.165) and slender ($\lambda_{L,20}$ = 0.743) cross section respectively. N_{Cmax} increases as the axial restraint increases. For different axial restrain, T_z and T_{cr} do not vary much with load ratio and cross section. Slender cross sections (200×150×4.4×6) undergoes buckling after T_{Cmax}, which can be seen from the sharp drop of axial compressive force as the temperature transits from T_{Cmax} to T_z.

The influence of load ratio (χ = 20%, 40% and 60%) with same axial restraint (β = 20% or 80%) in 200×80×6×11 ($\lambda_{L,20}$=0.18) and 200×150×3×4.5 ($\lambda_{L,20}$=0.99) on axial force in growth phase is presented in Figure 5.12. For same load ratio (β), the T_{Cmax} decreases as the axial restraint (χ) increases. The slope of the axial force curve remains almost similar as the temperature increases for similar β and cross section. T_z and T_{cr} decreases as the χ increases for same β. The force at the end of growth phase (N_{Tcr}) increases as χ increases.

The influence of load ratio (χ = 40%) and axial restraint (β = 50%) on 200×80×6×11 ($\lambda_{L,20}$=0.18) and 200×150×5.5×8 ($\lambda_{L,20}$=0.40) respectively on axial force in cooling phase is presented in Figure 5.13. The force (N_{Fmax}) at the end of cooling phase increases as the axial restraint and load ratio increases.

5.5.3 Analytical model

Analytical model to evaluate the maximum force (N_{Tcr}) and peak temperature (T_{cr}) at growth phase are proposed by many other researchers (Dwaikat and Kodur 2011; Pournaghshband et al. 2019; Sun and Burgess 2016; Yin and Wang 2005). Analytical formulation are formed based on integration of internal forces by assuming initial deflection profile (Yin and Wang 2005) or by solving force and moment equilibrium relationship (Dwaikat and Kodur 2011; Pournaghshband et al. 2019; Sun and Burgess 2016). The assumed initial deflection profile can consider only certain loading and boundary condition. Hence, to tackle general loading and boundary condition, internal forces are assessed from force moment equilibrium relationship for each temperature in growth phase. The second method is revisited in the present work with some co-efficient correction to appropriately incorporate material and geometric non-linearities. The proposed formulation is based on cross sectional capacity and support boundary condition. The correcting co-efficient are estimated based on the non-linear curve-fitting against the FE response.

Based on the change of temperature and stress flow in the beam, the event of natural life is split into 4 main stages. Stage 1: the compressive force is maximum -N_{Cmax} or T_{Cmax}; Stage 2: the axial force (N_{Tz}) is zero - T_z; Stage 3: the beam has reached the maximum temperature in growth

phase - N_{Tcr} or T_{cr}; and Stage 4: maximum axial force in the beam at the end of the heating and cooling cycle - N_{Fmax}.

5.3.1. Stage 1 – T_{Cmax} and N_{Cmax}

The beam undergoes thermal expansion as the temperature increase from room temperature (~20°C). Since, the beam is axially restrained, thermal expansion leads to development of axial force in the beam. The axial forces keep developing, till the beam starts to yield. The cross-sectional capacity of the beam is given by:

$$\frac{N_{Cmax}}{N_{Rd,T}} + \frac{M_{Ed,T}}{M_{Rd,T}} = 1 \tag{5.1}$$

$$\Rightarrow \frac{N_{Cmax}}{k_{y,T}^{\#} A_g f_{y,20}} + \frac{M_{Ed,T}}{k_{y,T}^{\#} M_{Rd,20}} = 1 \tag{5.2}$$

$$\Rightarrow \frac{N_{Cmax}}{k_{y,T} A_g f_{y,20}} + \frac{\chi}{k_{y,T}^{\#}} = 1 \tag{5.3}$$

$$\Rightarrow N_{Cmax} = (k_{y,T}^{\#} - \chi) A_g f_{y,20} \tag{5.4}$$

where the residual strength of the material $k_{y,T}^{\#} = C_1\beta^2 + C_2\beta + C_3\beta\chi + C_4\chi + C_5\chi^2 + C_6 + \beta^{C_7}\chi^{C_8}$. Here, C_1 = -0.528; C_2 = 0.1727; C_3 = -0.1003; C_4 = 1.065; C_5 = -0.1041; C_6 = -0.03063; C_7 = 0.692; C_8 = -0.06346

The axial force due to the thermal expansion

$$N_{Cmax} = \alpha L_b T_{Cmax} K_{eq,T} \tag{5.5}$$

where $K_{eq,T}$ is the effective beam stiffness at Temperature T.

$$K_{eq,T} = \frac{k_{E,T}\chi K_b}{\chi + 2k_{E,T}} \tag{5.6}$$

Eq (4) and (5) are solved simultaneously to find N_{Cmax} and T_{Cmax} (see Figure 5.14).

5.3.2. Stage 2 – T_z

The compressive axial force reduces in the beam as the temperature increase. At the end of this stage, the axial forces in the beam becomes nil.

$$\frac{N_{Tz}}{N_{Rd,T}} + \frac{M_{Ed,T}}{M_{Rd,T}} = 1 \tag{5.7}$$

where the axial force N_{Tz} is null, hence

$$M_{Ed,T} = M_{Rd,T} \tag{5.8}$$

$$\Rightarrow \beta = k_{y,T}{}^{\sim} \tag{5.9}$$

where $k_{y,T}{}^{\sim} = 0.7457\,\beta^{0.6583I}$. $k_{y,T}$ is back calculated to find T_z (see Figure 5.15)

5.3.3. Stage 3 – T_{cr} and N_{Tcr}

After T_z, catenary action develops in the beam. The limiting capacity of the beam at elevated temperature is the tensile capacity of the beam at that temperature (see Figure 5.16), which is given by

$$N_{T,cr} = k_{y,T}{}^{\phi} A_g f_{y,20} \tag{5.10}$$

where $k_{y,T}{}^{\phi} = b_{c1}\,\lambda^{b_{c2}} + b_{c3}\,\chi^{b_{c4}} + b_{c5}\,\beta^{b_{c6}} + b_{c7}$ where b_{c1} = -2.275; b_{c2} = 0.014477; b_{c3} = 0.33948; b_{c4} = 0.79119; b_{c5} = -0.085596; b_{c6} = -0.13663; b_{c7} = 2.3112

The temperature (T_{cr}) is estimated through a linear interpolation (see Figure 5.16)

$$T_{T,cr} = C_{cr}(T_z - T_{Cmax})\frac{N_{T,cr}}{N_{Cmax}} + T_z \tag{5.11}$$

$C_{cr} = b_{r1}\,\lambda^{b_{r2}} + b_{r3}\,\chi^{b_{r4}} + b_{r5}\,\beta^{b_{r6}} + b_{r7}$. Here, b_{r1} = 3.8251; b_{r2} = 0.001; b_{r3} = 2.94; b_{r4} = -0.007; b_{r5} = -9.68; b_{r6} = 0.003; b_{r7} = 4.05;

5.3.4. Stage 4 - N_{Fmax}

If the beam is allowed to cool before T_{cr} is reached, the catenary action in the beam continues. The axial force (N_{Fmax}) in the beam at the end of the heating and cooling phase (see Figure 5.17) is given by

$$N_{T,max} = k_{y,T}{}^{*} A_g f_{y,20} \quad (5.12)$$

where $k_{y,T}{}^{*}$ is given by $k_{y,T}{}^{*} = b_1 \beta^{b_2} + b_3 \chi^{b_4} + b_5 \lambda^{b_6} + b_7$. Here, b_1=0.2087; b_2= 0.7459; b_3 =1.625; b_4 =0.0817; b_5 = -0.2172; b_6 = 0.7259; b_7 =-1.0225

5.5.4 Failure modes

Failure modes are discussed for three beams: 200×80×8×12 ($\lambda_{L,20}$=0.165), 200×80×3×7.5 ($\lambda_{L,20}$=0.237) and 200×80×4.4×6 ($\lambda_{L,20}$=0.743) in Figure 5.15, 5.17 and 5.18 respectively. The principal stress (S11) is represented in these figures (see Figure 5.15, 5.17 and 5.18). In the figures, tensile and compressive yielding is presented with silver and black patches respectively

The beam - 200×80×8×12 ($\lambda_{L,20}$=0.165) is a plastic cross section (see Figure 5.18). As the temperature approaches T_{Cmax}, the web yields due to the compressive force. The top flange does not yield, indicating the stresses are axial in nature and not flexural type. At T_z, the compressive force reduces. Yielding of top and bottom flange is observed and neural axis can be seen on the mid height of the web, indicated that yielding is occurring due to the pure flexure. At T_{cr}, as the axial force increases, the yield contour spreads out from the bottom flange towards the web while the neutral axis lie near the top flange. At the end of simulation when the temperature cools to 20°C, the yielding appears in the web and top flange. The transition of yield location from bottom flange at T_{cr} to web and top flange at N_{Fmax} is explained in more detail in Figure 5.19. The stress pattern for intermediate temperature (654°C, 591°C, 472°C, 182°C and 85°C) during cooling phase are exhibited. At 645°C (in cooling phase), the yielding zone shrinks to the mid portion of the web from bottom flange and web at T_{cr}. As the temperature decreases, the yielding in the web reduces (at 591°C) and the neutral axis shift towards the bottom flanges. The yielding starts to spread out to the top flange from the upper web portion when the temperature decrease from 472°C to 182°C. The reason the tension yielding at bottom flange

at T_{cr} shifts to the top flange at the end of cooling phase, can be attributed to the following reason. At Tcr, the bottom flange and the lower portion of the web undergoes large plastic deformation. When the temperature drops, the beam starts to contract. Force during thermal contraction depends on unit length. Hence, the bottom flange experience compressive force due to higher plastic deformation in the bottom flange than the top flange. The top flange experience additional in-plane tensile force to maintain strain compatibility relationship.

200×80×3×7.5 ($\lambda_{L,20}$=0.24) is a beam (see Figure 5.20) with Class 2 web and Class 1 flange (according to Eurocode (EN 1993-1 2005)). At T_{Cmax}, the upper portion the web yields in compression with a sinusoidal like distribution. The top and bottom flange do not yield when the temperature is T_{Cmax}. As the temperature increase, the stress in the web region increases and then it undergoes buckling (at T_z) on the upper portion of the web (where the compressive stress is more dominant). At T_{cr}, the tensile yielding appears at the bottom flange. As the temperature drops (in cooling phase), the tensile yield zone shifts to the top flange from bottom flange.

Beam - 200×150×4.4×6 ($\lambda_{L,20}$=0.74) comprise of slender flange and plastic web (see Figure 5.21). The compressive yielding appears in the top flange at T_{Cmax}, with no yielding in the web and bottom flange. At T_z, the top flange undergoes inelastic buckling (since, the buckled portion at the top flange undergoes compressive yielding). The bottom flange and the lower portion of the web undergoes tensile yielding at T_{cr}. However, as temperature decreases (in cooling phase) the beam do not undergo yielding as seen in other examples (in Figure 5.20 and 5.19).

5.6 Example

The loads in the connection in axially restrained beams can be estimated through the analytical formulation. An example is presented for illustration and feasibility of the current approach.

The internal forces of a 3 m beam with nominal yield strength $\sigma_{y,20}$ = 350MPa is evaluated at the end of natural fire which is heated to its maximum temperature (T_{cr}). Design constraints: Beam length: 3m; Beam Dimension: 200×80×8×12; Load ratio: χ = 20%; Axial restrain β = 20%

Since, the beams are axially restrained, hence the load is transfer to adjacent member through shear connection. The factored shear connection of the beam is designed for a 100% of the beam capacity.

Factored shear force acting on the connection during fire (SF_T) due to χ = 20%	= 0.2 ×86 kN	= 17.2 kN
Reaction force at support due to 100% load during room temperature condition	= 86kN	
Factored shear capacity of the connection (SC_{20})	= 86 kN	
The bearing capacity of the connection (BC_{20})	=√3× SC_{20}	=~149kN
Axial force on the beam at the end of heating and cooling cycle for Load ratio: χ = 20%; Axial restrain: β = 20%; N_{Fmax} (see Equation 12)	= 473 kN	
Resultant force acting in the beam at the end of the cooling phase	$= \sqrt{{SF_T}^2 + {N_{Fmax}}^2}$	
	$= \sqrt{17.2^2 + 473^2}$	= ~ 474 kN
		$> \sqrt{{SF_{20}}^2 + {BC_{20}}^2}$ (Unsafe)

For the sake of simplicity, it has been assumed that the connections sustain 100% of their strength at the end of heating and cooling cycle. This assumption is not always true, since connection do not regain 100% of their strength when they are heated above 500-600^{o}C (Hanus et al. 2011).

The proposed approach shows that the axially restrained beams in ambient temperature cannot adequately sustain the force generated during cooling phase. Hence, the connections should be designed considering the axial force at the end of cooling phase (N_{Fmax}).

The axial force on the beam at end of cooling phase (N_{Fmax})	=473kN	
The connection should be design using N_{Fmax} as the minimum bearing capacity (BC_{20}^{*})	$=N_{Fmax}$	
Factored shear capacity of the connection (SC_{20}^{*})	$=N_{Fmax}/\sqrt{3}$	=273 kN

Here the new shear capacity of the beam (SC_{20}^{*}) is 3.2 times of conventional design (SC_{20}), such that the beam can sustain the internal forces at the end of cooling phase.

5.7 Conclusion

Internal forces developed in restrained beams during cooling phase are higher than the forces developed at the end of growth phase. A numerical study is carried out to estimate the internal forces in the restrained beam in natural fire condition (growth and cooling phase). In this study, two different set of material properties are employed in growth and cooling phase. A modified heating scheme is developed with fictitious temperature to handle two different material properties in a single simulation. After having validated the present numerical model with two experimental studies, parametric study is carried out for axially restrained beams in natural fire. The parameters considered in this study are: cross sectional slenderness, aspect ratio, load ratio and amount of axial restraint. 3 types of analysis are carried out. Firstly, moment capacity for each cross section is evaluated at 20^{o}C, 300^{o}C, 400^{o}C, 500^{o}C, 600^{o}C, 700^{o}C and 800^{o}C. Secondly, loads are applied on axially restrained beam of certain load ratio (χ) at growth phase. At the end of second step, the maximum temperature (T_{cr}) till which a certain cross section of restrained beam can survive for a certain load (- load ratio, χ) and axial restraint (β) is estimated. In the third type of analysis, beams are heated upto maximum temperature (T_{cr}) and then allowed to cool. The internal forces in the beam are estimated in cooling phase. Analytical model is proposed based on force equilibrium relations and numerical models. Typical failure modes are discussed for certain beams. It is observed that beam starts to yield as the axial force

in the beam reaches maximum compressive force (T_{Cmax} or N_{Cmax}). As the temperature increases, the axial force shifts from compressive to tensile, thereby undergoing catenary action. Beams with slender cross section or element undergo buckling during this stage. The beam can sustain heating till the residual strength in the beam (N_{Tcr}). As the beam cools, the internal forces keep increasing. A simple example is presented to show the significance of estimating axial force in cooling phase.

Table

Table 5.1 Flexural capacity of the beams at various elevated temperature

Sections		$M_{FEA,T}$ (in kNm)						
$(D\times B\times t_w\times t_f)$ †	$\lambda_{L,20}$	*20°C*	*300°C*	*400°C*	*500°C*	*600°C*	*700°C*	*800°C*
200×80×8×12	0.165	135	133	120	82	46	20	11
200×80×6×11	0.180	113	109	98	69	38	17	9
200×80×3×7.5	0.237	63	58	52	38	22	10	5
200×100×4×6	0.370	63	56	50	37	23	11	6
200×120×5.5×8	0.398	105	95	86	63	37	18	9
200×120×2.8×5	0.609	98	86	77	60	36	17	9
200×150×4.5×7	0.626	54	46	41	32	20	9	5
200×150×4.4×6	0.743	84	72	65	51	31	14	7
200×150×3×4.5	0.996	59	49	44	34	21	10	5

† in mm

Figures

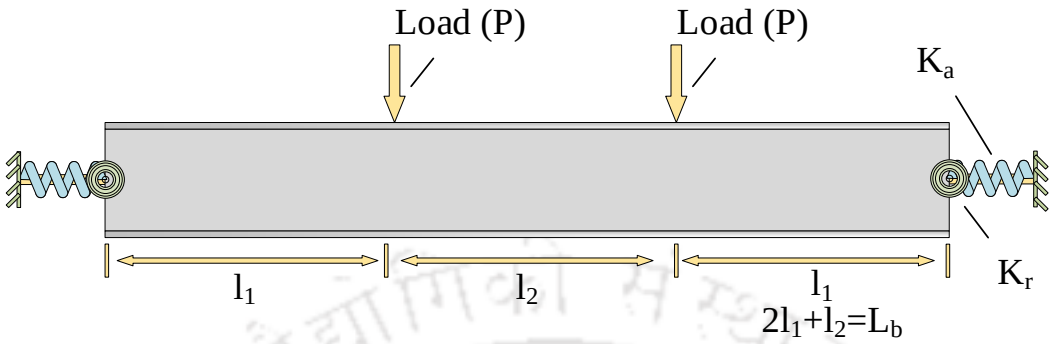

Figure 5-1 Schematic diagram for an axially and rotationally restrained beam under four-point bending load

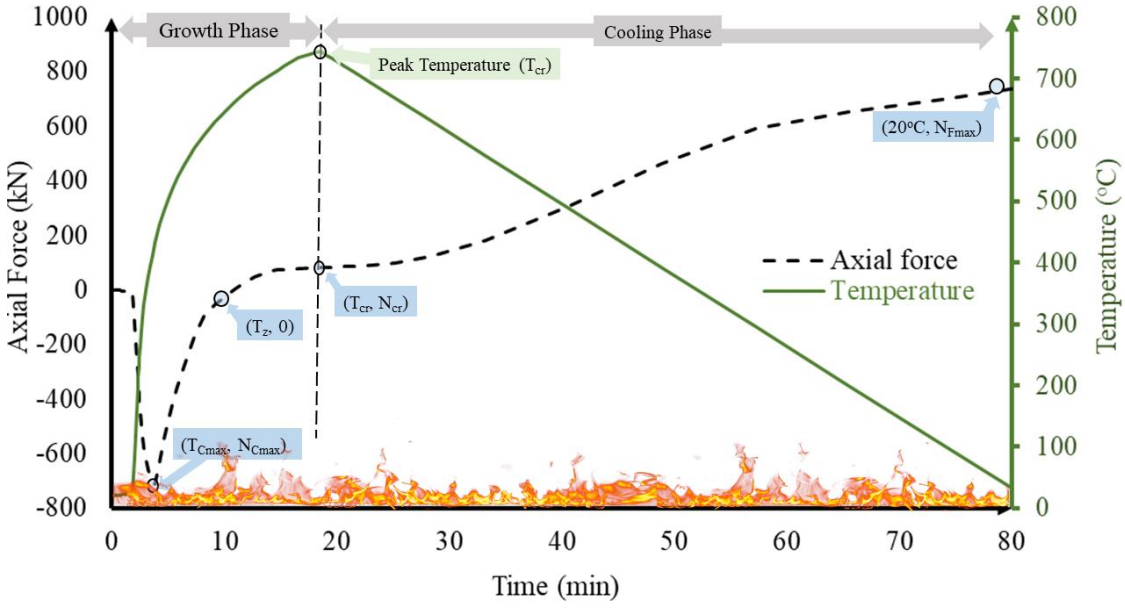

Figure 5-2 Typical representation of internal forces in a restrained beam in natural fire

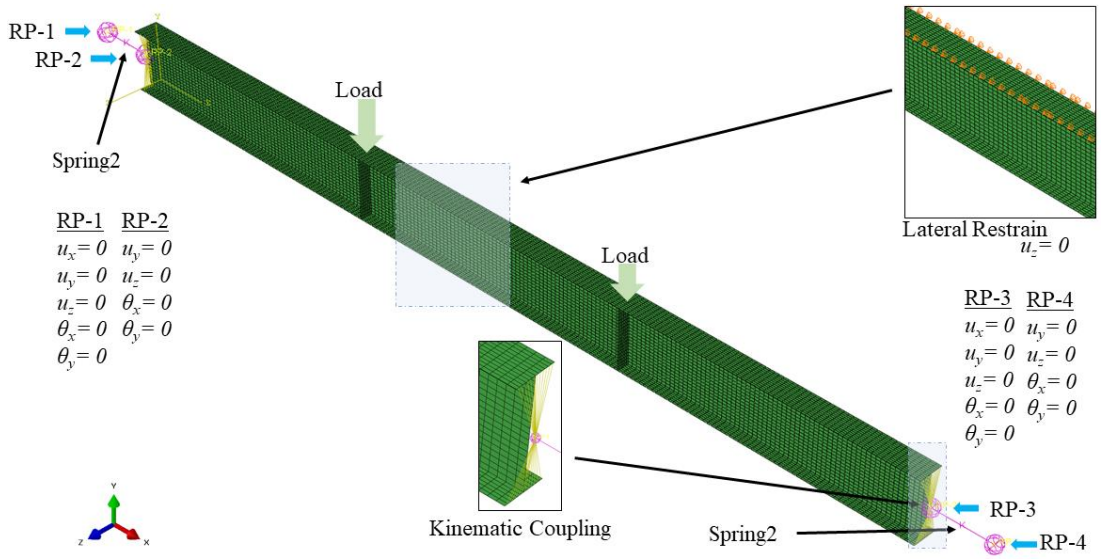

Figure 5-3 Boundary condition for current FE model

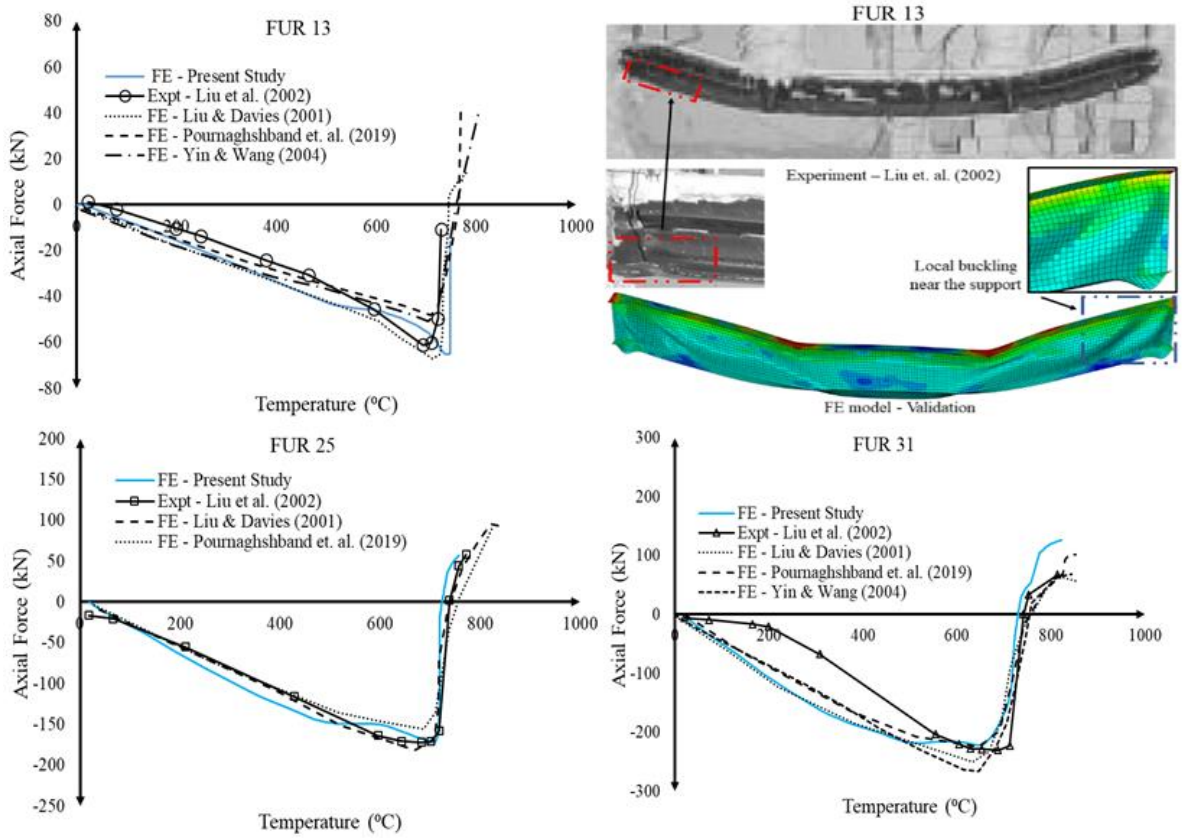

Figure 5-4 Present FE results compared with the experiments Li et al. (2002) - FUR 13, FUR 25 and FUR31. Comparison of failure model in the tested specimen (FUR 13) in Li et al. (2002) and current FE model

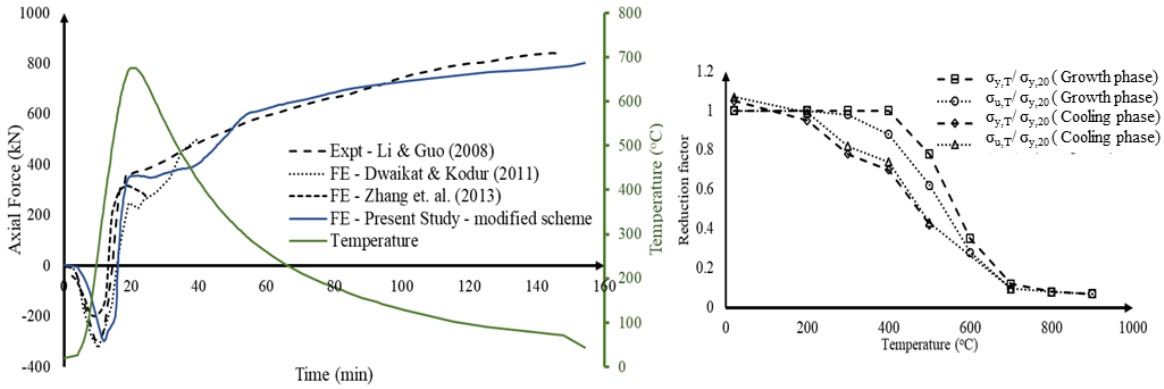

Figure 5-5 Comparison for axial force vs time between test (Li & Guo, 2008) and FE for Q235B grade steel. Reduction factor adopted in the present FE for growth and cooling phase.

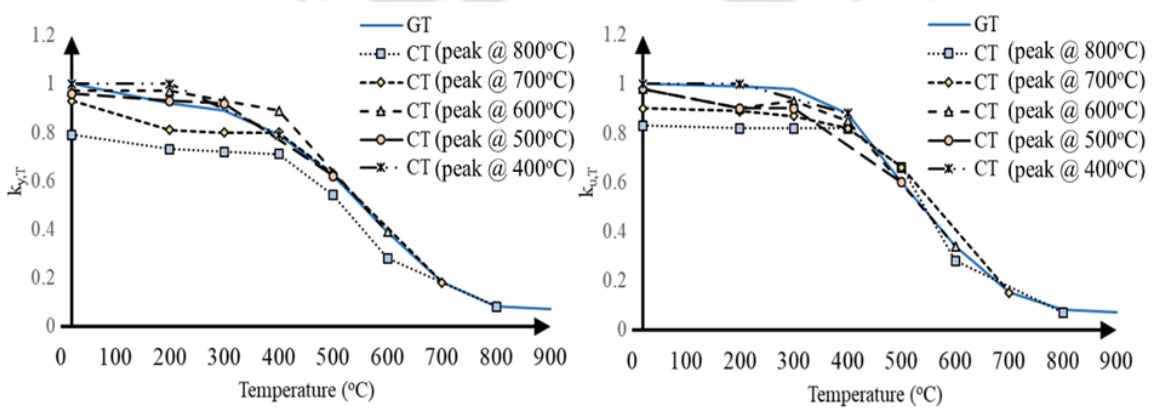

Figure 5-6 Reduction factor ($k_{y,T}$ and $k_{u,T}$) adopted in the FE models in growth (GT) and cooling (CT) phase

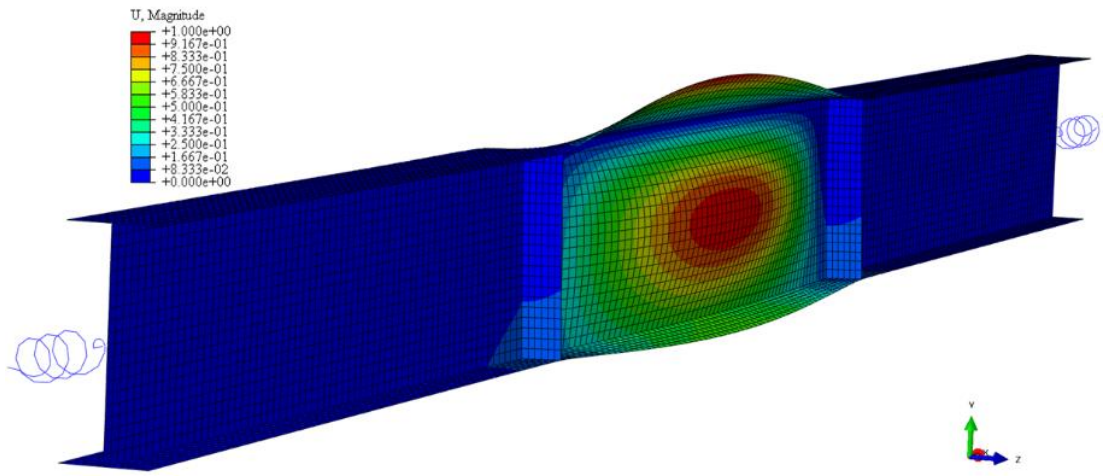

Figure 5-7 Imperfection mode in present FE model

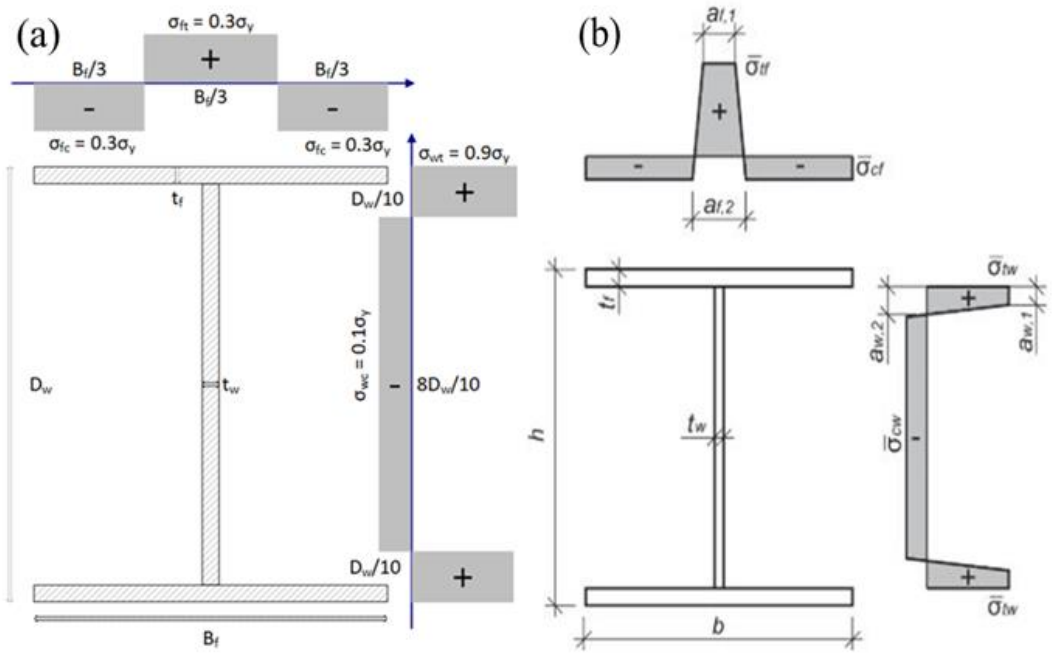

Figure 5-8 (a) Simplified residual stress model welded sections adopted in the current FE studies; (b) ECCS model

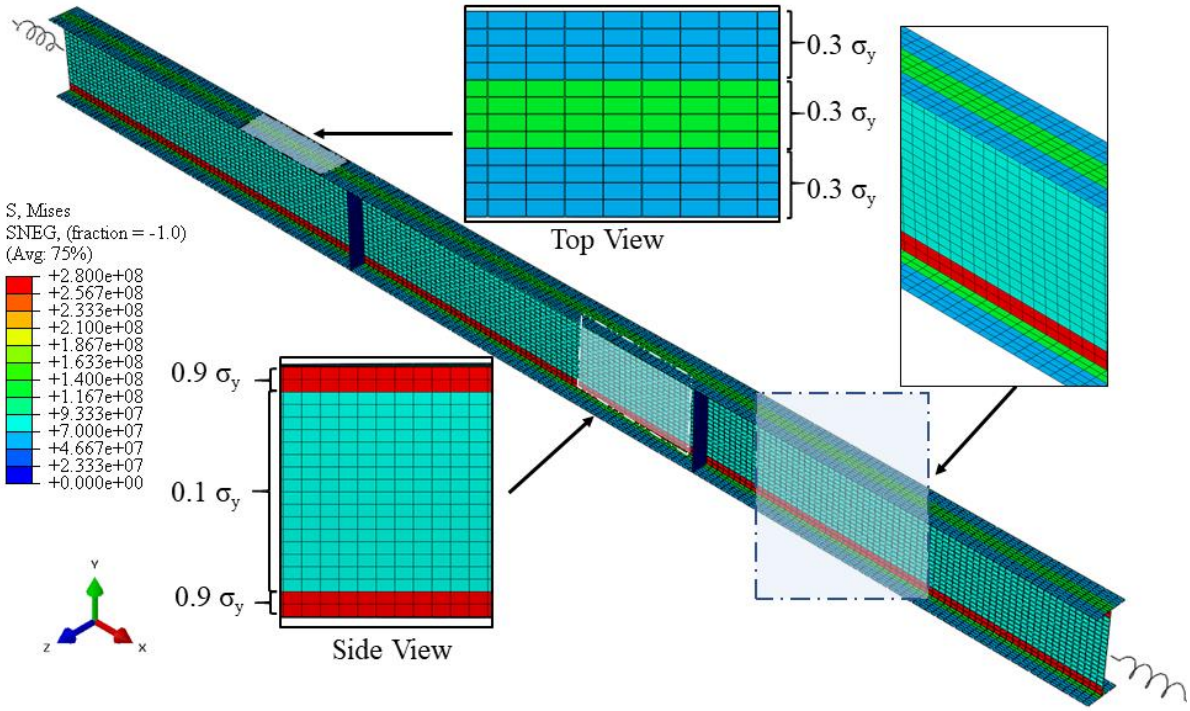

Figure 5-9 Residual stress pattern in current FE model

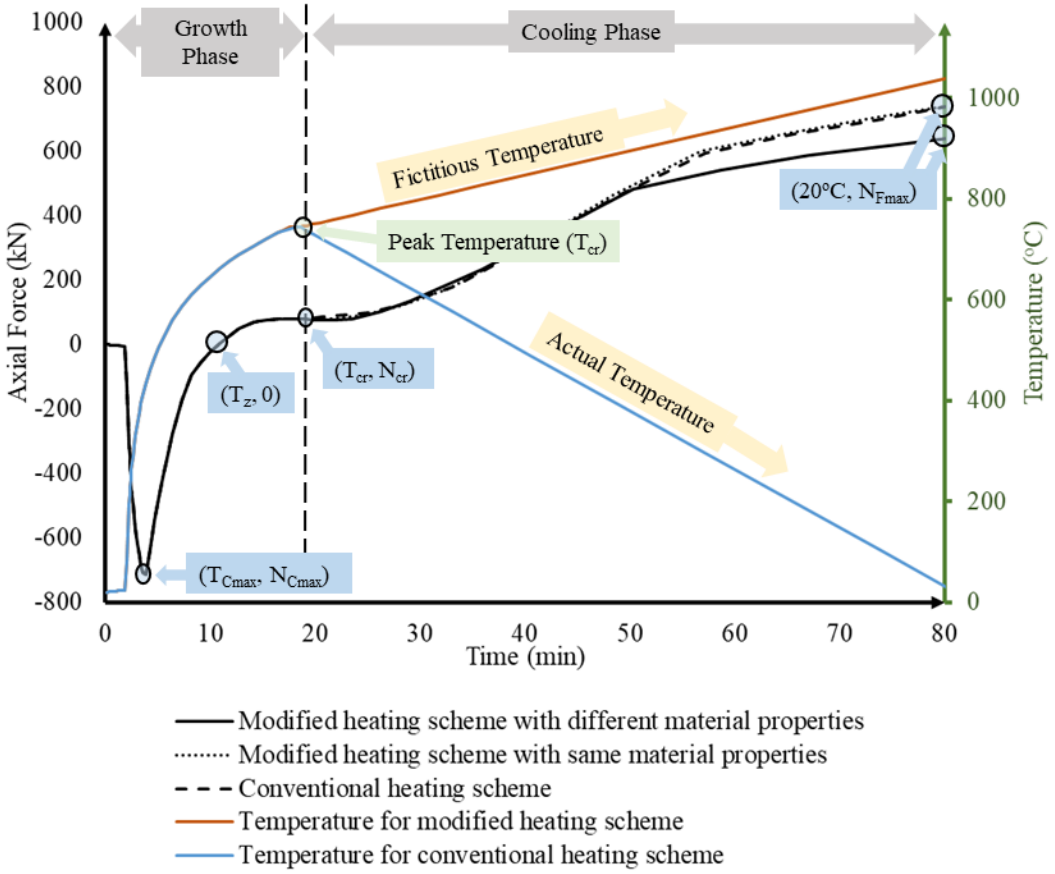

Figure 5-10 Illustration on numerical scheme for present FE models

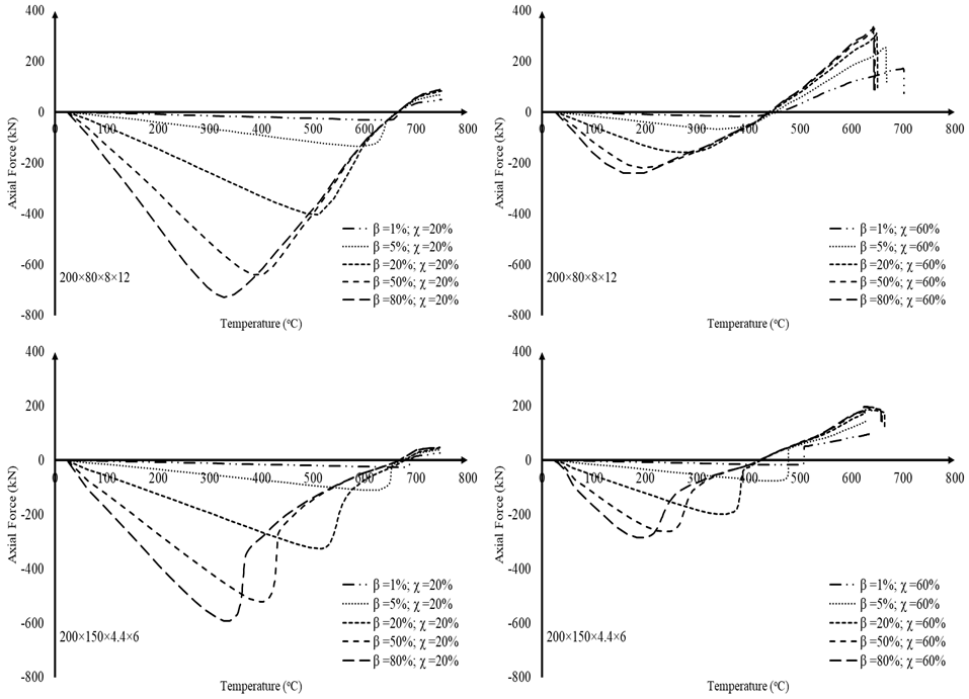

Figure 5-11 Effect of axial restraint (β = 1%, 5%, 20%, 50% and 80%) with same load ratio (χ = 20% or 60%) in 200×80×8×12 ($\lambda_{L,20}$ = 0.16) and 200×150×4.4×6 ($\lambda_{L,20}$=0.74) on axial force in growth phase

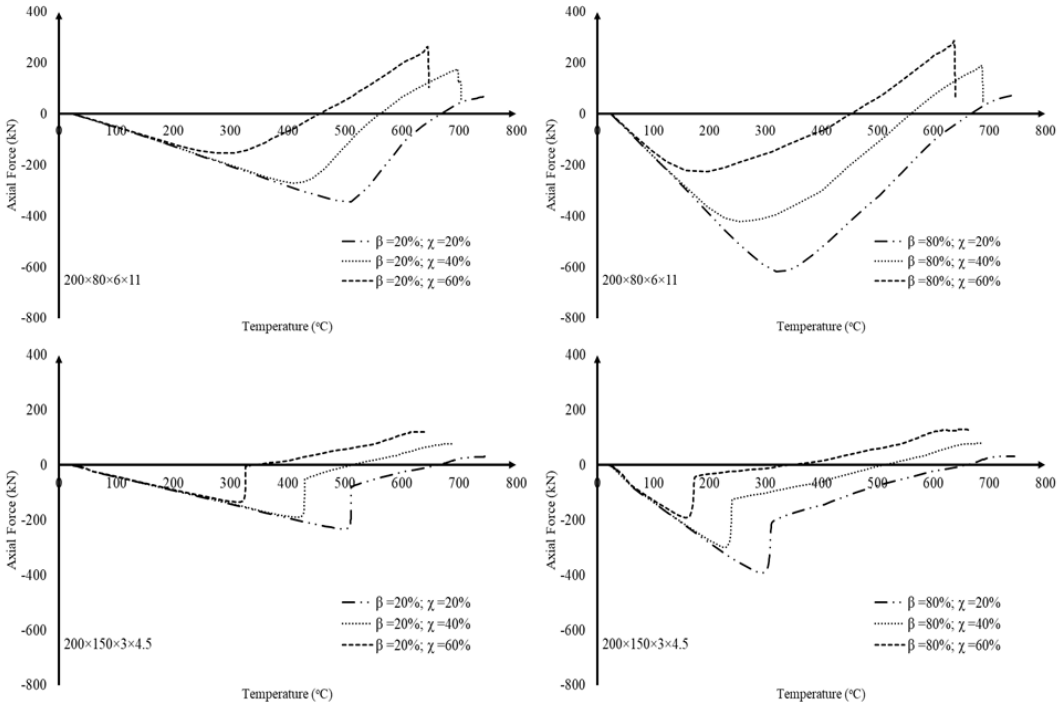

Figure 5-12 Effect of load ratio (χ = 20%, 40% and 60%) with same axial restraint (β = 20% or 80%) in 200×80×6×11 ($\lambda_{L,20}$ = 0.18) and 200×150×3×4.5 ($\lambda_{L,20}$ = 0.99) on axial force in growth phase

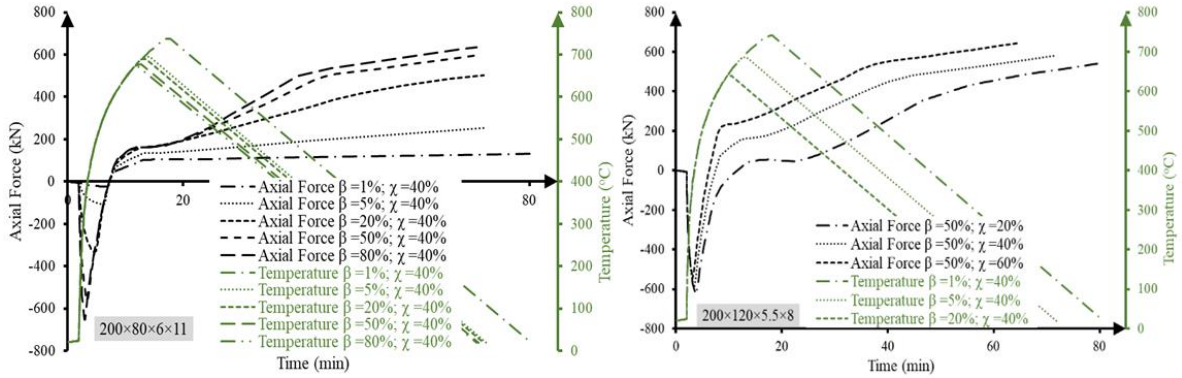

Figure 5-13 Effect of load ratio (χ = 40%) and axial restraint (β = 50%) in 200×80×6×11 ($\lambda_{L,20}$ = 0.18) and 200×150×5.5×8 ($\lambda_{L,20}$ = 0.40) respectively on axial force in cooling phase

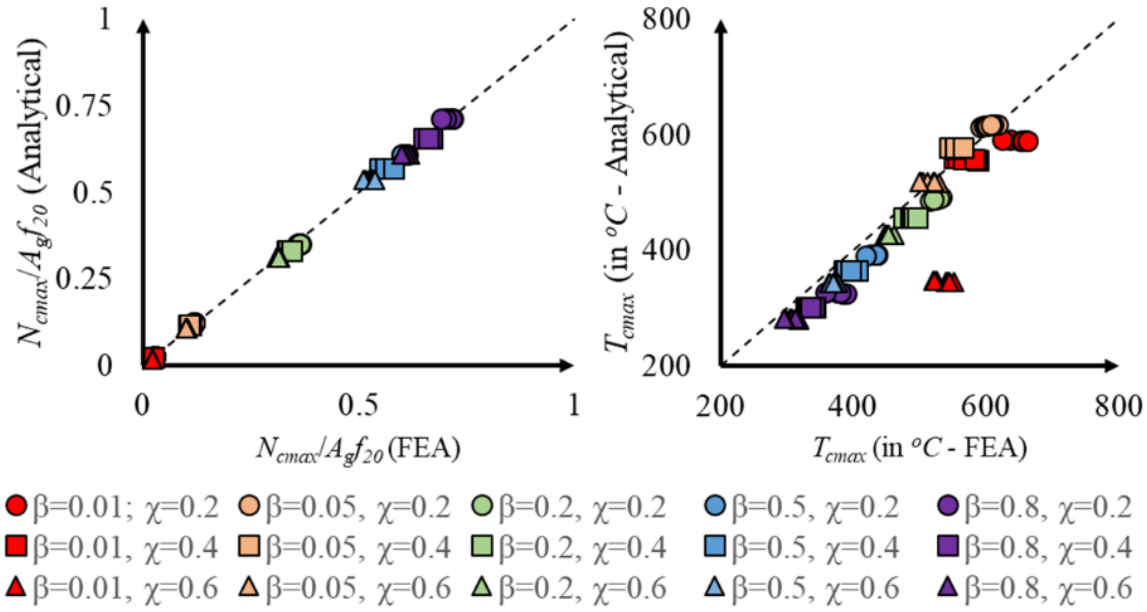

Figure 5-14 Comparison for the N_{Cmax} and T_{Cmax} estimated through Analytical and FE

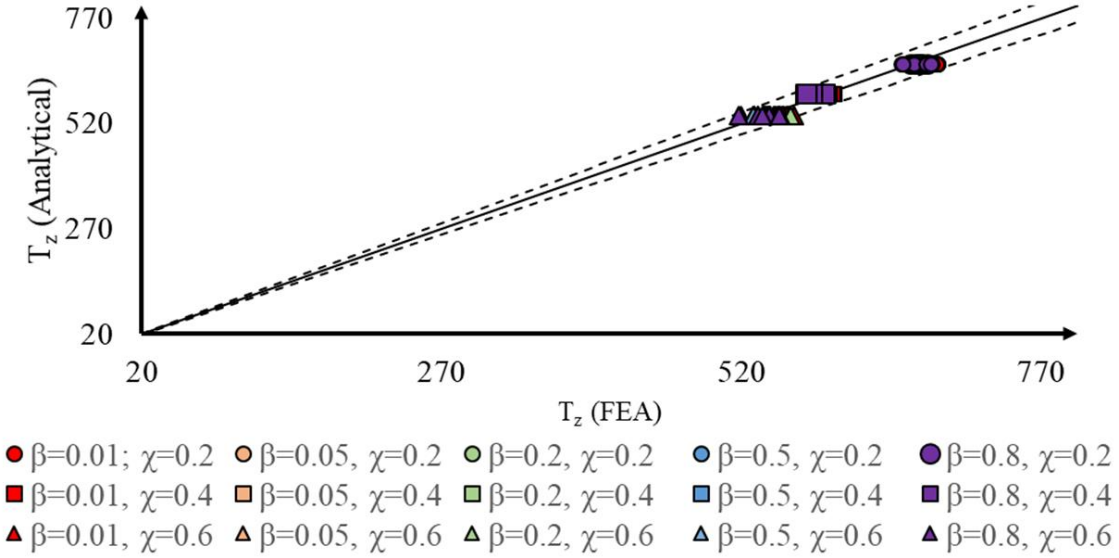

Figure 5-15 Comparison for the T_z estimated through Analytical and FE

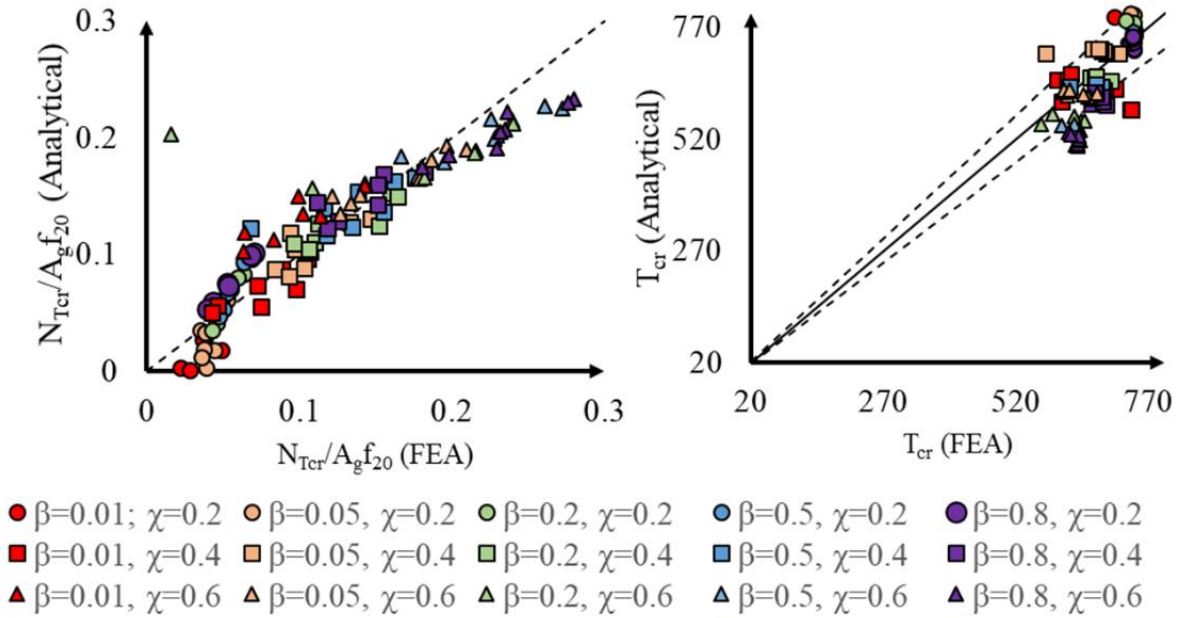

Figure 5-16 Comparison for the $N_{Tcr}/A_g\sigma_{y,20}$ and Tcr estimated through Analytical and FE

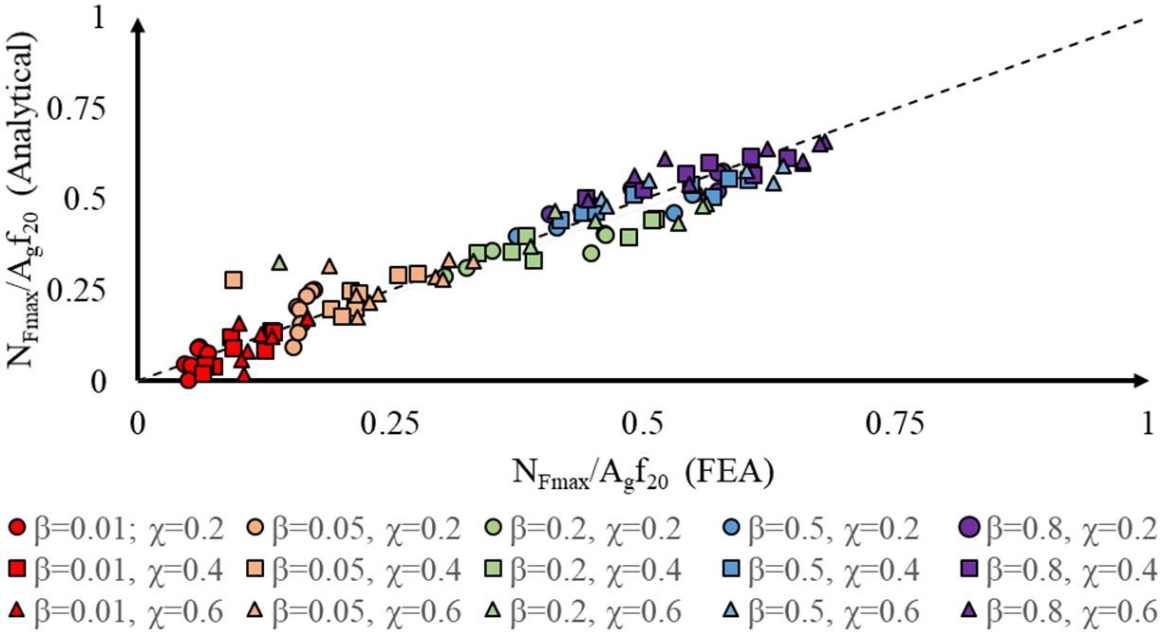

Figure 5-17 Comparison for the N_{Fmax} estimated through Analytical and FE

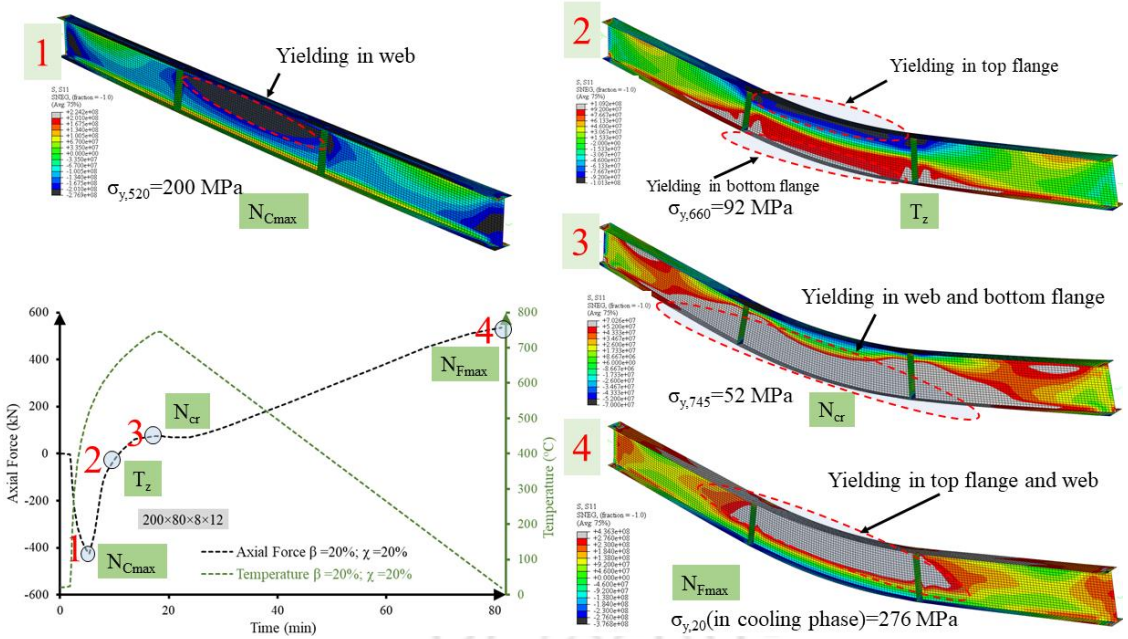

Figure 5-18 FE failure mode for 200×80×8×12 ($\lambda_{L,20}$=0.16)

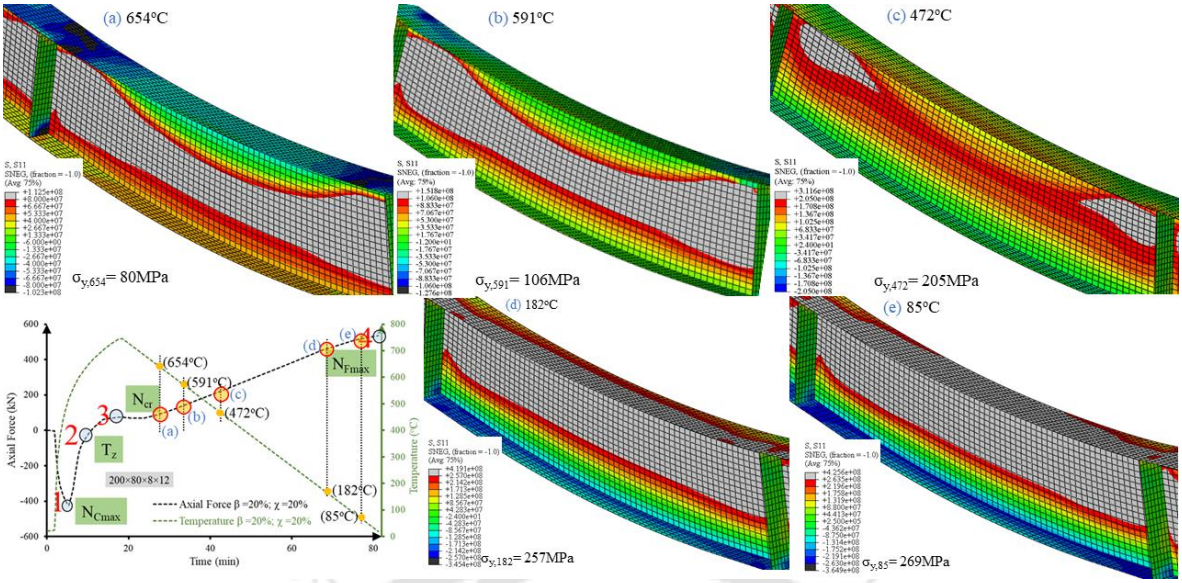

Figure 5-19 FE failure mode for 200×80×8×12 ($\lambda_{L,20}$ = 0.16) in cooling phase

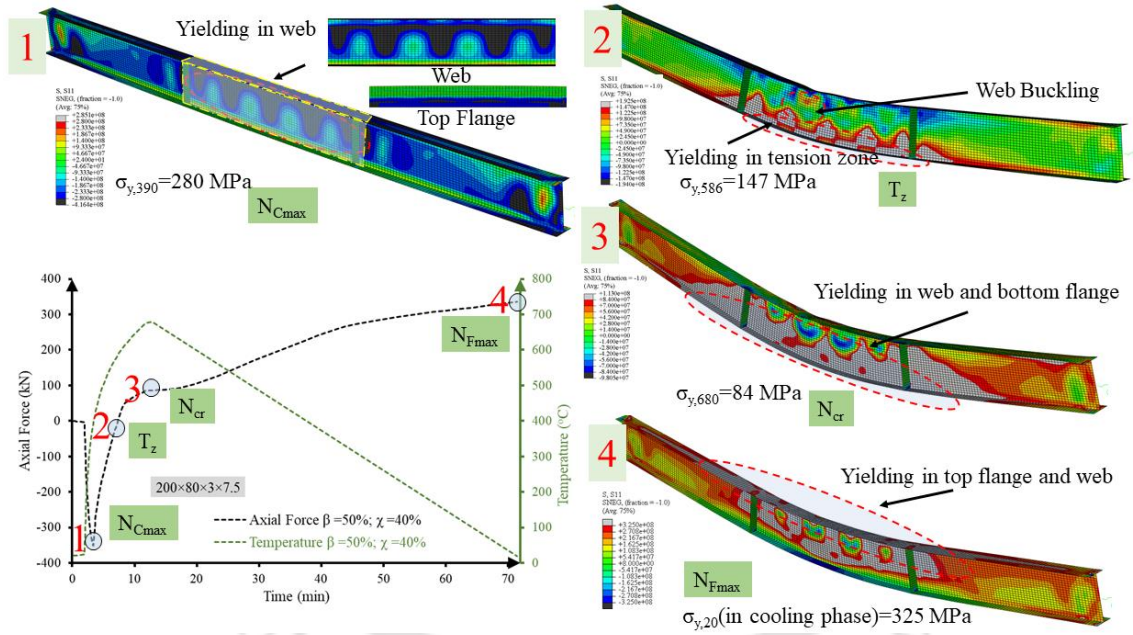

Figure 5-20 FE failure mode for 200×80×3×7.5 ($\lambda_{L,20}$ = 0.24)

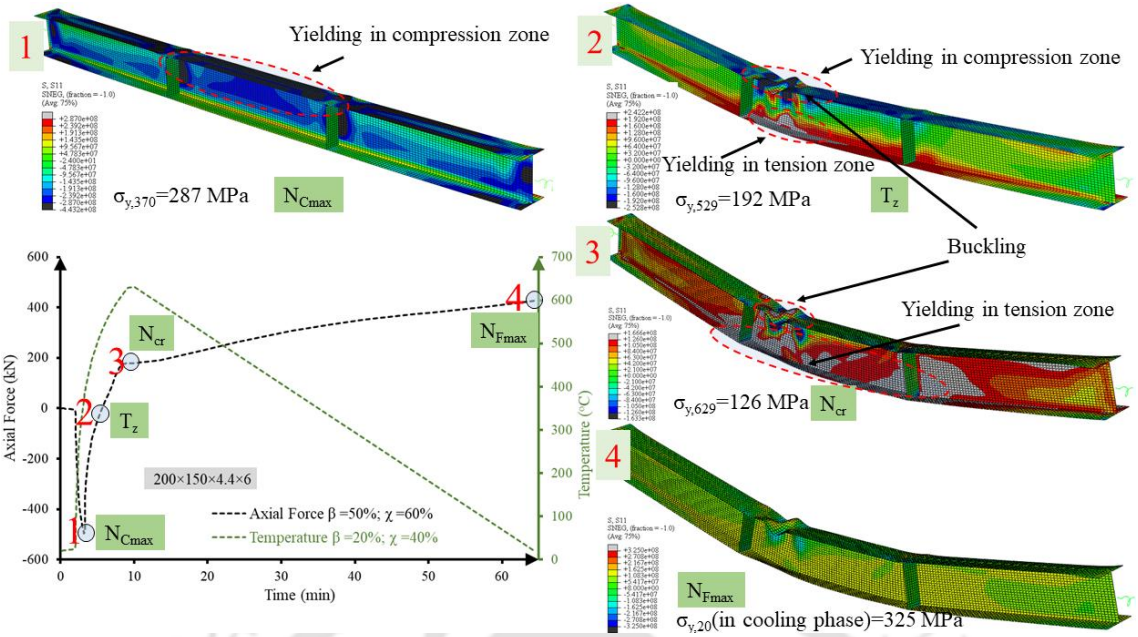

Figure 5-21 FE failure mode for 200×150×4.4×6 ($\lambda_{L,20}$ = 0.74)

CHAPTER 6: SUMMARY AND CONCLUSIONS

6.1 Summary of the present thesis work

In this thesis, mechanical tests are carried out on E350 steel and 10.9 Grade bolt in heating and cooling fire. Subsequently, the internal forces in axially restrained beams are assessed in heating and cooling fire. Summary of each work performed is briefly presented in the following subsections.

6.1.1 Mechanical properties of E350 in heating and cooling fire

The mechanical properties of E350 steel are evaluated in heating and cooling fire through experiments. Yield strength, ultimate strength and elastic modulus are estimated for specimens in growth, cooling and post fire phases, with a special emphasis on properties in cooling phase. Other studies like chemical analysis and micrographic studies are also carried out on post fire specimens. It has been found that, the existing model on reduction factors on growth phase fire is inadequate and hence, reduction factors are proposed for growth phase fire. The reduction factors in growth phase are proposed based on the present experimental and other literature. Since, there is no prior study on mechanical properties of steel in cooling fire, reduction factors are proposed on cooling phase based on present study. Stress strain models are proposed for heating and cooling fire based on the experimental results.

From the present study, it can be concluded that:

1) From the experimental results, it can be inferred that the mechanical properties in cooling phase are different from results in growth phase.

2) Interestingly, the rate of regain in strength in the cooling phase is lower than the rate of degradation in growth phase. Additionally, in general, it has been seen that, the mechanical properties have been able to regain complete strength, for elevated temperatures not exceeding 600°C.
3) Since, the stress strain relationship is not same in room temperature testing and growth and cooling phase fire, hence two stress strain models are proposed for (i) room temperature and post fire, and (ii) growth and cooling phase fire. Stress strain models are proposed based on the results from present experiments at room temperature, growth, cooling and post fire phases.
4) Large grain size micro-structures are seen in the micrographs of post fire specimen. The grain size increase as the peak temperature of the post fire specimen increase.
5) It is observed that heat treatment has no much affect on the chemical composition of the post fire specimen.

6.1.2 Mechanical strength of 10.9 Grade bolt in heating and cooling fire

The tensile and shear capacity of high strength steel 10.9 grade bolt in heating and cooling fire with emphasis on the mechanical respond of the bolts in cooling phase are found out in this section through experiments. Tensile and shear test set-up are developed to conduct tensile and shear tests respectively on 10.9 Grade bolt. M10 and M8 bolts are chosen for tensile and shear tests respectively. Reduction factors are proposed for growth and cooling phase fire. The growth phase reduction factor is proposed based on present experimental study and other experimental studies. The reduction factor in cooling phase is proposed based on the present experimental results. It is seen that the bolts do not regain much strength after 500^{o}C, after the specimen is heated above 600^{o}C.

From the present study, following conclusions are drawn:

1) The amount of strength reduction in tensile tests is more than the shear tests. Hence, separate reduction factors are proposed from tensile and shear specimens.

2) 10.9 Grade bolts do not regain much strength as compared to 8.8 Grade bolt in cooling phase.
3) In the cooling phase studies, below 500ºC - 400ºC, 10.9 Grade bolts do not further regain strength till they cool down completely.

6.1.3 Behavior of axially restrained beams in heating and cooling fire

There is a development of large internal forces in restrained beam during cooling phase fire. These forces are assessed in this work. After having validated the numerical models with existing experimental study, numerical investigation has been carried out to estimate the internal forces in axially restrained beams in heating and cooling fire. Two different materials are adopted in the numerical model based on the previous study on E350 steel in heating and cooling phase fire. A new heating scheme has been developed, called Modified Heating Scheme (MHS). This heating scheme allows keeping two different material properties in numerical model. After having displayed the suitability of the new scheme – MHS, parametric studies have been carried out. The parameters considered in this study are: cross sectional slenderness, aspect ratio, load ratio and amount of axial restraint. 3 types of analysis are carried out.

1. Firstly, moment capacity for each cross section is evaluated at 20ºC, 300ºC, 400ºC, 500ºC, 600ºC, 700ºC and 800ºC.
2. Secondly, loads are applied on axially restrained beam of certain load ratio (χ) at growth phase. At the end of second step, the maximum temperature (T_{cr}) till which a certain cross section of restrained beam can survive for a certain load (- load ratio, χ) and axial restraint (β) is estimated.
3. In the third type of analysis, beams are heated upto maximum temperature (T_{cr}) and then allowed to cool. The internal forces in the beam are estimated in cooling phase.

Analytical model is developed, which is the extension of previous work (other authors' studies) to cooling phase fire. Empirical coefficients are proposed in these analytical models, based on curve fitting with numerical results. Failure modes are presents for typical beams based on their

cross-sectional slenderness. An example is presented to evaluate the forces in restrained beam at the end of cooling phase fire.

Conclusions based on the present study are presented here:

1) In growth phase fire, the maximum compressive force increases and the temperature decreases as the axial restraint increases for same load ratio and cross section. Once, the catenary kicks in the beam, the axial restraint does not have influence critical temperature and axial force at the end of growth phase for same load ratio and member cross section.
2) In growth phase fire, the maximum compressive force in the beam decreases as load ratio increases for same axial restrained and member cross section. The peak temperature and maximum axial at the growth phase's end decrease and increase respectively.
3) In cooling phase fire, maximum tensile force in the beam at the end of cooling phase is higher for beams with larger amount of axial restrain, while load ratio has little influence on internal force.
4) The beam starts to yield (compressive yielding) when the beam reaches maximum compressive force. Based on cross sectional slenderness, the yielding appears in the top web for plastic section or in the flange in slender section. For slender cross section, the member buckles post maximum compressive force is reached.
5) At the end of growth phase, maximum portion of beam (bottom flange and most of the web) undergoes tensile yielding.The zone of tensile yielding changes as the member cools to accommodate thermal contraction and plastic deformation (during growth phase).

6.2 Scope of future work

It has been shown in the present work that it is important to assess the internal forces in the beam. Based on the present work, further works that can be carried out are listed below:

1. The internal force in restrained beam can exerts moment in the adjacent column; the internal moments in column can be assessed.
2. The internal forces can be assessed for different beam geometry (like channel, angle sections), slenderness (shear dominated beams), initial loading condition etc.
3. The material properties are evaluated only for E350 steel and can be found out for other grade of steel like E410, S700, S800 etc. and stainless steel – AISI 301, 304 etc. It is important to experimentally assess the mechanical properties of steel in cooling.
4. More detailed numerical studies using solid elements can be carried to understand the stress flow and failure mode in connection during cooling phase.
5. Bolts and welds constitute the connection in steel buildings. Welds and other grades of bolts can be tested in heating and cooling fire.

Appendix A: Numerical and analytical results for the restrained beams in heating and cooling fire

The results for the restrained beams in natural fire is presented here. The numerical and analytical values are annoted with phi symbol ($^{\varphi}$) and hash symbol ($^{\#}$) respectively. The results are presented for each beam cross section separately.

		200×80×8×12											
χ	β	N_{Cmax} (kN)	#N_{Cmax} (kN)	T_{Cmax} (°C)	$\#T_{Cmax}$ (°C)	T_z (°C)	$\#T_z$ (°C)	T_{cr} (°C)	$\#T_{cr}$ (°C)	N_{Tcr} (kN)	$\#N_{Tcr}$ (kN)	N_{Fmax} (kN)	$\#N_{Fmax}$ (kN)
0.2	0.01	31	30	636	591	662	663	743	751	44	34	70	113
0.2	0.05	137	144	592	613	661	663	743	797	61	71	202	295
0.2	0.2	424	409	521	488	661	663	744	751	74	97	537	473
0.2	0.5	713	708	433	393	660	663	744	733	80	111	641	602
0.2	0.8	835	829	377	327	660	663	743	718	82	118	674	672
0.4	0.01	27	28	551	560	583	592	736	586	121	115	152	162
0.4	0.05	124	137	551	577	581	592	714	710	171	152	322	345
0.4	0.2	392	387	484	456	580	592	686	632	186	178	595	523
0.4	0.5	664	663	395	365	579	592	689	614	205	192	680	652
0.4	0.8	767	763	331	302	579	592	690	596	212	199	706	722
0.6	0.01	25	17	521	347	543	538	688	--	167	187	194	206
0.6	0.05	115	122	502	517	541	538	660	613	229	224	358	388
0.6	0.2	361	363	449	427	540	538	637	547	279	250	654	566
0.6	0.5	601	623	377	344	539	538	633	528	304	265	766	695
0.6	0.8	710	708	319	281	538	538	636	503	326	272	791	765

200×80×6×11

χ	β	N_{Cmax} (kN)	$\#N_{Cmax}$ (kN)	T_{Cmax} (°C)	$\#T_{Cmax}$ (°C)	T_z (°C)	$\#T_z$ (°C)	T_{cr} (°C)	$\#T_{cr}$ (°C)	N_{Tcr} (kN)	$\#N_{Tcr}$ (kN)	N_{Fmax} (kN)	$\#N_{Fmax}$ (kN)
0.2	0.01	26	25	624	592	666	663	744	762	36	26	58	92
0.2	0.05	117	123	597	615	665	663	736	799	48	58	169	247
0.2	0.2	361	348	524	489	664	663	739	753	59	80	457	398
0.2	0.5	605	602	436	394	664	663	730	735	63	92	542	508
0.2	0.8	710	704	377	327	664	663	743	720	67	98	567	568
0.4	0.01	23	24	560	559	585	592	737	586	105	95	132	134
0.4	0.05	107	116	549	577	584	592	691	710	132	126	254	289
0.4	0.2	332	329	476	456	583	592	689	634	162	148	503	440
0.4	0.5	563	563	389	365	582	592	675	616	161	161	598	550
0.4	0.8	653	648	331	302	582	592	663	597	154	166	635	610
0.6	0.01	21	14	525	347	547	538	686	--	141	156	165	171
0.6	0.05	98	104	501	517	544	538	657	614	207	188	328	326
0.6	0.2	308	308	451	427	543	538	636	548	237	210	553	477
0.6	0.5	518	529	370	344	542	538	637	529	270	222	632	587
0.6	0.8	606	602	318	281	542	538	631	505	273	228	668	646

200×80×3×7.5

χ	β	N_{Cmax} (kN)	$\#N_{Cmax}$ (kN)	T_{Cmax} (°C)	$\#T_{Cmax}$ (°C)	T_z (°C)	$\#T_z$ (°C)	T_{cr} (°C)	$\#T_{cr}$ (°C)	N_{Tcr} (kN)	$\#N_{Tcr}$ (kN)	N_{Fmax} (kN)	$\#N_{Fmax}$ (kN)
0.2	0.01	17	16	659	589	678	663	705	793	30	11	42	49
0.2	0.05	72	76	610	616	672	663	742	805	26	30	102	145
0.4	0.01	14	15	556	559	592	592	605	604	55	53	56	75
0.4	0.05	67	72	553	575	575	592	575	710	58	73	58	171
0.4	0.5	351	350	391	365	586	592	676	620	85	94	335	333
0.4	0.8	400	402	329	302	583	592	685	602	93	98	347	370
0.6	0.01	13	9	541	345	559	538	559	--	61	92	61	98
0.6	0.05	62	65	521	517	548	538	617	615	114	111	116	194
0.6	0.2	191	191	461	427	561	538	567	553	10	125	253	288
0.6	0.5	326	328	364	344	551	538	636	533	139	132	370	356
0.6	0.8	374	374	307	281	550	538	636	510	145	136	382	393

200×100×4×6

χ	β	N_{Cmax} (kN)	$\#N_{Cmax}$ (kN)	T_{Cmax} (°C)	$\#T_{Cmax}$ (°C)	T_z (°C)	$\#T_z$ (°C)	T_{cr} (°C)	$\#T_{cr}$ (°C)	N_{Tcr} (kN)	$\#N_{Tcr}$ (kN)	N_{Fmax} (kN)	$\#N_{Fmax}$ (kN)
0.2	0.01	19	17	660	589	683	663	742	848	15	2	31	34
0.2	0.05	81	85	599	615	675	663	742	812	24	24	107	141
0.2	0.2	249	240	533	492	670	663	740	769	30	39	239	246
0.2	0.5	413	415	435	394	653	663	741	749	37	48	299	321
0.2	0.8	482	486	384	326	655	663	737	734	36	52	333	362
0.4	0.01	16	16	580	557	593	592	689	621	49	50	64	63
0.4	0.05	75	80	560	577	586	592	681	716	66	71	143	170
0.4	0.2	234	227	492	456	583	592	676	647	77	86	262	275
0.4	0.5	389	389	390	365	584	592	669	628	79	95	335	350
0.4	0.8	453	448	343	302	584	592	665	611	76	99	370	391
0.6	0.01	15	10	539	346	556	538	646	--	70	92	83	89
0.6	0.05	70	72	523	517	549	538	648	620	121	114	201	196
0.6	0.2	217	213	454	427	543	538	644	559	147	129	309	300
0.6	0.5	363	365	372	344	543	538	641	540	157	137	345	376
0.6	0.8	421	415	304	281	543	538	640	517	160	141	356	417

200×120×5.5×8

χ	β	N_{Cmax} (kN)	$\#N_{Cmax}$ (kN)	T_{Cmax} (°C)	$\#T_{Cmax}$ (°C)	T_z (°C)	$\#T_z$ (°C)	T_{cr} (°C)	$\#T_{cr}$ (°C)	N_{Tcr} (kN)	$\#N_{Tcr}$ (kN)	N_{Fmax} (kN)	$\#N_{Fmax}$ (kN)
0.2	0.01	28	26	651	590	676	663	740	857	29	1	53	45
0.2	0.05	122	127	600	615	676	663	741	814	39	33	164	206
0.2	0.2	374	360	528	490	675	663	743	770	49	56	459	363
0.2	0.5	624	624	425	392	672	663	738	750	54	69	544	477
0.2	0.8	734	730	389	326	674	663	742	736	55	75	588	538
0.4	0.01	25	24	566	558	595	592	709	631	100	72	129	89
0.4	0.05	112	120	545	577	593	592	687	716	110	105	223	250
0.4	0.2	350	341	486	456	591	592	700	648	156	127	498	407
0.4	0.5	592	584	406	365	589	592	686	629	160	140	583	520
0.4	0.8	687	672	341	302	589	592	682	612	155	146	624	582
0.6	0.01	22	15	523	347	557	538	657	--	117	136	135	127
0.6	0.05	103	108	505	517	555	538	673	621	183	168	309	288
0.6	0.2	324	320	448	427	553	538	649	560	220	191	548	445
0.6	0.5	548	549	371	344	552	538	637	541	234	204	645	559
0.6	0.8	634	624	307	281	552	538	639	519	237	210	674	620
0.2	0.05	72	75	618	618	669	663	737	822	27	11	98	96

200×120×2.8×5

χ	β	N_{Cmax} (kN)	$\#N_{Cmax}$ (kN)	T_{Cmax} (^oC)	$\#T_{Cmax}$ (^oC)	T_z (^oC)	$\#T_z$ (^oC)	T_{cr} (^oC)	$\#T_{cr}$ (^oC)	N_{Tcr} (kN)	$\#N_{Tcr}$ (kN)	N_{Fmax} (kN)	$\#N_{Fmax}$ (kN)
0.2	0.05	72	75	618	618	669	663	737	822	27	11	98	96
0.4	0.01	15	14	588	555	597	592	597	651	45	34	45	26
0.4	0.05	66	71	559	577	576	592	665	720	51	53	115	121
0.4	0.2	202	201	489	456	576	592	660	656	58	66	203	214
0.4	0.5	332	345	385	365	575	592	622	637	41	74	266	281
0.6	0.05	63	64	529	517	539	538	609	625	74	91	131	144
0.6	0.5	310	324	365	344	530	538	607	548	101	112	278	304

200×150×4.5×7

χ	β	N_{Cmax} (kN)	$\#N_{Cmax}$ (kN)	T_{Cmax} (^oC)	$\#T_{Cmax}$ (^oC)	T_z (^oC)	$\#T_z$ (^oC)	T_{cr} (^oC)	$\#T_{cr}$ (^oC)	N_{Tcr} (kN)	$\#N_{Tcr}$ (kN)	N_{Fmax} (kN)	$\#N_{Fmax}$ (kN)
0.2	0.01	28	26	655	589	683	663	739	910	26	- -	50	4
0.2	0.05	122	127	602	615	674	663	741	821	38	19	165	165
0.2	0.2	368	361	515	487	671	663	742	779	47	42	334	322
0.2	0.5	615	625	435	394	669	663	741	758	51	55	425	436
0.2	0.8	721	731	381	326	679	663	741	744	44	61	462	498
0.4	0.01	24	24	586	556	596	592	616	651	48	58	68	48
0.4	0.05	112	121	553	577	581	592	680	719	106	90	221	209
0.4	0.2	345	341	491	456	580	592	668	656	113	113	380	366
0.4	0.5	578	585	390	365	578	592	683	637	138	126	465	480
0.4	0.8	670	673	332	302	579	592	671	620	129	132	513	542
0.6	0.01	23	15	544	345	564	538	585	--	66	122	112	86
0.6	0.05	103	108	512	517	543	538	622	625	144	154	244	247
0.6	0.8	628	625	313	281	534	538	639	526	236	196	505	580

200×150×3×4.5													
χ	β	N_{Cmax} (kN)	$\#N_{Cmax}$ (kN)	T_{Cmax} (^oC)	$\#T_{Cmax}$ (^oC)	T_z (^oC)	$\#T_z$ (^oC)	T_{cr} (^oC)	$\#T_{cr}$ (^oC)	N_{Tcr} (kN)	$\#N_{Tcr}$ (kN)	N_{Fmax} (kN)	$\#N_{Fmax}$ (kN)
0.2	0.05	80	83	611	617	662	663	741	830	26	2	103	64
0.6	0.01	15	10	552	344	558	538	577	--	43	69	70	13
0.6	0.05	68	71	523	517	534	538	612	630	86	90	146	118
0.6	0.2	213	210	450	427	520	538	590	575	73	105	94	221
0.6	0.8	406	409	298	281	518	538	619	535	121	118	300	336

200×150×4.4×6													
χ	β	N_{Cmax} (kN)	$\#N_{Cmax}$ (kN)	T_{Cmax} (^oC)	$\#T_{Cmax}$ (^oC)	T_z (^oC)	$\#T_z$ (^oC)	T_{cr} (^oC)	$\#T_{cr}$ (^oC)	N_{Tcr} (kN)	$\#N_{Tcr}$ (kN)	N_{Fmax} (kN)	$\#N_{Fmax}$ (kN)
0.2	0.01	26	23	663	589	683	663	741	935	26	- -	46	-18
0.2	0.05	110	114	608	616	670	663	738	825	33	11	145	126
0.2	0.2	334	323	520	488	667	663	727	784	39	32	278	267
0.2	0.5	551	559	419	392	666	663	742	762	43	43	344	368
0.2	0.8	635	654	359	327	678	663	739	749	36	48	373	424
0.4	0.01	22	22	583	557	593	592	624	665	39	46	58	21
0.4	0.05	99	108	566	578	579	592	676	722	86	75	184	165
0.4	0.2	317	305	497	457	582	592	670	660	98	95	359	306
0.4	0.5	533	523	396	365	573	592	672	640	108	107	383	408
0.4	0.8	607	602	336	302	574	592	670	624	109	112	407	463
0.6	0.01	20	13	544	345	555	538	607	--	77	103	94	55
0.6	0.05	91	97	501	517	541	538	622	628	123	132	211	199
0.6	0.2	289	286	453	427	531	538	631	570	167	153	357	340
0.6	0.5	495	492	371	344	530	538	630	551	179	164	426	442
0.6	0.8	551	559	296	281	537	538	624	530	182	169	501	497

Appendix B: ABAQUS input file

Typical ABAQUS input file (annotated) for the cooling phase analysis

Annotated script	Remarks
*Heading	
*PARTS *Part, name=complete_beam	Parts of the model part: complete beam parts
*Node [: . . . :]	nodes of model
*Element, type=S4RT [: . . . :]	elements of model
*Nset, nset=Set_int_tf, internal [: . . . :]	nodes in top flange
*Elset, elset=Set_int_tf, internal [: . . . :]	elements in top flange
*Nset, nset=Set_int_bf, internal [: . . . :]	nodes in bottom flange
*Elset, elset=Set_int_bf, internal [: . . . :]	elements in bottom flange
*Nset, nset=Set_int_web, internal [: . . . :]	nodes in web
*Elset, elset=Set_int_web, internal [: . . . :]	elements in web
*Nset, nset=Set_int_stfr, internal [: . . . :]	nodes in stiffner
*Elset, elset=Set_int_stfr, internal [: . . . :]	Elements in stiffner
**Section: Top_Flange *Shell section, eleset= Set_int_tf, material= E350 t_f, 5	top flange thickness
**Section: Bottom_Flange *Shell section, eleset= Set_int_bf, material= E350 t_f, 5	bottom flange thickness
**Section: Web *Shell section, eleset= Set_int_web, material= E350 t_w, 5	web thickness
**Section: Stiffner *Shell section, eleset= Set_int_stfr, material= E350 t_w, 5	stiffner thickness
*End Part	

**	
**ASSEMBLY *Assembly, name=model_assembly *Instance, name=beam1, instance= complete_beam *End Instance **	
*Node 1, [rp_1] *Node 2, [rp_2] *Node 3, [rp_3] *Node 4, [rp_4]	Ref point rp_1 rp_2 rp_3 rp_4
*Nset, nset= Set_left_fixed 1 *Nset, nset= Set_rp2 2 *Nset, nset= Set_rp3 3 *Nset, nset= Set_right_fixed 4	Assigning nodes to ref point rp_1 to fixed support on left rp_2 to beam edge on left rp_3 to beam edge on right rp_4 to fixed support on right
*Nset, nset=loading, instance=beam1 [: . . . :] *Elset, elset=loading, instance=beam1 [: . . . :] *Nset, nset=lateral, instance=beam1 [: . . . :] *Elset, elset=lateral, instance=beam1 [: . . . :] *Nset, nset=set_bfc, instance=beam1 [: . . . :] *Elset, elset=set_bfc, instance=beam1 [: . . . :] *Nset, nset=set_bft, instance=beam1 [: . . . :] *Elset, elset=set_bft, instance=beam1 [: . . . :] *Nset, nset=set_tfc, instance=beam1 [: . . . :] *Elset, elset=set_tfc, instance=beam1 [: . . . :] *Nset, nset=set_tft, instance=beam1 [: . . . :] *Elset, elset=set_tft, instance=beam1	Assigning node and element set Points where load is applied edge of the top flange residual stress: bottom flange in compression residual stress: bottom flange in tension residual stress: top flange in tension

[: . . . :] *Elset, elset=set_wt, instance=beam1 [: . . . :] *Nset, nset=set_wc, instance=beam1 [: . . . :] *Elset, elset=set_wc, instance=beam1 [: . . . :]	residual stress: web in tension residual stress: web in compression
*Nset, nset=Set_rp1, internal 1 *Nset, nset=Set_rp4, internal 4	fixed end left fixed end right
*Elset, elset=_s_Surf_left_end_E3, internal, instance= beam1 [: . . . :] *Surfaces, type=ELEMENT, name=s_Surf_left_end _s_Surf_left_end_E3, E3 *Elset, elset=_s_Surf_right_end_E3, internal, instance= beam1 [: . . . :] *Surfaces, type=ELEMENT, name=s_Surf_right_end _s_Surf_right_end_E3, E3	elements on left edge of beam elements on right edge of beam
[: . . . :] *Surface, type= ELEMENT, name= stf_l2_heat _stf_l2_heat_SPOS,SPOS	
** Constraint: constrain_left *Coupling, constraint name= cnst_left, ref node= Set_rp2, surface= s_Surf_left_end *Kinematic ** Constraint: constrain_right *Coupling, constraint name= cnst_left, ref node= Set_rp3, surface= s_Surf_right_end	kinematic coupling rp_2 – left edge (beam) kinematic coupling rp_3 – right edge (beam)
*Kinematic *Spring, elset=Left-spring 1,1 βK_a *Element, type=Spring2, elset=Left-spring 1,2,1 *Spring, elset=Right-spring 1,1 βK_a *Element, type=Spring2, elset=Right-spring 3,3,4 *End Assembly	spring: rp_1 – rp_2 spring: rp_3 – rp_4
*Amplitude, name= Fire_amp [: . . . :] *Amplitude, name= Load_amp [: . . . :] **	fire input; time - temperature load input; time - load
**MATERIALS ** **Material, name= E350 *Conductivity [: . . . :] *Density	conductivity

[: . . . :] *Elastic [: . . . :] *Expansion [: . . . :] *Plastic [: . . . :] *Specific Heat [: . . . :] **	density elastic property expansion plastic property specific heat property
** PHYSICAL CONSTANTS ** *Physical Constants, absolute zero= -273.15, stefan boltzmann= 5.67e-8 **	Physical constants
**BOUNDARY CONDITIONS ** ** Name: Left Type: Displacement/Rotation *Boundary Set_left_fixed, 1, 1 Set_left_fixed, 2, 2 Set_left_fixed, 3, 3 Set_left_fixed, 5, 4 Set_left_fixed, 5, 5 ** Name: Left_spring Type: Displacement/Rotation *Boundary Set_rp2, 2, 2 Set_rp2, 3, 3 Set_rp2, 5, 4 Set_rp2, 5, 5 ** Name: Right_spring Type: Displacement/Rotation *Boundary Set_rp3, 2, 2 Set_rp3, 3, 3 Set_rp3, 5, 4 Set_rp3, 5, 5 ** Name: Right Type: Displacement/Rotation *Boundary Set_right_fixed, 1, 1 Set_right_fixed, 2, 2 Set_right_fixed, 3, 3 Set_right_fixed, 5, 4 Set_right_fixed, 5, 5 ** Name: lateralBC Type: Displacement/Rotation *Boundary lateral, 3, 3 **	boundary condition: left fixed end boundary condition: left beam edge boundary condition: right beam edge boundary condition: right beam end lateral support
**PREDEFINED FIELDS ** **Name: bfc Type: Stress *Initial Conditions, type=STRESS Set_bfc, σ_{fc}, 0, 0,	Residual stress bottom flange compressive stress

**Name: bft Type: Stress *Initial Conditions, type=STRESS Set_bft, σ_{ft}, 0, 0,	bottom flange tensile stress
**Name: tfc Type: Stress *Initial Conditions, type=STRESS Set_tfc, σ_{fc}, 0, 0,	top flange compressive stress
**Name: tft Type: Stress *Initial Conditions, type=STRESS Set_tft, σ_{ft}, 0, 0,	top flange tensile stress
**Name: wc Type: Stress *Initial Conditions, type=STRESS Set_wc, σ_{wc}, 0, 0,	web compressive stress
**Name: wt Type: Stress *Initial Conditions, type=STRESS Set_wt, σ_{wt}, 0, 0, **	web tensile stress
** STEP: fire_step **	
*imperfection, File= filename, Step=1 1,l_b/1000	global imperfection
*Step, name= fire_step, nlgeom=YES, inc= 200	Step: fire analysis
*Coupled Temperature-displacement, creep = none, deltmx= 200., stabilize = 0.0002, allsdtol = 0.05, continue = NO	stabilization parameters
10., total_fire_time., 1e-20, max_temperature_each_iteration. **	time steps
** BOUNDARY CONDITIONS **	
** Name: TEMPR_BC Type: Temperature *Boundary, amplitude=Fire_amp ALLNODE, 11, 11,1 **	Conduction heat: all nodes
** LOADS **	
** Name: CFOR_LOAD Type: Concerntrated force *Cload, amplitude= Load_amp Loadingset,2,-1 **	Loads
** OUTPUT REQUESTS **	
*Restart, write, frequency=0 **	field output
** FIELD OUTPUT: F-Output-1 **	
*Output, field, variable=PRESELECT **	
** HISTORY OUTPUT: H-Output-1 **	history output
*Output, history, variable=PRESELECT *End Step	

References

A572/A572M. 2018. “Standard Specification for High-Strength Low-Alloy Columbium-Vanadium Structural Steel 1.” *ASTM Int. West Conshohocken, PA 19428-2959, US*. https://doi.org/10.1520/A0572_A0572M-18.

Abaqus 6.19 [computer Software]. 2019. “Abaqus 6.19 User’s Manual.” *Dassault Syst. Simulia Corps.*

Aghakouchak, A. A., S. Garivani, A. Shahmari, and M. Heshmati. 2021. “Structural investigation of the collapse of the 16-story Plasco building due to fire.” *Struct. Des. Tall Spec. Build.*, 30 (1). John Wiley and Sons Ltd. https://doi.org/10.1002/tal.1815.

ANSI/AISC 360. 2016. “Specification for Structural Steel Buildings.” *AISC, Chicago, Illinois 60601-1802*.

AS 4100. 2016. “Steel Structures Standards.” *Stand. Aust. Sydney Aust.*

ASTM E21. 2017. “Standard Test Methods for Elevated Temperature Tension Tests of Metallic Materials.” *ASTM Int. West Conshohocken, PA 19428-2959, US*. https://doi.org/10.1520/E0021-17.

ASTM E8/E8M. 2016. “Standard Test Methods for Tension Testing of Metallic Materials.” *ASTM Int. West Conshohocken, PA 19428-2959, US*. https://doi.org/10.1520/E0008_E0008M-16A.

Aziz, E. M., and V. K. Kodur. 2016. “Effect of temperature and cooling regime on mechanical properties of high-strength low-alloy steel.” *Fire Mater.*, 40 (7): 926–939. John Wiley and Sons Ltd. https://doi.org/10.1002/fam.2352.

Bailey, C. G., I. W. Burgess, and R. J. Plank. 1996. “Analyses of the effects of cooling and fire spread on steel-framed buildings.” *Fire Saf. J.*, 26 (4): 273–291. https://doi.org/10.1016/S0379-7112(96)00027-6.

BS 5950-1. 2000. “Structural use of steelworks in building - Part 1.” *Br. Stand. Inst.*

BSI. 1990. “BS 5950 Structural Use of Steelwork in Building—Part 8.” *Code Pract. Fire*

Resist. Des. London, UK, 3.

Bull, L., E. J. Palmiere, R. P. Thackray, I. W. Burgess, and B. Davison. 2015. "Tensile behaviour of galvanised grade 8.8 bolt assemblies in fire." *J. Struct. Fire Eng.*, 6 (3): 197–212. https://doi.org/10.1260/2040-2317.6.3.197.

Callister, J. W. D., and D. G. Rethwisch. 2014. "Materials Science and Engineering: An Introduction." *Wiley*.

Chen, J., B. Young, and B. Uy. 2006. "Behavior of High Strength Structural Steel at Elevated Temperatures." *J. Struct. Eng.*, 132 (12): 1948–1954. https://doi.org/10.1061/(ASCE)0733-9445(2006)132:12(1948).

Chen, W., K. Liu, J. Ye, J. Jiang, C. Xu, L. Jin, and M. Zhang. 2020a. "High-temperature steady-state experiments on G550 cold-formed steel during heating and cooling stages." *Thin-Walled Struct.*, 151. Elsevier Ltd. https://doi.org/10.1016/j.tws.2020.106760.

Chen, W., J. Ye, L. Jin, J. Jiang, K. Liu, M. Zhang, W. Chen, and H. Zhang. 2020b. "High-temperature material degradation of Q345 cold-formed steel during full-range compartment fires." *J. Constr. Steel Res.*, 175. Elsevier Ltd. https://doi.org/10.1016/j.jcsr.2020.106366.

Chen, W., J. Ye, J. Peng, and B. Liu. 2019. "Experimental Investigation of Postfire Mechanical Properties of Q345 and G550 Cold-Formed Steel." *J. Mater. Civ. Eng.*, 31 (7). American Society of Civil Engineers (ASCE). https://doi.org/10.1061/(ASCE).

Dwaikat, M. M. S., and V. K. R. Kodur. 2011. "A performance based methodology for fire design of restrained steel beams." *J. Constr. Steel Res.*, 67 (3): 510–524. https://doi.org/10.1016/j.jcsr.2010.09.004.

El-Rimawi, J. A., I. W. Burgess, and R. J. Plank. 1996. "The Treatment of Strain Reversal in Structural Members during the Cooling Phase of a Fire." *J. Constr. Steel Res.*, 37 (2): 115–135. https://doi.org/10.1016/0143-974X(95)00023-O.

Elhami Khorasani, N., T. Gernay, and C. Fang. 2019. "Parametric Study for Performance-Based Fire Design of US Prototype Composite Floor Systems." *J. Struct. Eng.*, 145 (5). American Society of Civil Engineers (ASCE). https://doi.org/10.1061/(ASCE)ST.1943-541X.0002315.

EN 10025-2. 2019. "Hot rolled products of structural steels. Technical delivery conditions for non-alloy structural steels." *Eur. Committe Stand. (CEN), Brussels*.

EN 1991-1-2. 2002. "Actions on structures - Part 1-2: General actions - Actions on structures

exposed to fire." *Eur. Committe Stand. (CEN), Brussels*.

EN 1993-1-2. 2005. "Design of Steel Structures - Part 1-2: General Rules - Structural Fire Design." *Eur. Committe Stand. (CEN), Brussels*.

EN 1993-1. 2005. "Eurocode 3: Design of steel structures - Part 1-1: General rules and rules for buildings." *Eur. Committe Stand. (CEN), Brussels*.

Fan, S. G., G. P. Shu, C. S. Huo, C. L. Liu, and Y. L. Tao. 2013. "Research on performance of high-strength bolted connection in fire and after fire." *IES J. Part A Civ. Struct. Eng.*, 6 (2): 135–149. https://doi.org/10.1080/19373260.2013.765789.

Fischer, E. C., A. H. Varma, and A. Agarwal. 2019. "Performance-Based Structural Fire Engineering of Steel Building Structures: Design-Basis Compartment Fires." *J. Struct. Eng.*, 16 (9). https://doi.org/10.1061/(ASCE).

Flint, G., A. Usmani, S. Lamont, B. Lane, and J. Torero. 2007. "Structural Response of Tall Buildings to Multiple Floor Fires." *J. Struct. Div. Proc ASCE*, 133 (December): 1719–1732. https://doi.org/10.1061/(ASCE)0733-9445(2007)133:12(1719).

Franssen, J. M. 1990. "The unloading of building materials submitted to fire." *Fire Saf. J.*, 16 (3): 213–227. https://doi.org/10.1016/0379-7112(90)90034-C.

Gardner, L., A. Insausti, K. T. T. Ng, and M. Ashraf. 2010. "Elevated temperature material properties of stainless steel alloys." *J. Constr. Steel Res.*, 66 (5): 634–647. Elsevier. https://doi.org/10.1016/j.jcsr.2009.12.016.

Gardner, L., and D. A. Nethercot. 2004. "Experiments on stainless steel hollow sections-Part 1: Material and cross-sectional behaviour." *J. Constr. Steel Res.*, 60 (9): 1291–1318. https://doi.org/10.1016/j.jcsr.2003.11.006.

Gernay, T., and J. M. Franssen. 2015. "A performance indicator for structures under natural fire." *Eng. Struct.*, 100: 94–103. Elsevier Ltd. https://doi.org/10.1016/j.engstruct.2015.06.005.

Gernay, T., and N. E. Khorasani. 2020. "Recommendations for performance-based fire design of composite steel buildings using computational analysis." *J. Constr. Steel Res.*, 166. Elsevier Ltd. https://doi.org/10.1016/j.jcsr.2019.105906.

Gunalan, S., and M. Mahendran. 2014. "Experimental investigation of post-fire mechanical properties of cold-formed steels." *Thin-Walled Struct.*, 84: 241–254. https://doi.org/10.1016/j.tws.2014.06.010.

Guo, S. 2012. “Experimental and numerical study on restrained composite slab during heating and cooling.” *J. Constr. Steel Res.*, 69 (1): 95–105. https://doi.org/10.1016/j.jcsr.2011.08.009.

Guo, S., and C. G. Bailey. 2011. “Experimental behaviour of composite slabs during the heating and cooling fire stages.” *Eng. Struct.*, 33 (2): 563–571. https://doi.org/10.1016/j.engstruct.2010.11.014.

Hanus, F., G. Zilli, and J. M. Franssen. 2011. “Behaviour of Grade 8.8 bolts under natural fire conditions-Tests and model.” *J. Constr. Steel Res.* https://doi.org/10.1016/j.jcsr.2011.03.012.

Hill, H. N. 1944. “Determination of stress-strain relations from the offset yield strength values, Technical Note No. 927.” *Natl. Advis. Comm. Aeronaut.*

Hu, G., M. A. Morovat, J. Lee, E. Schell, and M. Engelhardt. 2009. “Elevated temperature properties of ASTM A992 steel.” *Proc. 2009 Struct. Congr. - Don’t Mess with Struct. Eng. Expand. Our Role*, 1067–1076.

Huang, Y., and B. Young. 2014. “The art of coupon tests.” *J. Constr. Steel Res.*, 96: 159–175. https://doi.org/10.1016/j.jcsr.2014.01.010.

Huang, Y., and B. Young. 2017. “Post-fire behaviour of ferritic stainless steel material.” *Constr. Build. Mater.*, 157: 654–667. Elsevier Ltd. https://doi.org/10.1016/j.conbuildmat.2017.09.082.

Imran, M., M. Mahendran, and P. Keerthan. 2018. “Mechanical properties of cold-formed steel tubular sections at elevated temperatures.” *J. Constr. Steel Res.*, 143: 131–147.

IS 1367-3. 2002. “Technical Supply Conditions for Threaded Steel Fasteners, Part 3: Mechanical Properties of Fasteners Made of Carbon Steel and Alloy Steel - Bolts, Screws and Studs.” *Indian Stand.*

IS 2062. 2011. “Hot Rolled Medium and Hot Rolled Medium and High Tensile Structural Steel - Specifaction.” *Bur. Indian Stand. New Delhi*.

IS 800. 2007. “General construction in steel - code of practice.” *Bur. Indian Stand. New Delhi*.

ISO 6892-1. 2016. “Metallic materials-Tensile testing.” *Br. Stand. Inst.*

ISO 898-1. 2009. “Mechanical properties of fasteners made of carbon steel and alloy steel - Part 1.” *Int. Organ. Stand. Geneva, Switz.*

Jiang, B., G. Q. Li, and A. Usmani. 2015. "Progressive collapse mechanisms investigation of planar steel moment frames under localized fire." *J. Constr. Steel Res.*, 115: 160–168. Elsevier Ltd. https://doi.org/10.1016/j.jcsr.2015.08.015.

Jiang, J., and G. Q. Li. 2017. "Disproportionate collapse of 3D steel-framed structures exposed to various compartment fires." *J. Constr. Steel Res.*, 138: 594–607. https://doi.org/10.1016/j.jcsr.2017.08.007.

Kankanamge, N. D., and M. Mahendran. 2011. "Mechanical properties of cold-formed steels at elevated temperatures." *Thin-Walled Struct.*, 49 (1): 26–44.

Kesawan, S., and M. Mahendran. 2018. "Post-fire mechanical properties of cold-formed steel hollow sections." *Constr. Build. Mater.* https://doi.org/10.1016/j.conbuildmat.2017.11.077.

Ketabdari, H., A. Saedi Daryan, and N. Hassani. 2019. "Predicting post-fire mechanical properties of grade 8.8 and 10.9 steel bolts." *J. Constr. Steel Res.*, 162. Elsevier Ltd. https://doi.org/10.1016/j.jcsr.2019.105735.

Khorasani, N. E., P. Gardoni, and M. Garlock. 2015. "Probabilistic Fire Analysis: Material Models and Evaluation of Steel Structural Members." *J. Struct. Eng. (United States)*, 141 (12). American Society of Civil Engineers (ASCE). https://doi.org/10.1061/(ASCE)ST.1943-541X.0001285.

Kirby, B. R. 1995. *The Behaviour of High-strength Grade 8.8 Bolts in Fire. J. Constr. Steel Res.*

Kirby, B. R., and R. R. Preston. 1988. "High Temperature Properties of Hot-rolled, Structural Steels for Use in Fire Engineering Design Studies." *Fire Saf. J.*, 13: 27–37.

Kodur, V. K. R., and M. M. S. Dwaikat. 2009. "Response of steel beam-columns exposed to fire." *Eng. Struct.*, 31 (2): 369–379. https://doi.org/10.1016/j.engstruct.2008.08.020.

Kodur, V., S. Kand, and W. Khaliq. 2012. "Effect of Temperature on Thermal and Mechanical Properties of Steel Bolts." *J. Mater. Civ. Eng.*, 24 (6): 765–774. American Society of Civil Engineers (ASCE). https://doi.org/10.1061/(asce)mt.1943-5533.0000445.

Kodur, V., M. Yahyai, A. Rezaeian, M. Eslami, and A. Poormohamadi. 2017. "Residual mechanical properties of high strength steel bolts subjected to heating-cooling cycle." *J. Constr. Steel Res.*, 131: 122–131. https://doi.org/10.1016/j.jcsr.2017.01.007.

Lamont, S., A. S. Usmani, and M. Gillie. 2004. "Behaviour of a small composite steel frame structure in a 'long-cool' and a 'short-hot' fire." *Fire Saf. J.*, 39 (5): 327–357.

https://doi.org/10.1016/j.firesaf.2004.01.002.

Lange, J., and F. González. 2012. “Behavior of high-strength grade 10.9 bolts under fire conditions.” *Struct. Eng. Int. J. Int. Assoc. Bridg. Struct. Eng.*, 22 (4): 470–475. https://doi.org/10.2749/101686612X13363929517451.

Li, D., B. Uy, J. Wang, and Y. Song. 2020. “Behaviour and design of high-strength Grade 12.9 bolts under combined tension and shear.” *J. Constr. Steel Res.*, 174. Elsevier Ltd. https://doi.org/10.1016/j.jcsr.2020.106305.

Li, G. Q., and S. X. Guo. 2008. “Experiment on restrained steel beams subjected to heating and cooling.” *J. Constr. Steel Res.*, 64 (3): 268–274. https://doi.org/10.1016/j.jcsr.2007.07.007.

Li, G. Q., S.-C. Jiang, Y.-Z. Yin, and M.-F. Li. 2003. *Experimental studies on the properties of constructional steel at elevated temperatures*. *J. Struct. Eng.*

Li, G., P. Wang, and J. Shouchao. 2007. “Non-linear finite element analysis of axially restrained steel beams at elevated temperatures in a fire.” *J. Constr. Steel Res.*, 63 (9): 1175–1183. https://doi.org/10.1016/j.jcsr.2006.11.009.

Li, H. T., and B. Young. 2017. “Material properties of cold-formed high strength steel at elevated temperatures.” *Thin-Walled Struct.*, 115: 289–299. https://doi.org/10.1016/j.tws.2017.02.019.

Liu, T. C. H., and J. M. Davies. 2001. “Performance of steel beams at elevated temperatures under the effect of axial restraints.” *Steel Compos. Struct.*, 1 (4): 427–440. https://doi.org/10.12989/scs.2001.1.4.427.

Liu, T. C. H., M. K. Fahad, and J. M. Davies. 2002. “Experimental investigation of behaviour of axially restrained steel beams in fire.” *J. Constr. Steel Res.*, 58 (9): 1211–1230. https://doi.org/10.1016/S0143-974X(01)00062-1.

Lou, G. B., S. Yu, R. Wang, and G. Q. Li. 2012. “Mechanical properties of high-strength bolts after fire.” *Proc. Inst. Civ. Eng. Struct. Build.*, 165 (7): 373–383. ICE Publishing Ltd. https://doi.org/10.1680/stbu.11.00015.

Lu, J., H. Liu, Z. Chen, and X. Liao. 2016. “Experimental investigation into the post-fire mechanical properties of hot-rolled and cold-formed steels.” *J. Constr. Steel Res.*, 121: 291–310. https://doi.org/10.1016/j.jcsr.2016.03.005.

Luecke, W., S. W. Banovic, and J. D. McColskey. 2013. *High-temperature tensile constitutive data and models for structural steels in fire*. *Natl. Inst. Stand. Technol.* Gaithersburg, MD.

Manach, P. Y., S. Thuillier, J. W. Yoon, J. Coër, and H. Laurent. 2014. "Kinematics of Portevin-Le Chatelier bands in simple shear." *Int. J. Plast.*, 58: 66–83. Elsevier Ltd. https://doi.org/10.1016/j.ijplas.2014.02.005.

Mander, J. B. 1983. "Seismic design of bridge piers." University of Canterburry, Christchurch, New Zealand.

McCann, F., L. Gardner, and S. Kirk. 2015. "Elevated temperature material properties of cold-formed steel hollow sections." *Thin-Walled Struct.*, 90: 84–94. Elsevier Ltd. https://doi.org/10.1016/j.tws.2015.01.007.

Mirambell, E., and E. Real. 2000. "On the calculation of deflections in structural stainless steel beams: An experimental and numerical investigation." *J. Constr. Steel Res.*, 54 (1): 109–133. https://doi.org/10.1016/S0143-974X(99)00051-6.

Neuenschwander, M., M. Knobloch, and M. Fontana. 2017. "Elevated temperature mechanical properties of solid section structural steel." *Constr. Build. Mater.*, 149: 186–201.

Outinen, J., O. Kaitila, and P. Miikeliiinen. 2001. "High-Temperature testing of structural steel and modelling of struuctures at fire temperatures." *Helsinki Univ. Technol. Dept Civ. Environ. Eng. Lab. Steel Struct.*, 126.

Outinen, J., and P. Makelainen. 2004. "Mechanical properties of structural steel at elevated temperatures and after cooling down." *Fire Mater.*, 28 (2–4): 237–251. https://doi.org/Doi 10.1002/Fam.849.

Peixoto, R. M., M. S. Seif, and L. C. M. Vieira. 2017. "Double-shear tests of high-strength structural bolts at elevated temperatures." *Fire Saf. J.*, 94: 8–21. Elsevier Ltd. https://doi.org/10.1016/j.firesaf.2017.09.003.

Pournaghshband, A., S. Afshan, and M. Theofanous. 2019. "Elevated temperature performance of restrained stainless steel beams." *Structures*, 22: 278–290. https://doi.org/10.1016/j.istruc.2019.08.015.

Rackauskaite, E., P. Kotsovinos, A. Jeffers, and G. Rein. 2017. "Structural analysis of multi-storey steel frames exposed to travelling fires and traditional design fires." *Eng. Struct.*, 150: 271–287. https://doi.org/10.1016/j.engstruct.2017.06.055.

Ramberg, W., and W. R. Osgood. 1943. *Description of stress-strain curves by three parameters/NACA, Technical Note No. 902*.

Ramesh, S., L. Choe, and C. Zhang. 2020. "Experimental investigation of structural steel beams subjected to localized fire." *Eng. Struct.*, 218. Elsevier Ltd.

https://doi.org/10.1016/j.engstruct.2020.110844.

Ranawaka, T., and M. Mahendran. 2009. “Experimental study of the mechanical properties of light gauge cold-formed steels at elevated temperatures.” *Fire Saf. J.*, 44 (2): 219–229. https://doi.org/10.1016/j.firesaf.2008.06.006.

Rasmussen, K. J. R. 2003. “Full-range stress–strain curves for stainless steel alloys Kim.” *J. Constr. Steel Res.*, 59: 47–61.

Rokilan, M., and M. Mahendran. 2020. “Elevated temperature mechanical properties of cold-rolled steel sheets and cold-formed steel sections.” *J. Constr. Steel Res.*, 167. Elsevier Ltd. https://doi.org/10.1016/j.jcsr.2019.105851.

Rokilan, M., and M. Mahendran. 2022. “Design of cold-formed steel wall studs subject to non-uniform elevated temperature distributions.” *Thin-Walled Struct.*, 171. Elsevier Ltd. https://doi.org/10.1016/j.tws.2021.108625.

Shaheen, M. A., A. S. J. Foster, L. S. Cunningham, and S. Afshan. 2020. “Behaviour of stainless and high strength steel bolt assemblies at elevated temperatures — A review.” *Fire Saf. J.* Elsevier Ltd.

Singh, T. G., and K. D. Singh. 2019a. “Mechanical properties of YSt-310 cold-formed steel hollow sections at elevated temperatures.” *J. Constr. Steel Res.*, 158: 53–70.

Singh, T. G., and K. D. Singh. 2019b. “Post-fire mechanical properties of YSt-310 cold-formed steel tubular sections.” *J. Constr. Steel Res.*, 153: 654–666. https://doi.org/10.1016/j.jcsr.2018.11.014.

Smith, C. I., B. R. Kirby, D. G. Lapwood, K. J. Cole, A. P. Cunningham, and R. R. Preston. 1981. “The reinstatement of fire damaged steel framed structures.” *Fire Saf. J.*, 4: 21–62. https://doi.org/10.1016/0379-7112(81)90004-7.

Song, Y., J. Wang, B. Uy, and D. Li. 2020. “Stainless steel bolts subjected to combined tension and shear: Behaviour and design.” *J. Constr. Steel Res.*, 170. Elsevier Ltd. https://doi.org/10.1016/j.jcsr.2020.106122.

Standards Australia. 1998. “Steel structures (AS 4100).” *Aust. Build. Codes Board*.

Sun, R., and I. W. Burgess. 2016. “An analytical and numerical prediction for ductility demand on steel beam-to-column connections in fire.” *Eng. Struct.*, 115: 55–66. Elsevier Ltd. https://doi.org/10.1016/j.engstruct.2016.02.036.

Tan, K.-H. H., and Z.-F. F. Huang. 2005. “Structural Responses of Axially Restrained Steel

Beams with Semirigid Moment Connection in Fire." *J. Struct. Eng.*, 131 (4): 541–551. https://doi.org/10.1061/ASCE0733-94452005131:4541.

Tao, Z., X.-Q. Wang, and B. Uy. 2012. "Stress-Strain Curves of Structural and Reinforcing Steels after Exposure to Elevated Temperatures." *J. Mater. Civ. Eng.*, 25 (9): 1306–1316. American Society of Civil Engineers (ASCE). https://doi.org/10.1061/(asce)mt.1943-5533.0000676.

Torić, N., J. Brnić, I. Boko, M. Brčić, I. W. Burgess, and I. U. Glavinić. 2017. "Development of a high temperature material model for grade S275JR steel." *J. Constr. Steel Res.*, 137: 161–168.

Usmani, A. S., Y. C. Chung, and J. L. Torero. 2003. "How did the WTC towers collapse: A new theory." *Fire Saf. J.*, 38 (6): 501–533. Elsevier Ltd. https://doi.org/10.1016/S0379-7112(03)00069-9.

Wang, H., and Y. F. Chen. 2021. "Behaviour of austenitic stainless steel bolts at elevated temperatures." *Eng. Struct.*, 235. Elsevier Ltd. https://doi.org/10.1016/j.engstruct.2021.111973.

Wang, H., X. Hu, and C. Chen. 2005. "Experimental research of ultimate bearing capacity of high-strength bolt at high temperature." *Steel Constr.*, 3.

Wang, X.-Q., Z. Tao, U. Katwal, and C. Hou. 2021. "Tensile stress-strain models for high strength steels." *J. Constr. Steel Res.*, 186: 106879. https://doi.org/10.1016/j.jcsr.2021.106879.

Wang, Y. C. 2000. "An analysis of the global structural behaviour of the Cardington steel-framed building during the two BRE fire tests." *Eng. Struct.*, 22: 401–412.

Yang, K. C., R. J. Hsu, and Y. J. Chen. 2011. "Shear strength of high-strength bolts at elevated temperature." *Constr. Build. Mater.*, 25 (8): 3656–3660. https://doi.org/10.1016/j.conbuildmat.2011.03.003.

Ye, J., and W. Chen. 2012. "Elevated Temperature Material Degradation of Cold-Formed Steels under Steady- and Transient-State Conditions." *J. Mater. Civ. Eng.*, 25 (8): 947–957. American Society of Civil Engineers (ASCE). https://doi.org/10.1061/(asce)mt.1943-5533.0000640.

Yilmaz, A. 2011. "The Portevin-Le Chatelier effect: A review of experimental findings." *Sci. Technol. Adv. Mater.*

Yin, Y. Z., and Y. C. Wang. 2004. "A numerical study of large deflection behaviour of

restrained steel beams at elevated temperatures." *J. Constr. Steel Res.*, 60 (7): 1029–1047. https://doi.org/10.1016/j.jcsr.2003.09.005.

Yin, Y. Z., and Y. C. Wang. 2005. "Analysis of catenary action in steel beams using a simplified hand calculation method, Part 1: Theory and validation for uniform temperature distribution." *J. Constr. Steel Res.*, 61 (2): 183–211. https://doi.org/10.1016/j.jcsr.2004.07.002.

Yuan, G., Q. Shu, Z. Huang, and Q. Li. 2016. "An experimental investigation of properties of Q345 steel pipe at elevated temperatures." *J. Constr. Steel Res.*, 118: 41–48.

Zhang, C., G. Q. Li, and A. Usmani. 2013. "Simulating the behavior of restrained steel beams to flame impingement from localized-fires." *J. Constr. Steel Res.*, 83: 156–165. https://doi.org/10.1016/j.jcsr.2013.02.001.

Zhang, C., R. Wang, and L. Zhu. 2021. "Mechanical properties of Q345 structural steel after artificial cooling from elevated temperatures." *J. Constr. Steel Res.*, 176. Elsevier Ltd. https://doi.org/10.1016/j.jcsr.2020.106432.

Zuev, L. B., V. V. Gorbatenko, and V. I. Danilov. 2017. "Chernov–Lüders bands and the Portevin–Le Chatelier effect as plastic flow instabilities." *Russ. Metall.*, 2017 (4): 231–236. Maik Nauka-Interperiodica Publishing. https://doi.org/10.1134/S0036029517040243.

List of publication based on this thesis

Peer reviewed journal

1) ***SK Mushahary****; KD Singh; SA Jayachandran (2021)*, 'Mechanical properties of E350 steel during heating and cooling, Thin – walled Structures, Vol 160, https://doi.org/10.1016/j.tws.2020.107351.
2) ***S.K. Mushahary****, K.D. Singh, S.A. Jayachandran (2022)*, Tensile and shear strength of 10.9 grade bolts in heating and cooling fire, J. Constr. Steel Res. 197 107503. https://doi.org/10.1016/j.jcsr.2022.107503
3) ***SK Mushahary****; KD Singh; SA Jayachandran (----)*, 'Numerical study of restrained steel beam in natural fire', **(***under review*).

Conference paper

1) ***SK Mushahary;*** *KD Singh; SA Jayachandran (2018),* 'Complementing effects of axial restraints in steel beam at elevated temperature' 11th Structural Engineering convention, Jadavpur University, Kolkata